

REPORT DOCUMENTATION PAGE			Form Approved OMB NO. 0704-0188		
<p>The public reporting burden for this collection of information is estimated to average 1 hour per response, including the time for reviewing instructions, searching existing data sources, gathering and maintaining the data needed, and completing and reviewing the collection of information. Send comments regarding this burden estimate or any other aspect of this collection of information, including suggestions for reducing this burden, to Washington Headquarters Services, Directorate for Information Operations and Reports, 1215 Jefferson Davis Highway, Suite 1204, Arlington VA, 22202-4302. Respondents should be aware that notwithstanding any other provision of law, no person shall be subject to any penalty for failing to comply with a collection of information if it does not display a currently valid OMB control number.</p> <p>PLEASE DO NOT RETURN YOUR FORM TO THE ABOVE ADDRESS.</p>					
1. REPORT DATE (DD-MM-YYYY) 05-02-2013		2. REPORT TYPE Final Report		3. DATES COVERED (From - To) 21-Dec-2011 - 20-Mar-2012	
4. TITLE AND SUBTITLE Design and Delivery of HMT Half-Shaft Prototype			5a. CONTRACT NUMBER W911NF-12-1-0038		
			5b. GRANT NUMBER		
			5c. PROGRAM ELEMENT NUMBER 1720BA		
6. AUTHORS Chau Tran, Eric Boros, Ryan Soukup, Caitlin Winnike, Tyler Hull, Brandon Novak			5d. PROJECT NUMBER		
			5e. TASK NUMBER		
			5f. WORK UNIT NUMBER		
7. PERFORMING ORGANIZATION NAMES AND ADDRESSES North Carolina State University Research Administration 2701 Sullivan Drive, Suite 240 Raleigh, NC 27695 -7514			8. PERFORMING ORGANIZATION REPORT NUMBER		
9. SPONSORING/MONITORING AGENCY NAME(S) AND ADDRESS(ES) U.S. Army Research Office P.O. Box 12211 Research Triangle Park, NC 27709-2211			10. SPONSOR/MONITOR'S ACRONYM(S) ARO		
			11. SPONSOR/MONITOR'S REPORT NUMBER(S) 61711-ST-II.1		
12. DISTRIBUTION AVAILABILITY STATEMENT Approved for Public Release; Distribution Unlimited					
13. SUPPLEMENTARY NOTES The views, opinions and/or findings contained in this report are those of the author(s) and should not be construed as an official Department of the Army position, policy or decision, unless so designated by other documentation.					
14. ABSTRACT The Mechanical and Aerospace Engineering Department's MAE 416 senior design section at NC State University will redesign and build a prototype of the half-shaft assembly for SUPACAT HMT 400/600 for the United States Army Special Operations Command (USASOC) under the Combat Development Directive (CDD). The new design is to eliminate failure of half-shaft joints and related components while maintaining current articulation angles, torque capacity, part interchangeability, and compatibility with existing drive train connections.					
15. SUBJECT TERMS HMT, Joints, Coupling, Half-Shaft					
16. SECURITY CLASSIFICATION OF:			17. LIMITATION OF ABSTRACT UU	15. NUMBER OF PAGES	19a. NAME OF RESPONSIBLE PERSON Chau Tran
a. REPORT UU	b. ABSTRACT UU	c. THIS PAGE UU			19b. TELEPHONE NUMBER 919-515-3025

Report Title

Design and Delivery of HMT Half-Shaft Prototype

ABSTRACT

The Mechanical and Aerospace Engineering Department’s MAE 416 senior design section at NC State University will redesign and build a prototype of the half-shaft assembly for SUPACAT HMT 400/600 for the United States Army Special Operations Command (USASOC) under the Combat Development Directive (CDD). The new design is to eliminate failure of half-shaft joints and related components while maintaining current articulation angles, torque capacity, part interchangeability, and compatibility with existing drive train connections.

Enter List of papers submitted or published that acknowledge ARO support from the start of the project to the date of this printing. List the papers, including journal references, in the following categories:

(a) Papers published in peer-reviewed journals (N/A for none)

<u>Received</u>	<u>Paper</u>
-----------------	--------------

TOTAL:

Number of Papers published in peer-reviewed journals:

(b) Papers published in non-peer-reviewed journals (N/A for none)

<u>Received</u>	<u>Paper</u>
-----------------	--------------

TOTAL:

Number of Papers published in non peer-reviewed journals:

(c) Presentations

Number of Presentations: 0.00

Non Peer-Reviewed Conference Proceeding publications (other than abstracts):

Received

Paper

TOTAL:

Number of Non Peer-Reviewed Conference Proceeding publications (other than abstracts):

Peer-Reviewed Conference Proceeding publications (other than abstracts):

Received

Paper

TOTAL:

Number of Peer-Reviewed Conference Proceeding publications (other than abstracts):

(d) Manuscripts

Received

Paper

TOTAL:

Number of Manuscripts:

Books

Received

Paper

TOTAL:

Patents Submitted

Patents Awarded

Awards

Graduate Students

<u>NAME</u>	<u>PERCENT SUPPORTED</u>
-------------	--------------------------

FTE Equivalent:

Total Number:

Names of Post Doctorates

<u>NAME</u>	<u>PERCENT SUPPORTED</u>
-------------	--------------------------

FTE Equivalent:

Total Number:

Names of Faculty Supported

<u>NAME</u>	<u>PERCENT SUPPORTED</u>
-------------	--------------------------

FTE Equivalent:

Total Number:

Names of Under Graduate students supported

<u>NAME</u>	<u>PERCENT SUPPORTED</u>
-------------	--------------------------

FTE Equivalent:

Total Number:

Student Metrics

This section only applies to graduating undergraduates supported by this agreement in this reporting period

The number of undergraduates funded by this agreement who graduated during this period: 0.00

The number of undergraduates funded by this agreement who graduated during this period with a degree in science, mathematics, engineering, or technology fields:..... 0.00

The number of undergraduates funded by your agreement who graduated during this period and will continue to pursue a graduate or Ph.D. degree in science, mathematics, engineering, or technology fields:..... 0.00

Number of graduating undergraduates who achieved a 3.5 GPA to 4.0 (4.0 max scale):..... 0.00

Number of graduating undergraduates funded by a DoD funded Center of Excellence grant for Education, Research and Engineering:..... 0.00

The number of undergraduates funded by your agreement who graduated during this period and intend to work for the Department of Defense 0.00

The number of undergraduates funded by your agreement who graduated during this period and will receive scholarships or fellowships for further studies in science, mathematics, engineering or technology fields: 0.00

Names of Personnel receiving masters degrees

<u>NAME</u>
Total Number:

Names of personnel receiving PHDs

<u>NAME</u>
Total Number:

Names of other research staff

<u>NAME</u>	<u>PERCENT SUPPORTED</u>
FTE Equivalent:	
Total Number:	

Sub Contractors (DD882)

Inventions (DD882)

Scientific Progress

The shortcomings of the Supacat HMT 400/600's current half-shaft assembly have made themselves evident through the high failure rate of CV boots. These failures prompted the development of an improved, bootless design intended to increase product life and robustness.

The decision to pursue the design outlined above did not come about without the investigation of alternative solutions. These included dual cardan joints, Thompson couplings, and alternative boot designs. Ultimately, the dual Cornay® joints were deemed superior for the application, with their high range of articulation and torque capacity.

The dual Cornay® joint configuration detailed in this report has many advantages over the current design. Most importantly, the catastrophic boot failure problem has been solved. With the implementation of twin bootless joints, there is no potential for lubricant loss due to extreme thermal conditions or abrupt impact caused by debris. The increase in reliability, in combination with the advantage of the design's relative ease of installation and removal, means less vehicle down time and higher confidence in performance over questionable terrain. Equally important are the financial savings associated with this design. Savings projections of \$8766.62 over 50,000 miles for each half-shaft were found, along with a break-even point of only 13,092 miles.

The proposed design, combined with a joint geometry redesign or variations in vehicle suspension components, provide an excellent solution to the Supacat HMT 400/600's boot joint failure problem.

Despite its advantages, the proposed design does have its drawbacks, particularly in fitment. The joint model used for the prototype fails to fit into the HMT's suspension assembly without considerable modification. The Cornay® joints being used are off-the-shelf models, Cornay® would be able to manufacture and design a proprietary joint for the use particularly for the HMT 400 to fix the clearance issues without modifying the suspension. Combined with stronger components, a smaller design with similar torque capacity is feasible. Another means of addressing the fitment problem is through a redesign of a few suspension components of the vehicle, particularly the pushrod assembly, which limits available assembly space currently. This redesign could allow the prototype to be installed into the HMT 400/600 without interference to suspension components.

Technology Transfer

Design and Delivery of HMT Half-Shaft Prototype

Final Report
Reference Number W911NF-12-1-0038
Army Research Office
P.O. Box 12211
RTP, NC 27709-2211



Submitted by: Dr. Chau M. Tran

North Carolina State University
Department of Mechanical & Aerospace Engineering
Engineering Bldg III, Campus Box 7910
911 Oval Drive
Raleigh, NC 27695-7910
Phone: (919) 515-3025
E-mail: cmtran@eos.ncsu.edu
November 1, 2012

Table of Contents

1.	Introduction.....	1
1.1.	Background	1
1.2.	Problem Statement	3
1.3.	Literature Review	3
1.4.	Personnel	13
1.5.	Design Methodology	15
1.6.	Schedule	18
2.	Modeling and Simulation.....	20
2.1.	Description of Design.....	20
2.2.	Analysis.....	24
2.3.	Simulation	50
3.	Optimization	55
3.1.	Feasibility Study.....	55
3.2.	Optimization Methods.....	62
4.	Materials and Design for Manufacturing.....	63
4.1.	Material Selection	63
4.2.	Mechanisms.....	66
4.3.	Assembly Details.....	74
4.4.	Design for Manufacturing	81
5.	Prototype Testing	82
5.1.	Test Design.....	82
5.2.	Statistical Analysis of Data	86
6.	Economics/Cost	89
6.1.	General Economics	89
6.2.	Cost.....	91
7.	Quality Engineering.....	92
7.1.	Deliverables.....	92
7.2.	Safety.....	92
7.3.	Impact on Society.....	93
7.4.	Ethics.....	94
8.	Concluding Remarks.....	95
	References.....	97
	Appendices.....	97

1. Introduction

The United States Army Special Operations Command (USASOC) under the Combat Development Directive (CDD) based on Fort Bragg in Fayetteville, North Carolina is the sponsor for this mechanical engineering senior design project at North Carolina State University. The sponsor sent the senior design engineer for the CDD, Jamie Villamil, and two combat developers, Sean Cantrell, and Joe Woodall to present the half-shaft project to the class. They established the three primary failure modes of the current half-shaft design and stated the project goals they hope to achieve, as well as a short overview of the HMT 400. The primary concern was boot failure which in turn leads to an overall failure of the joint itself due to debris intrusion and grease loss.

1.1. Background

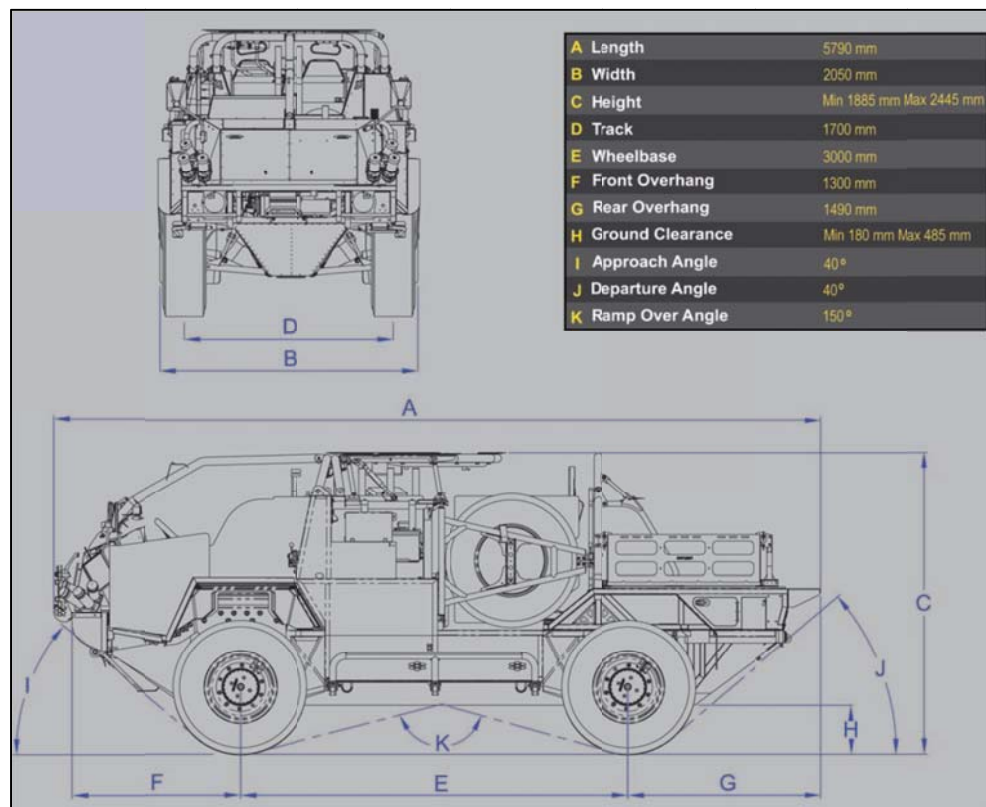


Figure 1: Supacat HMT400

The SUPACAT HMT (High Mobility Transport) 400/600 shown above in Figure 1 was designed based on the already existing ATMP (All Terrain Mobility Platform) by SUPACAT under license from Lockheed Martin. The HMT design was to implement self-deployability while increasing the driving range of the vehicle for use in military operations. The HMT was also designed to be able to fit inside a CH-47 Chinook helicopter, thus constraining its overall size. Since the initial design in 1990's and its enlistment in service in 2004 there will soon be over 600 in service worldwide. This vehicle can be equipped with runflat tires, locking

differentials, self-recovery winches, weapon mounts, remote weapons stations, smoke grenade launchers, IR lights and right or left hand drive.

In order to accommodate for the terrain on the battlefield and to fit into the Chinook the HMT uses an innovative air suspension system which allows for selectable ride height based on the current operating conditions. The current suspension vertical travel is 15 inches between the lowest and highest ride heights; this range of motion combined with the angle caused by steering results in a maximum half-shaft angle of 35° which puts great stress on the CV joints of the half-shafts driving each wheel.

The current design implements the use of Rzeppa joints on both the inner and outer joints of the half-shaft, shown below in Figure 2.

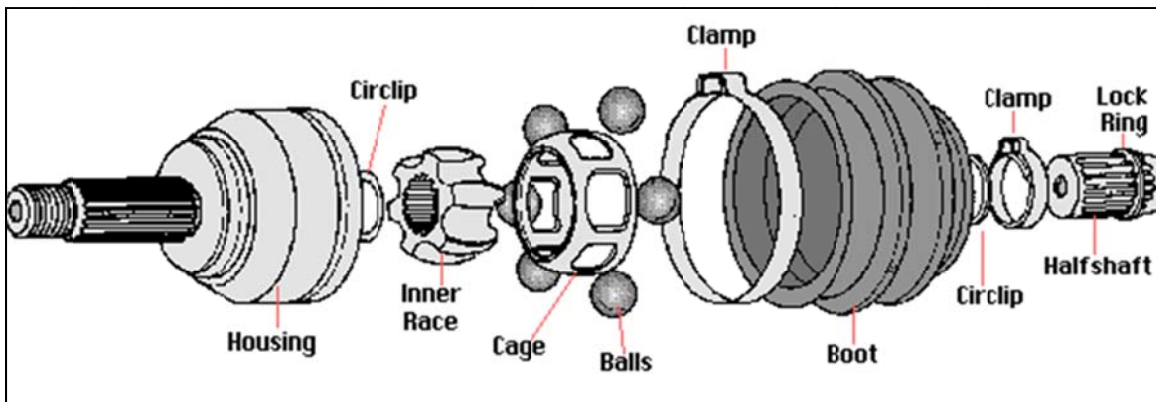


Figure 2: Rzeppa Joint Exploded View

The Rzeppa is a constant velocity joint invented in 1926 and was improved in 1936 by Alfred Hanz Rzeppa. The Rzeppa joint uses six balls and an inner and outer race to provide almost constant velocity torque transfer regardless of joint angle.¹ The balls are the means of transferring the torque in the joint, much like the teeth of a bevel gear. However, the Rzeppa transfers torque at the price of friction. The joint does not easily rotate at high articulation angles and causes an immense amount of heat build-up. Also this joint design must be packed with grease which is why a boot is necessary to keep out contamination and to contain the grease. When the boot fails the joint soon follows because the grease quickly leaks out causing joint lock up. Common causes of current boot failure include fatigue due to self-contact, heat failure, and tearing.

The combination of the HMT's harsh operating conditions, the maximum half-shaft angle of 35° , and the formidable maximum transmitted torque of $3000 \text{ N}\cdot\text{m}$ causes these Rzeppa joints to have an abysmal life-span. Due to this problem with the HMT and their interest in improving the performance of one of their personnel transports, the research and development engineers of the United States Special Operations Command, among other efforts, have enlisted outside aid to improve on their design.

The USASOC has established professional relationships with several North Carolina Universities, including Western Carolina University, UNC Charlotte, and, more recently, North Carolina State University. The universities have historically offered the assistance of their engineering departments to help solve various engineering problems encountered by the USASOC. In August of 2011, this led to the approach of NCSU's Mechanical and Aerospace

Engineering Department's senior design class to improve HMT 400/600 half-shaft performance.

In response to this approach and in an effort to remedy the design flaws in the current design, a bootless design will be implemented, using two Cornay® CVX-50 joints in place of both the cross-groove inner CV joint and the outer Rzeppa CV joint. Also, to expedite the replacement process a involute spline will be executed in between the joints to allow for the lateral plunge due to articulation and suspension travel, as well as the collapsing and separation of the shaft to remove each joint separately without removing the wheel assembly.

1.2. Problem Statement

The project goal is to redesign the half-shaft assembly between the differential and the gear hub of a SUPACAT HMT 400/600 for the United States Army Special Operations Command (USASOC) under the Combat Development Directive (CDD). The new design should extend the life-span of the half-shaft. Specifically, the design objective is to eliminate failure of half-shaft joints and related components while maintaining current articulation, torque capacity, part interchangeability, and compatibility with existing drive train connections. The new design will satisfy the following constraints:

- Operate at “on-road” suspension setting of $+5.6^\circ$
- Withstand the maximum torque applied of 3,000 Nm
- 15 inches of wheel travel
- Operating speed of 2,000 RPM
- Approximate lateral movement of 7 mm
- Lateral steering angle of $\pm 30^\circ$
- Prototype budget of \$800
- While maintaining clearances, commonality, and compatibility with existing parts.

1.3. Literature Review

The literature review for this project will consist of researching a variety of different methods to transmit rotational motion along a shaft throughout an articulation range which includes varying angles in several different directions. It will also include some brief research on other components involved with protecting and covering the necessary components. Among the material researched are joint designs for transferring motion at an angle, mechanical designs for transferring torque along a shaft at varying lengths, and various devices for protecting said mechanisms.

The Rzeppa joint currently utilized in the HMT400 half-shaft is a special design of universal joint capable of transmitting rotational motion at constant angular velocity.² More details on the Rzeppa joint can be found in Section 1.1 above. The following will cover the remaining literature review of other possible solutions to the failing half-shaft joints.

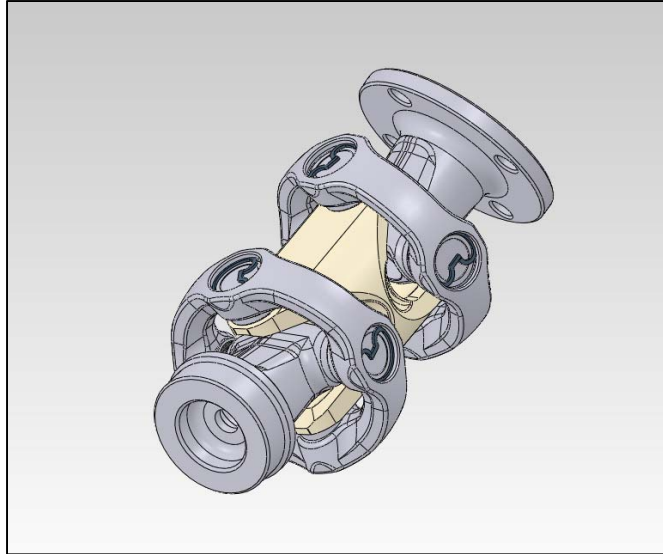


Figure 3: Cornay® CVX-50 Joint

Shown above in Figure 3 is the Cornay® CVX-50 CV joint. This particular CV joint operates at true constant velocity at angles up to 50°. ³ The joint also delivers extended durability over existing CV technology in high-speed, high-torque, and high-angle applications. In addition this joint is particularly suited to specialty 4x4 vehicles, military and light commercial vehicle applications that require high angle functionality at high speed operation and low vibration characteristics both on, and off road. The main components of the Cornay® joint shown below in Figure 4 include a centering mechanism which forces the two joint halves to operate at the same angle thereby causing the joint to operate at constant velocity at all angles (104). Two shafts (134,135) are rotatably connected to the centering mechanism. Movement of one of the shafts at an angle relative to the longitudinal axis of the coupling yoke (136) is transmitted to the other shaft by the centering mechanism. The joint also includes a flanged end as well as weldable connection to receive a 3 OD x 0.083 inch wall tubing at the other. Additionally the joint contains sealed needle roller bearings in the coupling yokes.

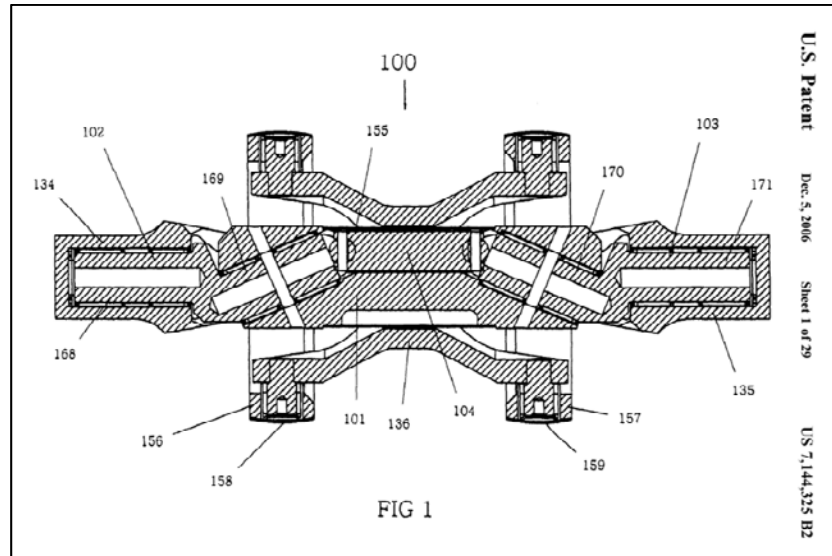


Figure 4: Cornay® CVX-50 Joint Patent Drawing

One route that was investigated was improving the current boot design. In order to improve the robustness and overall resistance to puncture and wear of the boot a look into laminates for the boot revealed other possibilities. One such laminate was the invisibleSHIELD by ZAGG®. This laminate is a 0.2 mm thick clear plastic like coating that comes in sheets, shown in Figure 5 below. This particular laminate can withstand over 1,000 lbs. of force without tearing or breaking. Also, it is very scratch resistant and puncture resistant. The invisibleSHIELD is designed as a covering for smartphones and iPods® to protect the screen and overall cosmetics of the subject in which they are applied to.⁴



Figure 5: invisibleSHIELD Laminate Sheet

Another route involved the use of a split boot rather than a conventional type closed boot, seen below in Figure 6. The motivation behind this design was the ease of installation and removal of the boot in case of maintenance needs, as these boots do not require half-shaft removal to install. These boots are prevalent in the automotive aftermarket industry, specifically for off-roading. Though convenient in the installation process, split boots inherently lose lubricant over time at the open seam. They are also just as prone to failure due to heat and puncture as closed boots.



Figure 6: Split-Type CV Boot

Another bootless joint design that was researched was the Thompson Coupling shown below in Figure 7. The main benefit of the Thompson joint is the fact it is a very low friction CV joint that can operate over a range of articulations at speed. Additionally, the joint can be loaded axially and continue to maintain a constant velocity over a range of input and output shaft angles. This joint is a vast improvement over the Rzeppa CV joint because there is very little frictional loss. The basis of this design is two Cardan joints assembled within one another using a control yoke. There is also a spherical four bar linkage that is utilized by the control yoke to geometrically constrain the alignment of the Cardan joints. The control yoke also utilizes this spherical pantograph scissor mechanism to bisect the angle between the input and output shafts.⁵ All of the parts associated in this design are labeled and color coded below in Figure 7.

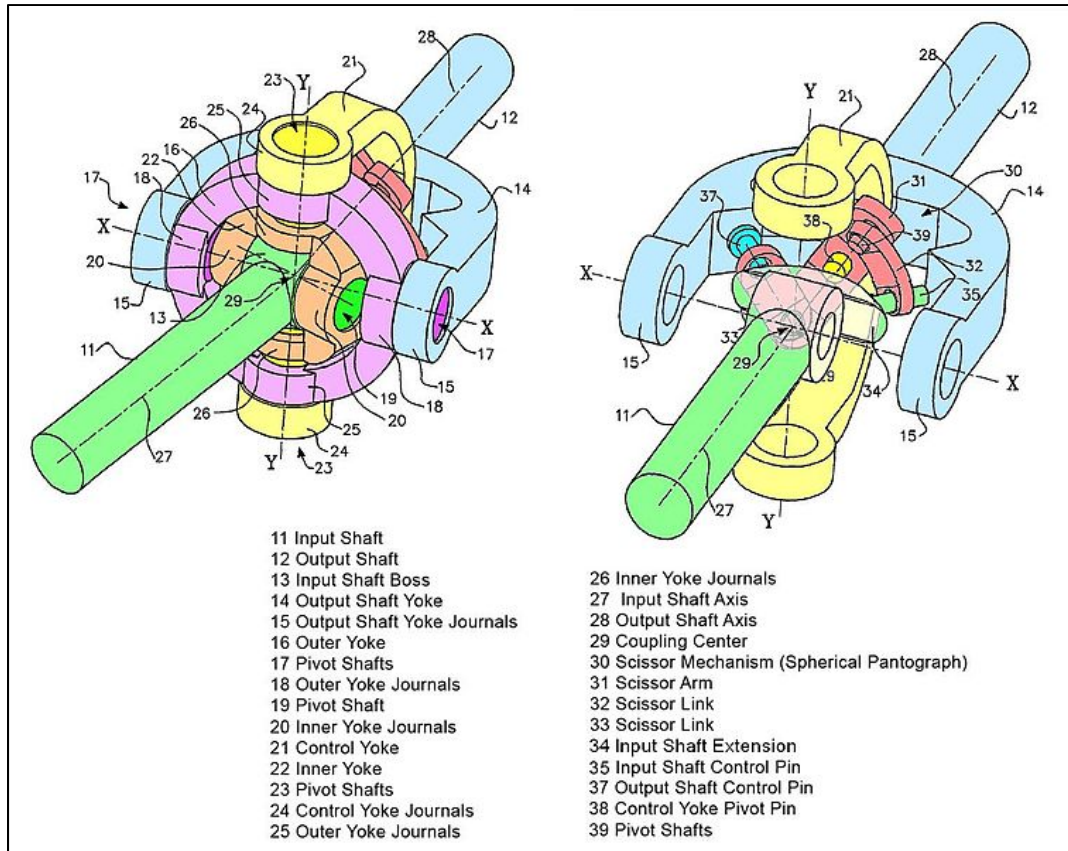


Figure 7: Thompson Coupling Patent Drawing

Another possible bootless invention was the Dual Cardan Constant Velocity (CV) joint. This joint is utilized in many light-duty applications to transfer rotational motion through an angle at near constant rotational velocity. The component breakdown of the Dual Cardan CV joint is shown below in Figure 8. The joint consists of two end yokes of different possible mating arrangements, two universal joints, a coupling yoke and a centering mechanism. The centering mechanism is necessary for the joint to maintain near constant velocity operation.

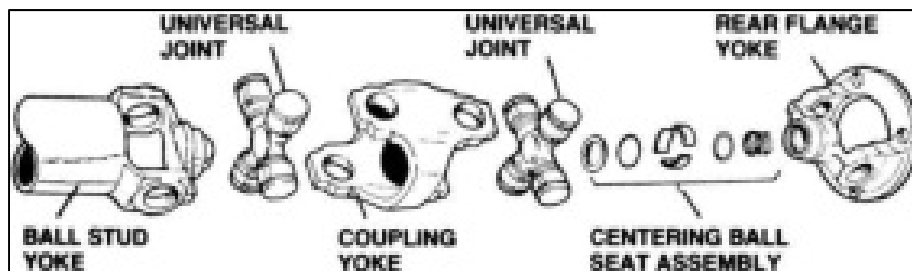


Figure 8: Dual Cardan Constant Velocity (CV) Joint

This centering mechanism is capable of maintaining constant velocity operation of the joint by splitting the overall angle evenly between the two universal joints. Technically a Dual Cardan joint is any type of joint that consists of an input shaft, an output shaft, a coupling yoke and two universal joints. There exist many more variations of the Dual Cardan joint that do not

utilize the centering mechanism preventing them from maintaining constant velocity at more than one angle. This operational phenomenon has to do with the rotational characteristics of the universal joint itself. As constant velocity rotation is transferred from an input shaft to a universal joint at an angle, the two caps of the joint attached to the input shaft will rotate at constant velocity as well. However, the other two caps attached to the opposite or output shaft will maintain a sinusoidal wave motion of velocity. This sinusoidal wave of velocity experienced is due to the fact that the universal joint will have to rotate in-and-out with respect to the axis of the input shaft. Essentially, the caps attached to the output shaft must travel a rotational distance that is longer than those attached to the input shaft. This motion is then transferred to the output shaft, which at high RPMs will cause vibration thus damaging the universal joint itself as well as components attached to the shaft. In Figure 9 below, the relationship between output shaft speed and input shaft angle can be realized.

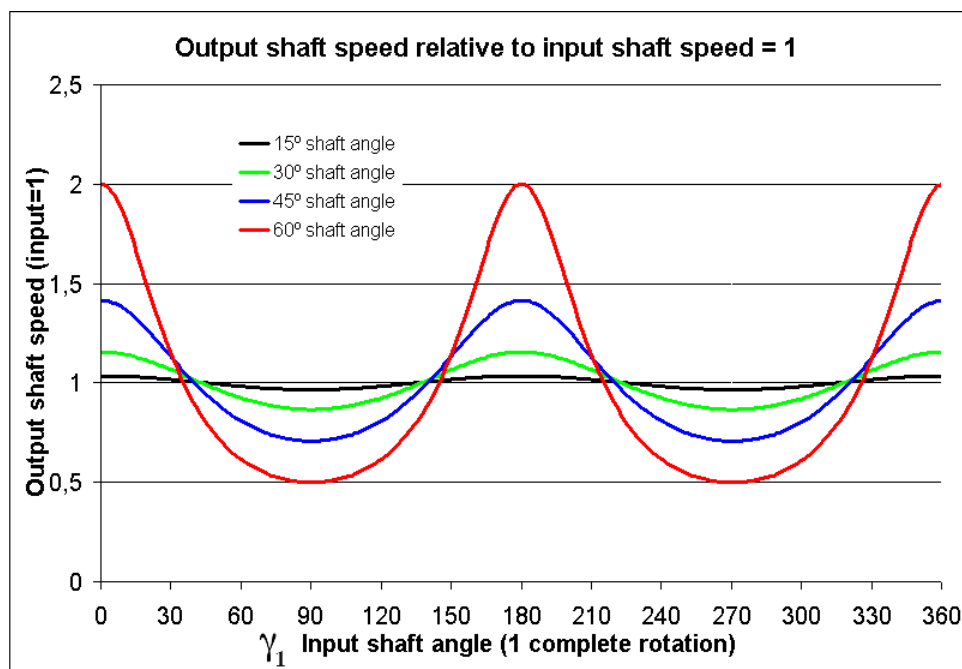


Figure 9: Universal Joint Output Speed vs. Input Angle⁶

By incorporating an intermediate shaft known as the coupling yoke, along with another universal joint, this sinusoidal wave caused by the first universal joint can be cancelled out by the second universal joint. In doing this, the intermediate shaft or coupling yoke will in fact rotate in a sinusoidal pattern, but this mass rotating in this fashion is very small and will eliminate damaging vibration over a specified operating range. The centering mechanism is not required for transmitting constant velocity across an angle where the input and output shaft are at fixed angles. In this constant velocity application of the Dual Cardan joint, the centering mechanism is necessary to allow for changing articulation angles. As the angle changes, the centering mechanism ensures the angle is split evenly between each universal joint allowing the sinusoidal wave pattern to eliminate itself across the entirety of the joint. For this specific application it is absolutely necessary to maintain constant velocity operation as the articulation angles are dynamic.

The Tracta joint shown in Figure 10 below is a type of universal joint capable of maintaining constant velocity operation. It was patented by Jean-Albert Grégoire in 1926, and used in the front wheel drive cars manufactured by his company, Asnières.

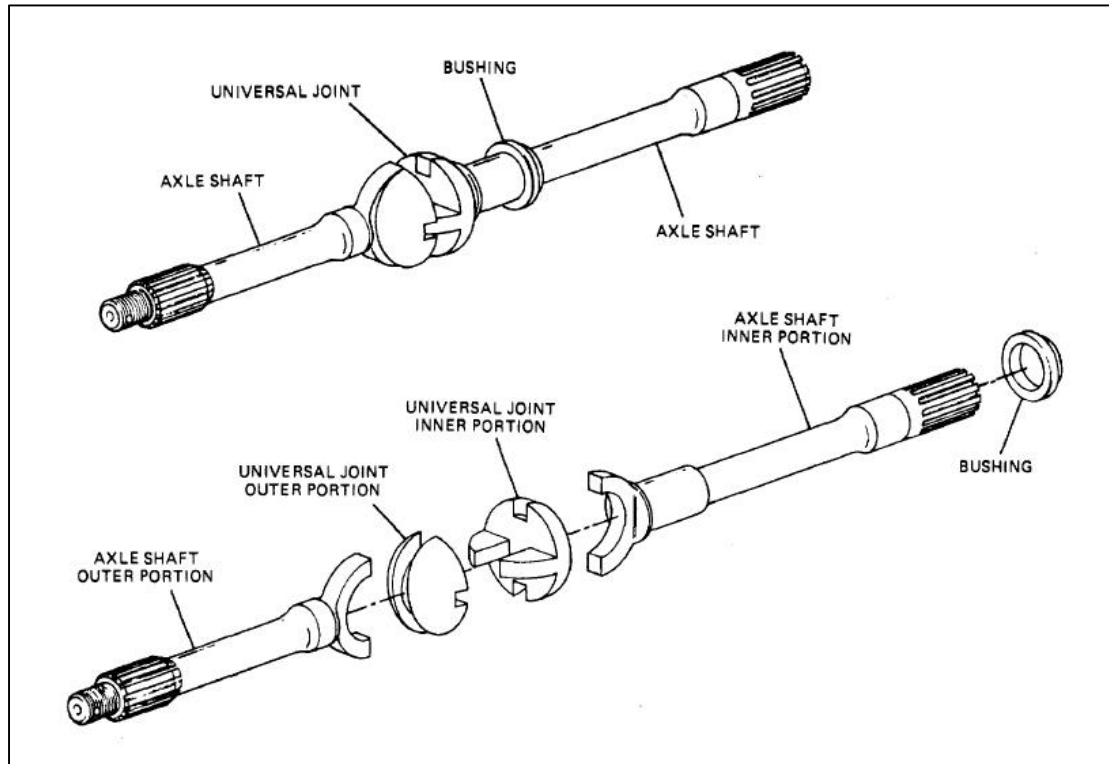


Figure 10: Tracta Joint

The Tracta joint consists of four parts: A forked driving shaft, a female (slotted joint), a male (spigot joint), and a forked driven shaft. In Figure 10 above, one can see that both the input and output shafts are of near identical design having semicircular forks which ride within the guides of each side of the universal joint. Also shown in the figure are both sides of the universal joint, the female (outer) and male (inner). The axis of articulation of each fork is perpendicular to that of the axis of articulation of the universal joint thus rendering it capable of operating at constant velocity. In fact the principles that allow this joint to operate at constant velocity are the exact same as a dual Cardan joint. The slot in the very middle of the male joint (inner), allows the universal joint to divide the angle of articulation evenly between either shaft/joint interface in the same fashion that the centering mechanism in a dual Cardan joint does. It is key to note that this joint does not incorporate any sort of roller or ball bearing and relies solely on sliding friction. It is easy to see why the dual Cardan is a much more popular design as it incorporates sealed needle roller bearings thus increasing the life and reliability of the joint.

Another type of constant velocity joint that was researched was the tripod joint. This joint operates in a very similar fashion to an Rzeppa joint, with points of rolling friction arranged in a circular fashion on a “spider assembly”, and a “slide housing: which the roller discs can articulate and plunge within. The tripod joint can be seen in Figure 11 below.

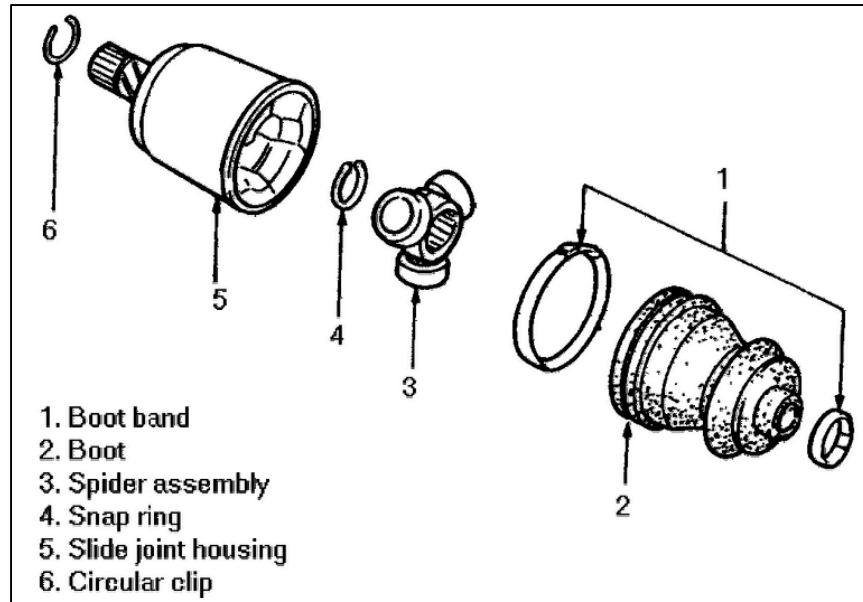


Figure 11: Tripod Joint

Shown in Figure 11, the main components of the tripod joint are the outer race, labeled 5, and the inner race and rolling discs, labeled 3. The outer race houses three grooves with widths slightly larger than the diameter of each rolling disc, and a specified depth to facilitate plunge. Any shaft utilizing this tripod joint does not require a spline located along the shaft to account for axial plunge. The roller discs, which contain needle roller bearings, in this assembly press against one wall of each groove to transfer motion. As articulation angles change, the roller discs must roll in and out along these grooves as they make the circular path around the axis of rotation of the spider assembly.

For the shaft application in the HMT400 it was important to maintain a shaft design that allowed for axial “plunge”, which is the change in overall length of the shaft. As can be seen above, there are universal joints that can cope with axial plunge and there are some that cannot. For those joints that cannot, it was necessary to investigate the available types of splines. Wikipedia defines mechanical splines as: *“ridges or teeth on a drive shaft that mesh with grooves in a mating piece and transfer torque to it, maintaining the angular correspondence between them.”*⁷ The first mechanical spline was the straight spline, which consists of ridges spaced along the circumference of the shaft that run the length of a shaft and are of a specified height and width. Figure 12 below shows several arrangements of straight splines.

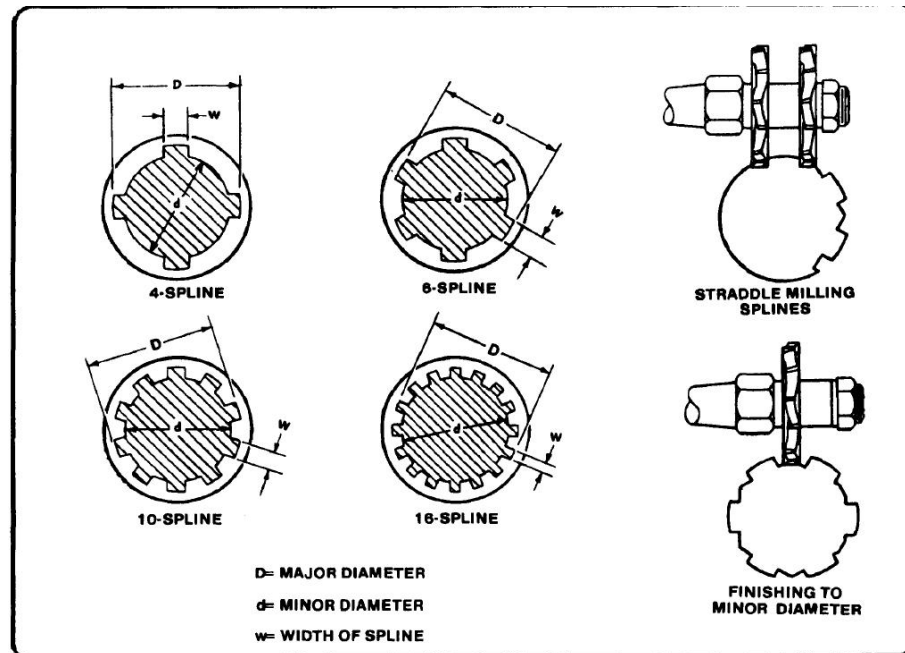


Figure 12: Straight Spline

The splines shown above provide a similar way to transmit torque to that of the tripod joint, however this method of transferring torque does not allow for any articulation. The male spline teeth will push against the female spline teeth as the male spline rotates, transferring the motion to the female spline. The downside to this design is that there is sliding friction as the male shaft plunges into the female shaft. Grease can typically remedy this problem, but at high torque transference can be significant enough to cause lock up, preventing the shaft from sliding as needed.

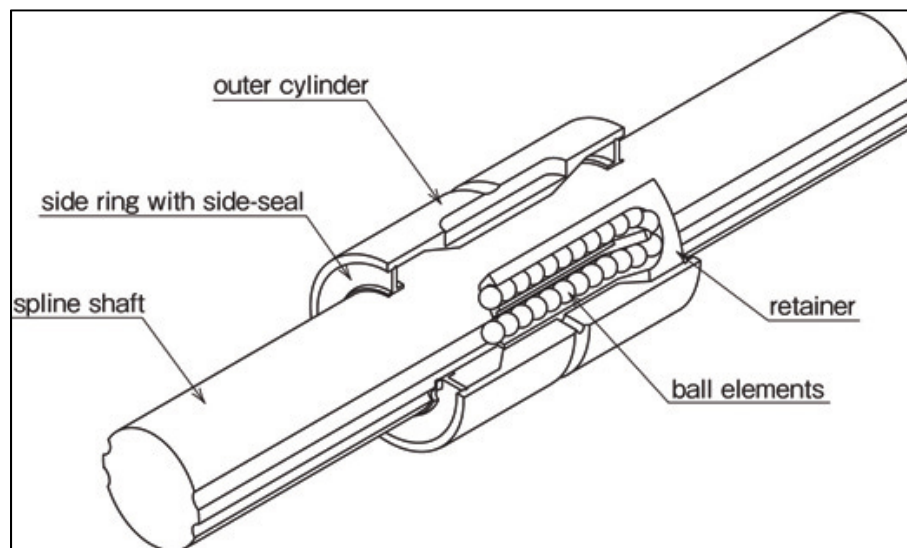


Figure 13: Ball Spline

Figure 13 shown above is that of the ball spline. The operational function is identical to that of a straight spline, however does not incorporate sliding friction. The ball spline uses many ball bearings situated within an outer cylinder that roll within longitudinal grooves on the spline shaft. Unfortunately, in order to transfer high amounts of torque using this type of bearing requires very large ball bearings which results in a very large outside diameter of both the spline shaft and outer cylinder.

Other investigation that did not include literature involved the interviews of several industry professionals. One such person that was contacted was Jesse Jaynes at High Angle Driveline in Paradise, CA. In this interview the current designs and their downfalls were discussed. It was Jesse's recommendation that an Rzeppa joint was maintained for the outer joint, and possibly a single universal joint utilized for the inner joint. Upon further analysis it was ruled that due to the high articulation angles and torque experienced by the HMT400 that a single universal joint not be utilized as premature failure could result. Also discussed in this interview were possible alternatives to the boot containing the Rzeppa and Cross Groove joints. Jesse recommended that thermoplastics were not suitable as they have been known to fail in this application, especially when subjected to large amounts of particulate such as sand, clay and dirt. The thermoplastic is great for withstanding the heat produced by the joint, but was not capable of withstanding the abrasiveness of particulates on the outside of the boot. It was suggested that a dual boot design be investigated, which incorporates a rubber boot interior for withstanding the heat of the joint, and an exterior boot made from leather to prevent particulate and large debris from damaging the interior boot.

Another industry professional that was contacted was Matt Craddock at Brakes Inc. in Raleigh, NC. His expertise was in the area of custom Dual Cardan joint shafts. Although a specific Dual Cardan joint laid along the lower range of our necessary torque requirement, he advised that this joint has been successfully implemented in vehicles capable of producing higher power ratings than the HMT400.

1.4. Personnel



Eric Boros – Company Contact, Weldor

Eric Boros of Chapel Hill, NC is currently completing the last year of his undergraduate double major in mechanical and electrical engineering here at NCSU. He plans to attend graduate school and hopes to eventually start his own company. Eric's professional experience includes internships at SpaceDev and Applied Research Associates as well as a year spent as an undergraduate research assistant in the Mechanical and Aerospace Engineering Department.



Ryan Soukup – Professor Contact, Shop Fabricator

Ryan is from Boone, NC and is set to graduate in the fall of 2012 with a Bachelor's Degree in Mechanical Engineering. His relevant work experience includes an internship as a product engineer at Teledyne Continental Motors, where he worked on a valve train design project for internal combustion engines of prop-driven aircraft. More recently, he has filled a co-op position at BMW US Factory as a supplier quality associate for glass- and painted hang-on parts. As a hobby, Ryan works on automobiles, and has gained experience installing engines, suspension components, and various other automotive systems.



Caitlin Winnike – Treasurer, Shop Fabricator

Caitlin, who is from Chapel Hill, NC, is graduating this December and will continue at NCSU to pursue her Master's Degree in Mechanical Engineering. Over the summers she has interned for GE Aviation working on the quality team of the turbine blade manufacturing floor, Volvo executing complete vehicle simulations for braking distance, and Schlumberger performing fatigue analysis on drill collar design variations. Caitlin also has international experience studying abroad in Italy.

Design and Delivery of HMT Half-Shaft Prototype



Tyler Hull – Weldor

Tyler, of Charlotte, NC, is planning on graduating in May of 2012 with a Major in Mechanical Engineering and a Minor in Business at NC State. Tyler's professional experience includes working for a Civil/Environmental Engineering firm here in Raleigh, RSG Engineers. This past summer he completed his third rotation as a manufacturing engineer with Daimler Trucks North America at the Freightliner Manufacturing plant in Cleveland, NC. His job responsibilities centered on the streamlining of manufacturing processes which involved many principles of Lean Manufacturing. As a hobby, Tyler works on automobiles, and has gained experience rebuilding and installing engines, transmissions and transfer cases, as well as other drivetrain, suspension and electrical components.



Brandon Novak – Machinist

Brandon Novak of Vestal, NY is graduating this December and has a job offer from Static Control Components in Sanford, North Carolina, either in automation or as a systems engineer. Last summer he interned at Static working in the systems engineering department, designing in house open-cell polyurethane foams for use in laser printer cartridges. Brandon also spent a summer working for KNS Brakes located locally in Cary, North Carolina recommending and designing brake system upgrades and replacements for customers with cars ranging from Subarus to Lotus's. Brandon is also an automotive enthusiast who enjoys working on cars in his free time. Such work entailing fuel systems, turbochargers, intercoolers, porting work on intake and exhaust manifolds, brake and suspension systems, and tuning his car. Also, he is proficient at the instillation, wiring and tuning of aftermarket stereo systems as well as the fiberglass fabrication of speaker enclosures.

1.5. Design Methodology

In order to produce and test a prototype of the optimal design solution chosen, the design methodology in Figure 14 will be implemented.

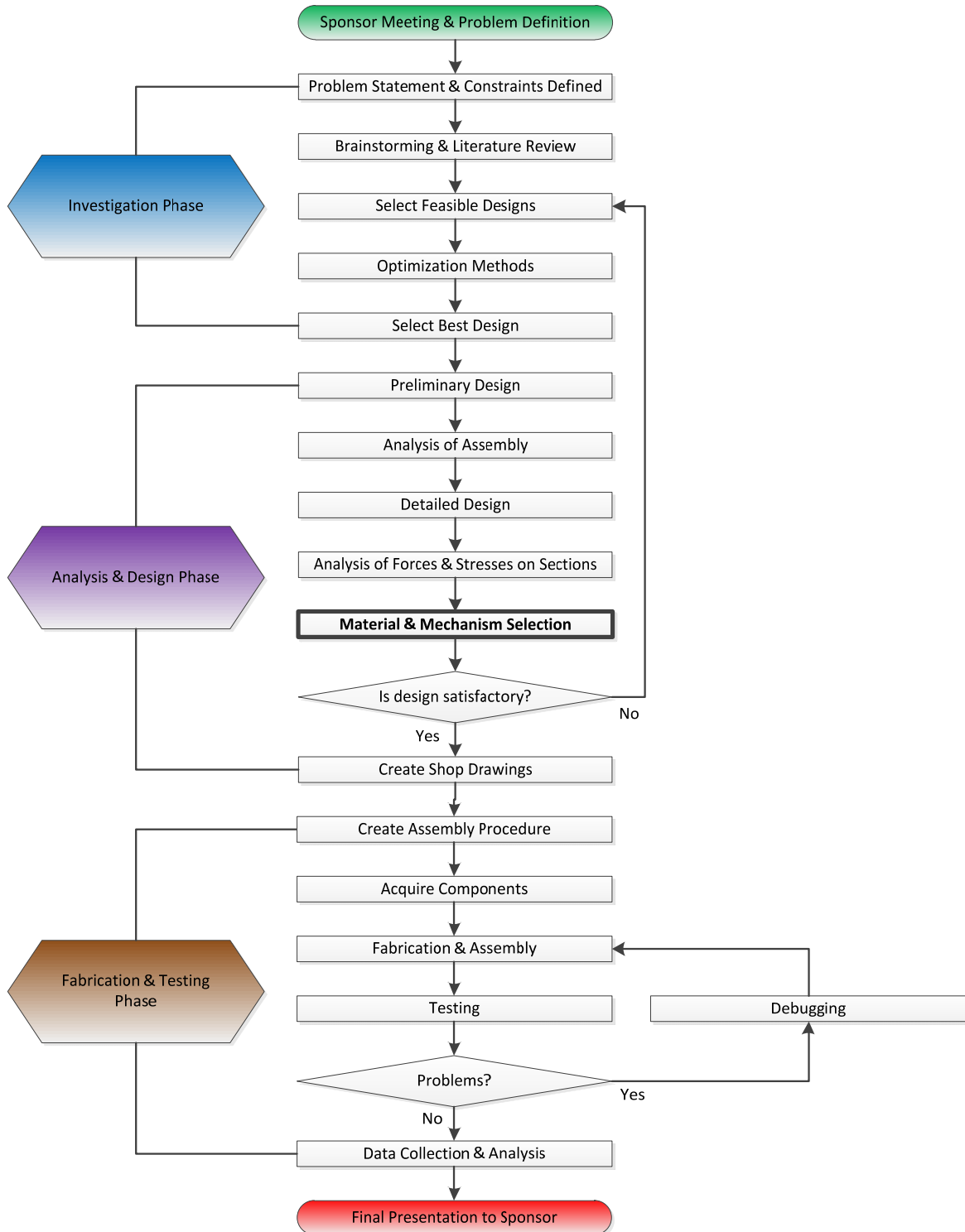


Figure 14: Design Methodology Flowchart

Sponsor Meeting and Problem Definition: The sponsor will present an initial overview and background of the product along with their problems, components and any other pertinent information regarding the objective of the project. The group will also take a trip to Fort Bragg to gather more information about the vehicle.

Investigation Phase

Problem Statement & Constraints Defined: Using the information from the sponsor presentation and trip, the class will formulate the problem statement and constraints that every group would accept.

Brainstorming & Literature Review: The group will complete research and a literature review of joints, boots, and other technologies to come up with unique design solutions to the problem the HMT 400/600 is experiencing.

Select Feasible Designs: Out of all of the designs considered, preliminary calculations will be performed to determine which ones are feasible.

Optimization Methods: Criteria will be selected to rate the feasible designs and determine which one is the optimal design.

Select Best Design: The optimal design will be chosen as the preliminary design for the group.

Analysis & Design Phase

Preliminary Design: A preliminary design will be constructed of the optimal design, which includes a basic assembly and preliminary calculations.

Analysis of Assembly: Preliminary calculations will be completed on the assembly to determine dimensions and details.

Detailed Design: All dimensions and details will be computed to construct a detailed design of the final solution proposed.

Analysis of Forces & Stresses on Sections: Calculations will be run on the whole assembly and the parts to calculate the forces and stresses each section of the design will experience.

Material & Mechanism Selection: Using the calculated stresses on the sections, the materials and mechanisms required to withstand them will be initially selected. Availability, cost, machinability and safety will be analyzed as shown below in **Figure 15** to determine if the selection is acceptable or not. If not, and there are no acceptable alternatives, the design will have to be changed by going back to the feasible designs stage.

Design and Delivery of HMT Half-Shaft Prototype

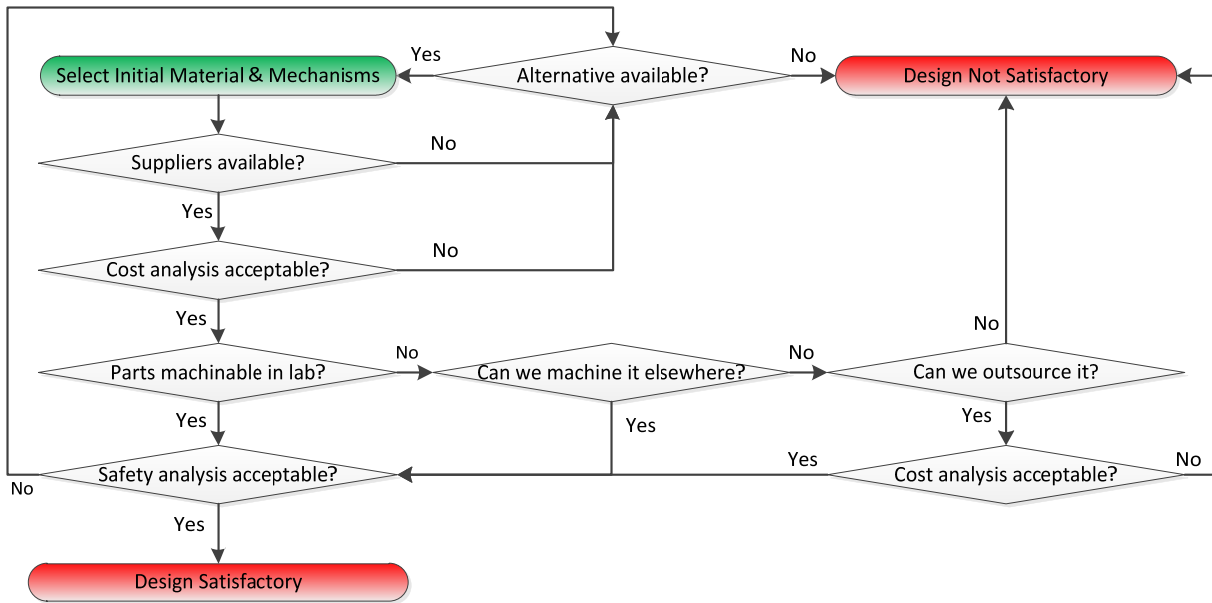


Figure 15: Material and Mechanism Selection Flowchart

Create Shop Drawings: Knowing which components need to be purchased, shop drawings will be completed of the parts the group will fabricate in-house and of the whole assembly.

Fabrication & Testing Phase

Create Assembly Procedure: The group will create the assembly procedure that details the steps for manufacturing the prototype.

Acquire Components: The necessary materials and mechanisms will be purchased by the suppliers chosen in the material and mechanism selection step.

Fabrication & Assembly: The components of the half-shaft prototype will be constructed and assembled according to the assembly procedure.

Testing: The prototype will be tested in the test rig to determine the operating torque values with vertical articulation and steering angles at high and low speeds.

Debugging: The prototype will be debugged to fix any major and minor problems with the design.

Data Collection & Analysis: Data will be collected and analyzed according to the test procedure to determine the performance of the prototype.

Final Presentation to Sponsor: The group will conclude with a formal presentation and demonstration of the design to the USASOC representatives.

1.6. Schedule

Investigation Phase

The primary phase in the overall problem solution process, beginning in late August and ending in September, is the Investigation Phase. This time will be spent creating a problem statement and required constraints, as well as brainstorming possible solutions to the problem, creating feasibility designs, and presenting two possible solutions in a feasibility study. All of the feasible designs will be analyzed through optimization methods to choose the solution that most suitably fits the needs of the problem statement.

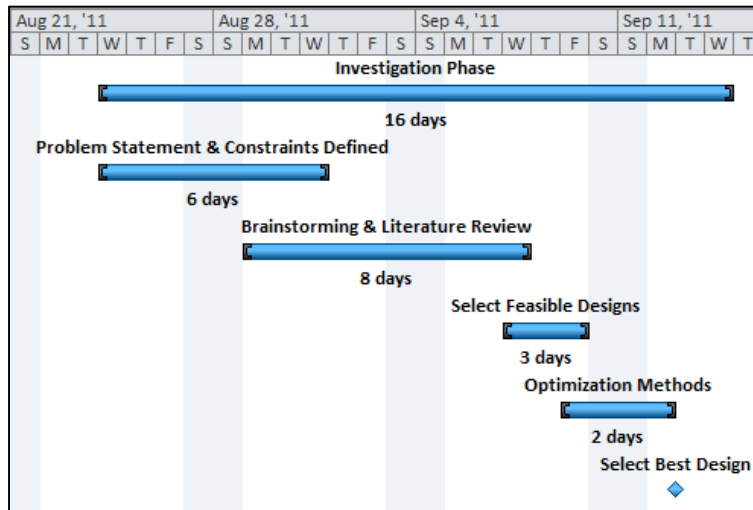


Figure 16: Investigation Phase Gantt Chart

Design and Analysis Phase

The second phase in the problem solution process is the Design and Analysis Phase. This phase will begin in September and follow through into October. During the design phase, a preliminary design will be constructed using the selected design from the previous phase. This is followed by an analysis of the assembly and the different sections to calculate the forces and stresses. With this information, a more detailed design and shop drawings will be created. The stresses found from the analysis will also enable the selection of materials and mechanisms.

Design and Delivery of HMT Half-Shaft Prototype

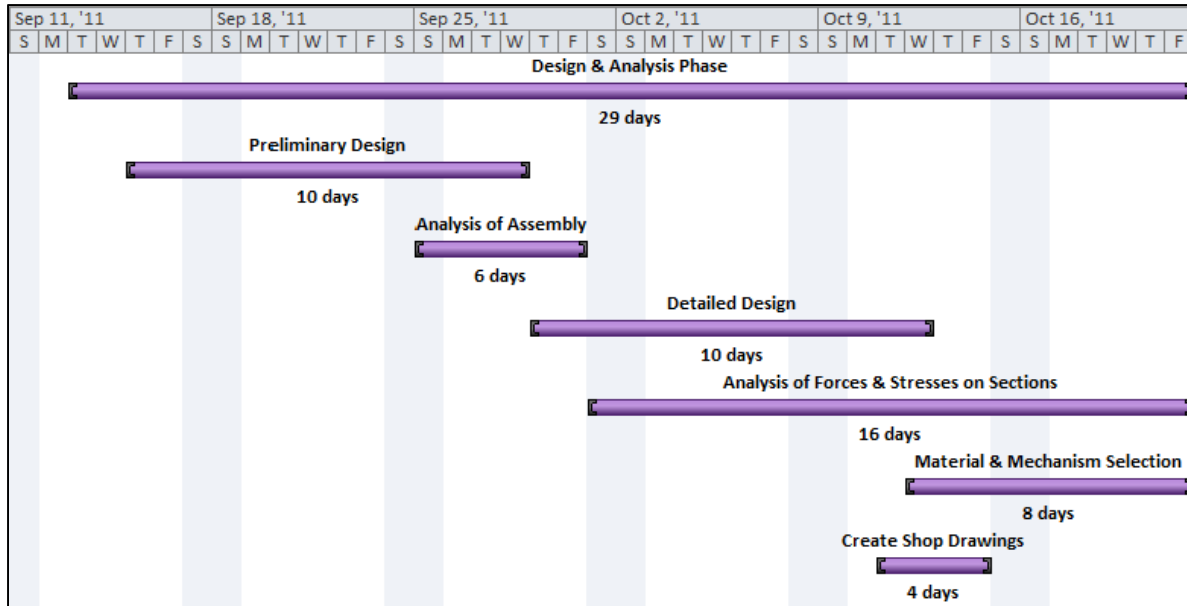


Figure 17: Design and Analysis Phase Gantt Chart

Fabrication and Testing Phase

The final phase of the problem solution process will begin in mid-October and follow through into late-November. During this final stage an outline for the remaining tasks will be constructed which will include the procurement of materials and components, the machining and welding of the components, the necessary assembly required and testing. If necessary, debugging will take place after preliminary testing. Finally, with the completed prototype, data will be collected and analyzed to be presented to the sponsor.

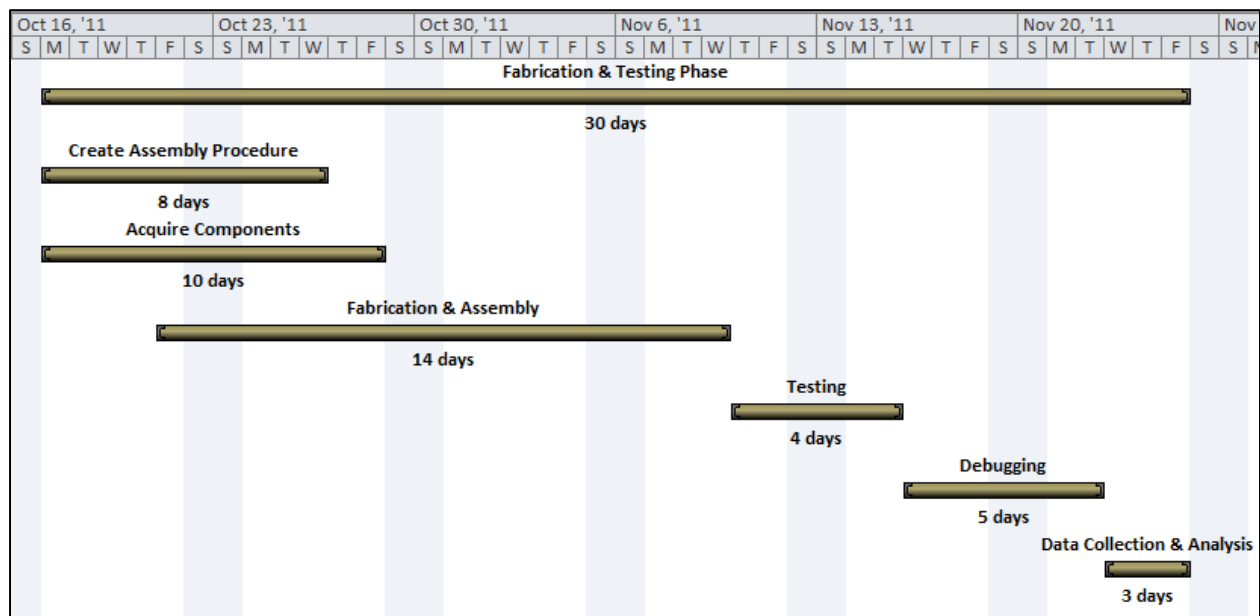


Figure 18: Fabrication and Testing Phase Gantt Chart

2. Modeling and Simulation

2.1. Description of Design

The key feature of the new Cornay® half-shaft design is the use of twin Cornay® joints to account for steering and ride height articulation. These joints are effectively replacements for the current inner cross groove plunging Rzeppa and the outer 6-ball Rzeppa. This half-shaft assembly will be comprised of the following components, seen in Figure 19 below.

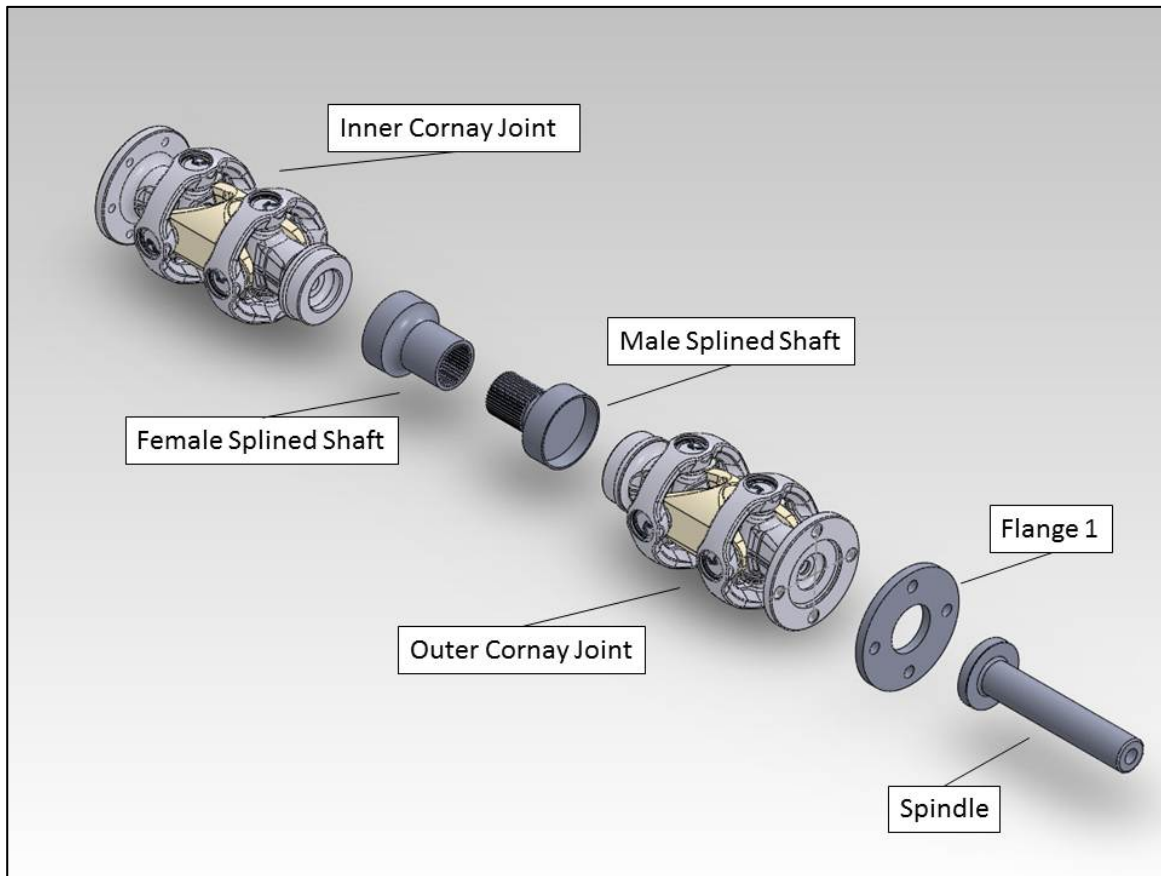


Figure 19: Half Shaft Assembly, Exploded View

Inner Cornay® Joint

As stated, the inner joint of this design will be a Cornay® CVX-50, shown in Figure 4 of Section 1.3. This particular joint includes a centering mechanism that ensures true constant velocity at all angles of specified articulation, in this joint's case, that articulation is 50°. The centering mechanism featured in this joint is shown below in Figure 20. The centering mechanism creates true constant velocity in a few ways. The centering mechanism does not move laterally in order to split the angle of articulation amongst the two shafts by use of the cam design, labeled as components 102 and 103 in Figure 20. The centering mechanism uses rotation of these cams to transmit equal angles of the bisecting plane. This allows the centering mechanism to remain in the bisecting angle planes of the two joint halves causing the joint to operate at true constant velocity. In addition to providing true constant velocity at

all angles up to the joint's maximum misalignment capability the centering mechanism allows the joint to be self-aligning and self-supporting by utilizing end support bearings, components 145 and 106 in Figure 20, for the input and output shafts. Eliminating lateral movement of the centering mechanism allows the concentration of mass of the coupling yokes to be moved closer to the center of rotation thereby reducing inertia excitation (vibration) in the joint.

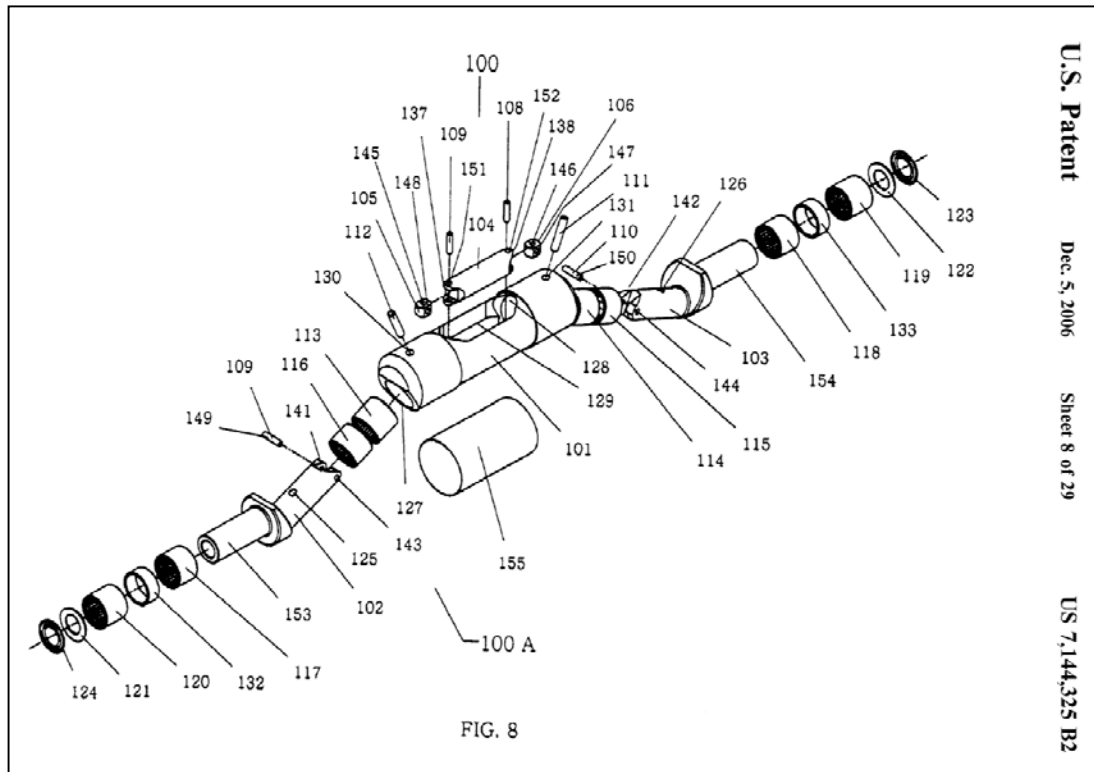


Figure 20: Cornay® Joint Centering Mechanism, Exploded View

The inner Cornay® joint seen in Figure 19 is attached directly to the output of the HMT Supacat's transfer case. This is possible through the joint's input flange bolt pattern, which is drilled to match that of the transfer case, shown below in Figure 21. The use of this component allows for the transmission of over 3000 Nm of torque at angles of up to 50° at truly constant velocity. This torque is transferred by the joint to the female splined shaft through a welded connection around the joint output displayed in the lower right corner of Figure 22.

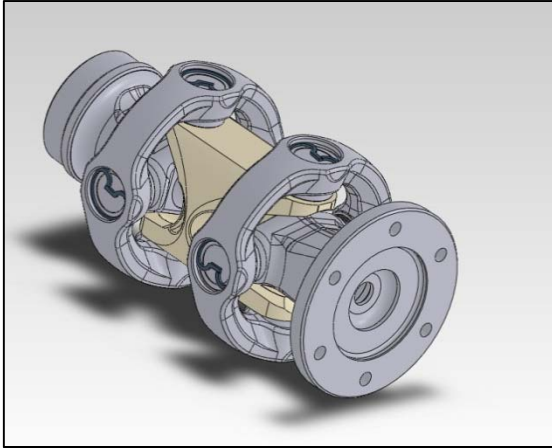


Figure 21: Inner Cornay® Joint - Input View

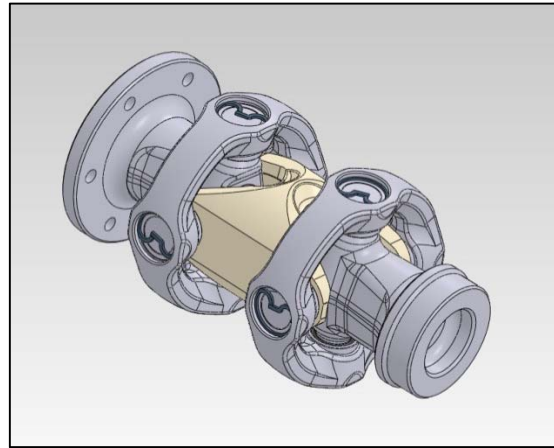


Figure 22: Inner Cornay® Joint - Output View

Female Splined Shaft

The output shaft of the inner Cornay® joint is welded to a female splined shaft shown below in Figure 23 and Figure 24. The splined segment of this shaft is sufficiently long to accommodate the 7 mm axial plunge introduced by HMT's pushrod suspension design. Due to this axial motion, this spline will be lubricated, with the lubricant contained through the use of a boot or dust cap. The shaft is bored to fit over the Cornay® joint's output as in Figure 23. It is fixed to the inner Cornay® joint by a weld around the outside of its larger diameter.

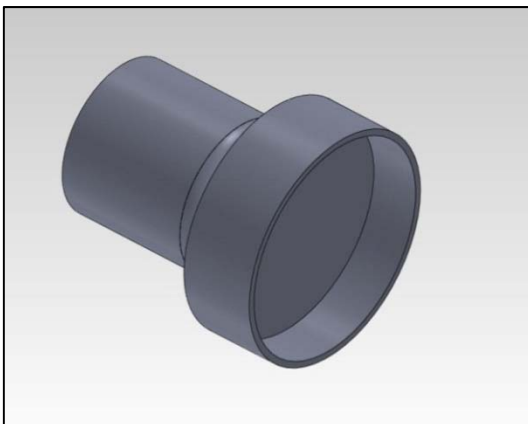


Figure 23: Female Splined Shaft - Input View

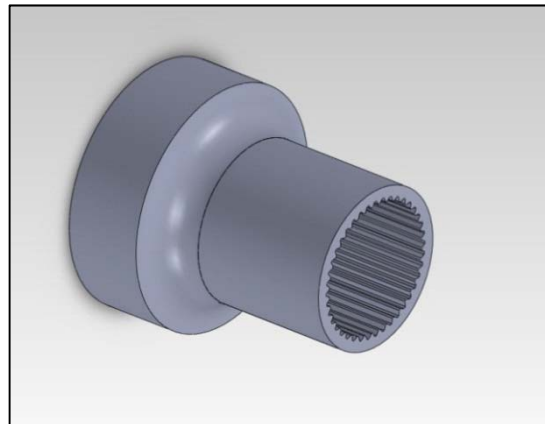


Figure 24: Female Splined Shaft - Output View

Male Splined Shaft

Transferring power from the female splined shaft is a male splined shaft, pictured below in Figure 25 and Figure 26. The characteristics of this shaft [splined length, diameter, number of splines, etc.] were selected to suit the torque and plunge needs of the assembly. This male shaft is welded to the outer joint, mirroring the connection of the inner joint and female shaft.

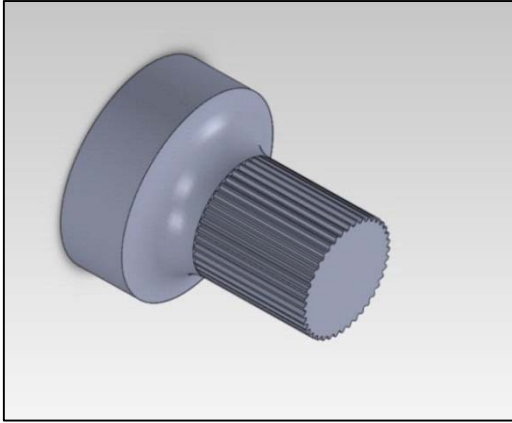


Figure 25: Male Splined Shaft - Input View

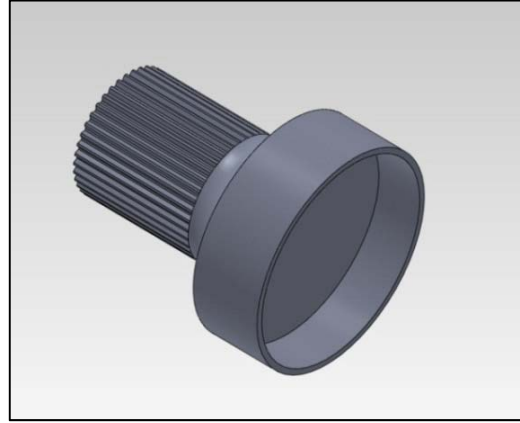


Figure 26: Male Splined Shaft - Output View

The splined shaft for the production half-shaft should be ball-splines. Conventional involute splines introduce excessive axial force due to high friction. Ball-splines translate this sliding friction to rolling friction, greatly reducing the axial forces on the half-shaft assembly.

Outer Cornay® Joint

The outer joint is the same model as the one used for the inner joint. This joint inherently accounts for more articulation than the inner shaft, including any steering angle. The output flange of this outer joint differs from that of the inner joint in its bolt pattern, which is a 4 bolt pattern with a larger radius as in Figure 28 below.

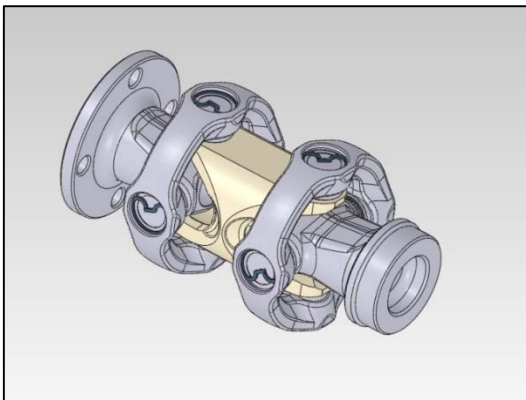


Figure 27: Outer Cornay® Joint - Input View

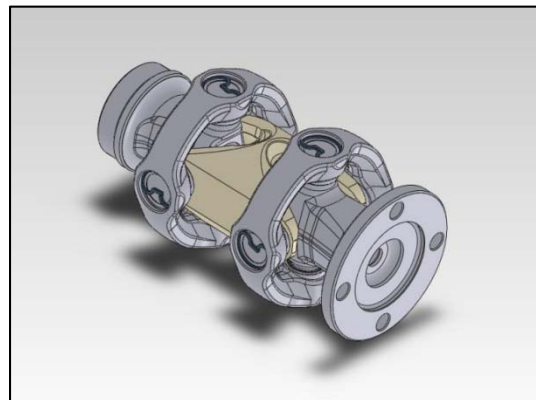


Figure 28: Outer Cornay® Joint - Output View

Flange 1/Spindle

The outer flange is bolted to the output end of the outer joint and a spindle welded to its output face. As with the inner flange, the dimensions and materials of this flange, viewed in Figure 29, and associated hardware and weld pattern were selected for suitable use in this application. The spindle in Figure 30 contains a tapped and threaded hole matching the retaining bolt seen in the hub of the HMT 400/600 and the test rig. The advantage of the flanged connection of this design over a spindle welded to the outer joint output is ease of

assembly. Flange 1 contains threaded holes for the bolts, which eliminates the need for nuts as well as simplifying the installation and removal of the shaft, which currently requires wheel and hub removal.

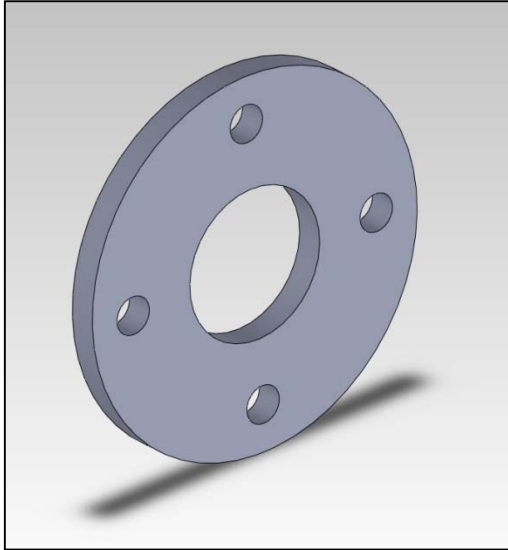


Figure 29: Flange 1

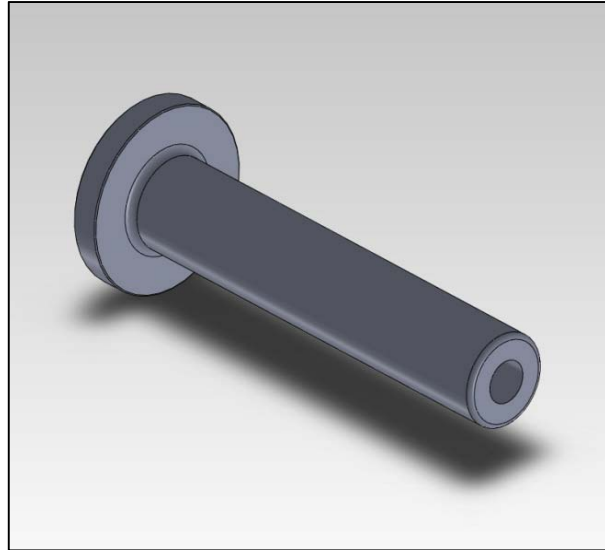


Figure 30: Spindle

This assembly was developed with two features in mind: robustness and ease of maintenance. The bootless Cornay® design eliminates the current boot failure issue, increasing assembly robustness. The flanged and splined connections are developed to make half-shaft install and removal a process that does not require hub removal. Between the increased robustness and ease of removal, maintenance on this design should be less demanding than current maintenance.

Design Differences between Prototype and Production Design

There are a few design details distinguishing the production design from the prototype. Material differences exist for the flange, spindle, and splined shafts. Also, the spindle of the production design is splined to match the splines of the hub internals.

2.2. Analysis

The following section will cover the analysis of the entire half-shaft as well as the individual components while utilizing free body diagrams (FBDs). This process is essential to verifying the overall strength of the half-shaft and the individual components. If there exist any weaknesses in the original design, this will help to locate and diagnose those weaknesses to ensure that the half-shaft will perform as required.

Full Half-Shaft Analysis

When in operation, the half-shaft is subject to certain forces and moments. In order to be able to accurately size parts and to appropriately choose materials, the forces which the half-

shaft experiences must be computed. To find these forces, the free-body diagram (FBD) for each component will be examined starting at the wheel of the Supacat and ending with the inner joint. All components will be assumed to be rigid-bodies in this analysis. Also, as a simplification, the half-shaft will be considered to be rotating only; the wheel of the Supacat will be considered to be spinning only with no suspension travel or steering motion.

The wheel is considered first. Shown in Figure 31 is the FBD for one wheel of the Supacat. The term “wheel” includes the steering knuckle and the hub in addition to the tire; Figure 31 only shows the tire of this assembly. There are three points where forces act on the wheel: the contact point with the ground, the connection with the suspension, and the connection with the half-shaft. The suspension consists of both an upper and a lower A-arm in addition to a tie-rod, but this system is simplified in the FBD as a single point of contact at which the combined suspension reaction is applied.

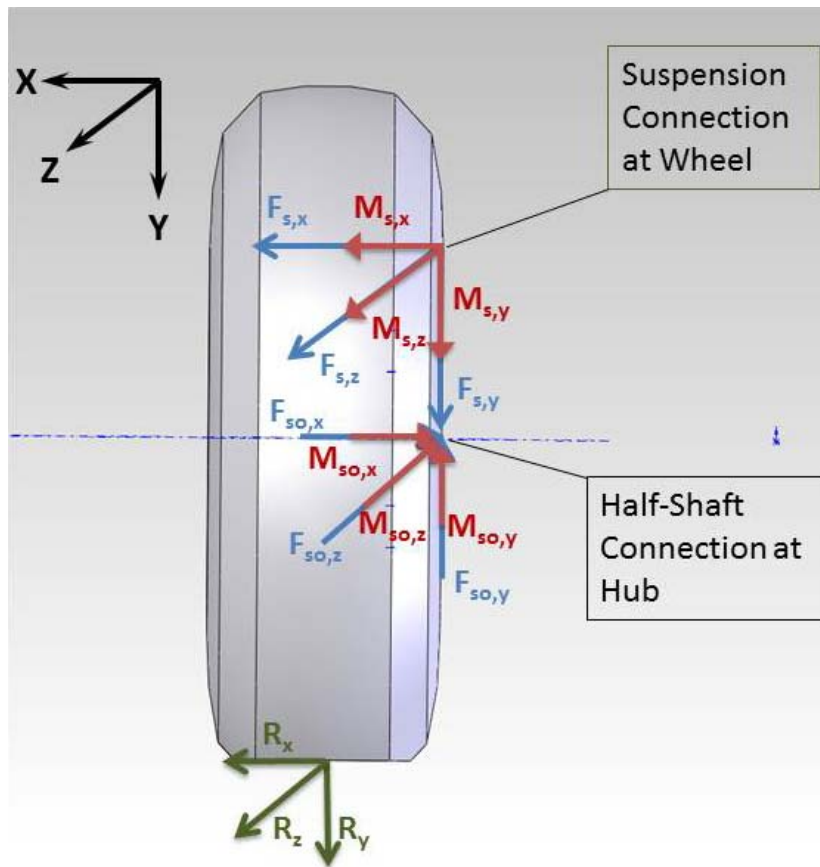


Figure 31: Entire Half-Shaft Assembly with Reactions At Input and Output

A glance at Figure 31 will show that this is an over-determined system. In order to avoid extraordinarily complex strain analysis on the wheel, an assumption about the load distribution between the suspension and the half-shaft must be made. It will be assumed that the resultant of the reaction, \mathbf{R} , except any moment about the wheel's x-axis, is completely and solely supported by the suspension.

$$R_x = F_{so,x}$$

$$R_y = F_{so,y}$$

$$R_z = F_{so,z}$$

The forces and moments contributing to the reactions \mathbf{F}_{ho} and \mathbf{M}_{ho} are those generated by the action of the half-shaft during torque transmission. These include the transmitted torque and whatever forces are generated by the acceleration, both angular and linear, of the half-shaft itself. As a result of this assumption, the rest of the half-shaft assembly must be analyzed to obtain \mathbf{F}_{ho} and \mathbf{M}_{ho} .

Considering the half-shaft as a whole, Figure 32 shows it removed from the suspension with the forces and moments exerted by the hub and the transfer case displayed. Notice where the forces act. At the transfer case, while the joint flange is a bolted connection, the individual forces and moments at each bolt are combined into a single reaction force, \mathbf{F}_{ijf} , and a single reaction moment, \mathbf{M}_{ijf} , at the flange's center. At the hub side, the forces are placed where the supporting bearing inside the hub is relative to the spindle.

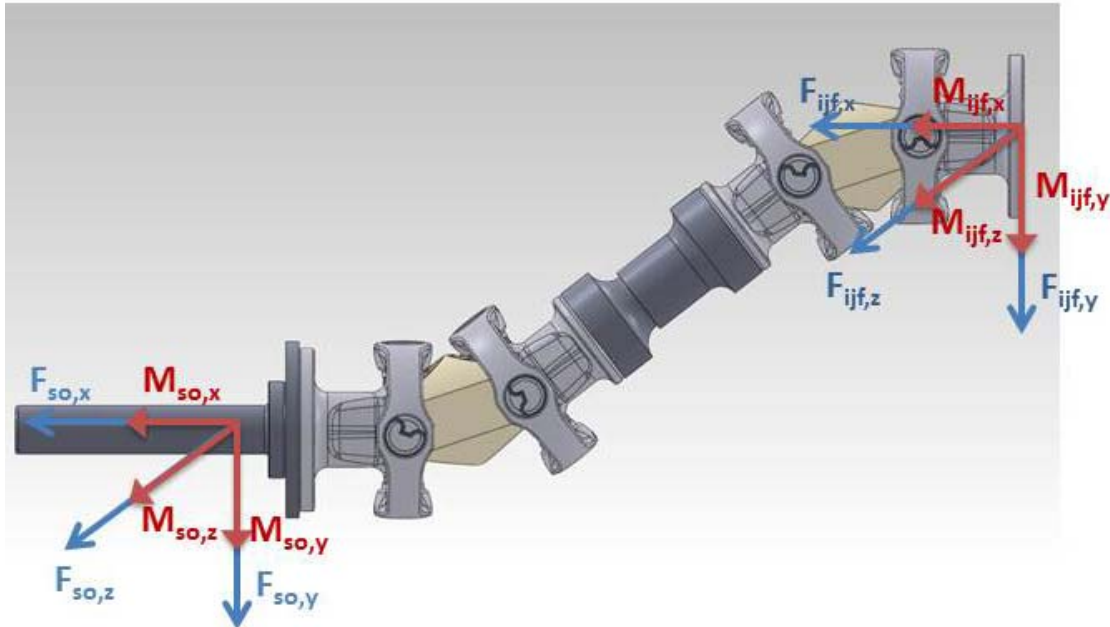


Figure 32: FBD of Supacat Wheel

The part of the half-shaft attached to the bearing inside the wheel is the flanged spindle that is attached to the inner-joint (Figure 33).

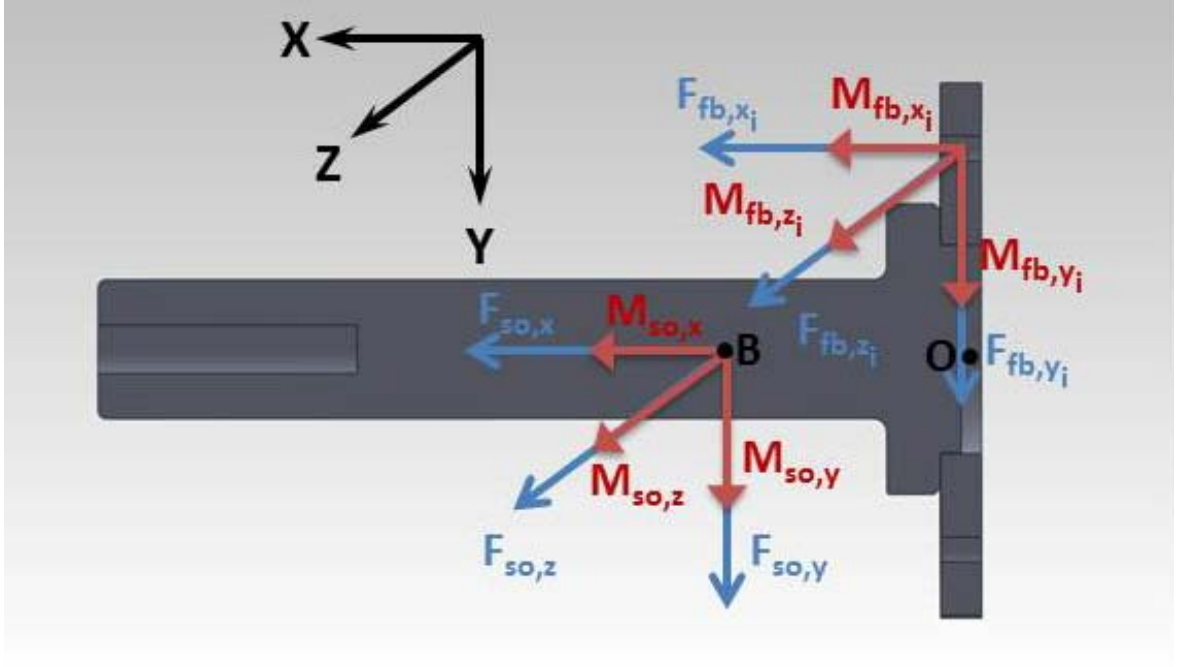


Figure 33: FBD of Flange/Spindle

Applying Newton's Laws to the spindle results in the following equations. All accelerations are set to zero since the spindle does not move linearly.

$$\sum F_X = \sum_{i=1}^4 F_{fb,x_i} + F_{so,x} = ma_{X,spindle} \quad (1)$$

$$\sum F_Y = \sum_{i=1}^4 F_{fb,y_i} + F_{so,y} = ma_{Y,spindle} \quad (2)$$

$$\sum F_Z = \sum_{i=1}^4 F_{fb,z_i} + F_{so,z} = ma_{Z,spindle} \quad (3)$$

The spindle is stationary linearly, so all accelerations can be set to zero.

$$\sum_{i=1}^4 F_{fb,x_i} = -F_{so,x} \quad (4)$$

$$\sum_{i=1}^4 F_{fb,y_i} = -F_{so,y} \quad (5)$$

$$\sum_{i=1}^4 F_{fb,z_i} = -F_{so,z} \quad (6)$$

The moment equations can be written similarly. The torques are summed around the point O at the center of the flange as shown in Figure 33. Forces that act through this point or that have a zero length moment arm are ignored.

$$\sum M_X = \sum_{i=1}^4 M_{fb,x_i} + M_{so,x} + \sum_{i=1}^4 (r_{b_i/O,z} F_{fb,y_i} + r_{b_i/O,y} F_{fb,z_i}) = J_{xx,O} \alpha_{X,spindle} \quad (7)$$

$$\sum M_Y = \sum_{i=1}^4 M_{fb,y_i} + M_{so,y} + \sum_{i=1}^4 (r_{b_i/O,z} F_{fb,x_i}) + r_{B/O,x} F_{so,z} = J_{yy,O} \alpha_{Y,spindle} \quad (8)$$

$$\sum M_Z = \sum_{i=1}^4 M_{fb,z_i} + M_{so,z} + \sum_{i=1}^4 (r_{b_i/O,y} F_{fb,x_i}) + r_{B/O,x} F_{so,y} = J_{zz,O} \alpha_{Z,spindle} \quad (9)$$

There are a couple of simplifying observations that can be made. First, the bolts are assumed to not support any moments. Secondly, the spindle is constrained to rotate only in the x-axis; thus all angular accelerations except α_X will be zero. Using these assumptions and solving for the forces on the bolts, the equations can be simplified.

$$\sum_{i=1}^4 (r_{b_i/O,z} F_{fb,y_i} + r_{b_i/O,y} F_{fb,z_i}) = J_{xx,O} \alpha_{X,spindle} - M_{so,x} \quad (10)$$

$$\sum_{i=1}^4 (r_{b_i/O,z} F_{fb,x_i}) = -M_{so,y} - r_{B/O,x} F_{so,z} \quad (11)$$

$$\sum_{i=1}^4 (r_{b_i/O,y} F_{fb,x_i}) = -M_{so,z} - r_{B/O,x} F_{so,y} \quad (12)$$

Now that the forces and moments on the spindle and flange have been related, the outer joint (Figure 34) can be analyzed. Note that the coordinate axes have been drawn shifted away from their true locations to preserve the clarity of the picture.

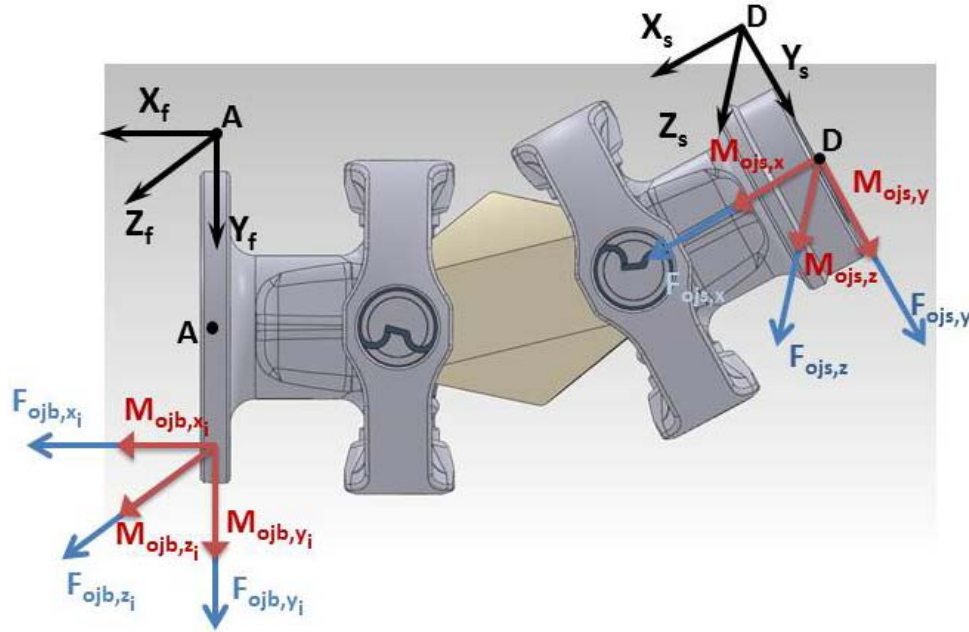


Figure 34: FBD of Outer Cornay® Joint

Since the internal mechanisms of the joint are overly complex for a detailed analysis, an abstraction must be found that relates the forces and moments on the shaft end to those on the flange end of the joint. In order to do this, each of the load components applied at the shaft end are considered individually; after accounting for how the joint articulates under the considered load, the reaction at the flange is determined. Note that this construct assumes that the maximum operating articulation angle of the joint is never reached.

A force, $\mathbf{F} = (F_{ojs,y}, F_{ojs,z})$, in the y-z plane of the shaft, (Z_s, Y_s) , is considered first. Since such a force would cause the joint to articulate, only a negligible portion would be transmitted through the joint to the flange. As a result, the reaction at the flange due to a force in the shaft's y-z plane will be considered to be zero. A similar situation occurs when a moment $\mathbf{M} = (M_{ojs,y}, M_{ojs,z})$ is applied. Since the joint does not support such a load but rather articulates under it, the resultant reaction at the flange will be considered to be zero.

While no reaction at the flange will be considered to be generated by any loading in the shaft's y-z plane, the same cannot be said about an axial force, $F_{ojs,x}$, or an axial moment, $M_{ojs,x}$. The joint's primary function is to transmit an axial torque, and, as a result, any applied axial moment at the shaft of the joint will be assumed to be fully and solely transmitted to the flange as an axial moment.

For an axial force, however, only a portion of the force will be seen at the flange. To determine how much of the applied axial force, $F_{ojs,x}$, is transmitted to the flange, the joint is approximated as a four bar linkage with one unpinned end (Figure 35).

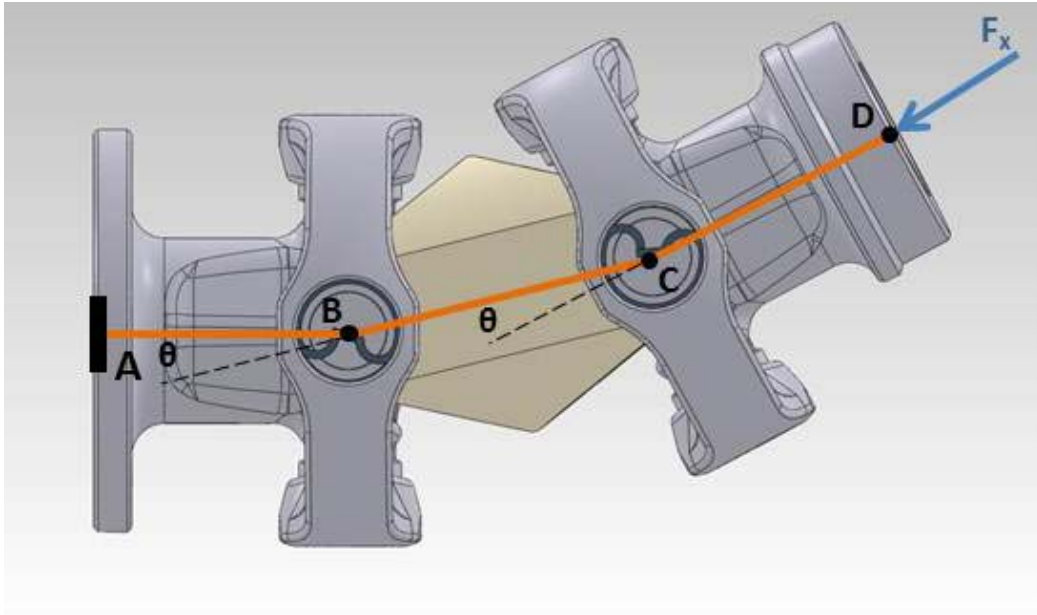


Figure 35: Four-Bar Linkage Approximation of Outer Joint

By computing the component of the force, F_x , that is transmitted along the length of each bar in the linkage ABCD, the reaction at A can be found. The first step is to move the point of contact of F_x to the point C (Figure 36). The two systems are equivalent since F_x is oriented along the length of CD.

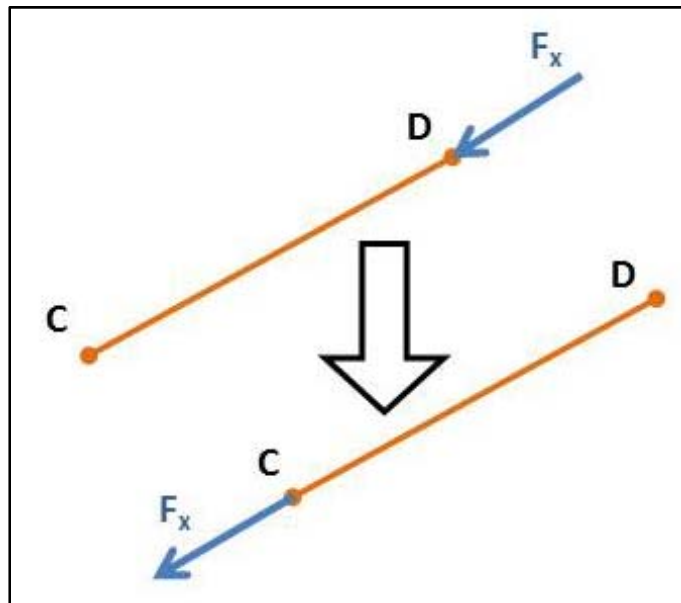


Figure 36: Transformation of Axial Force from D to C

Now, noting that the force is acting on C the bar BC can be drawn. F_x can also be split into components parallel and perpendicular to BC's length (Figure 37).

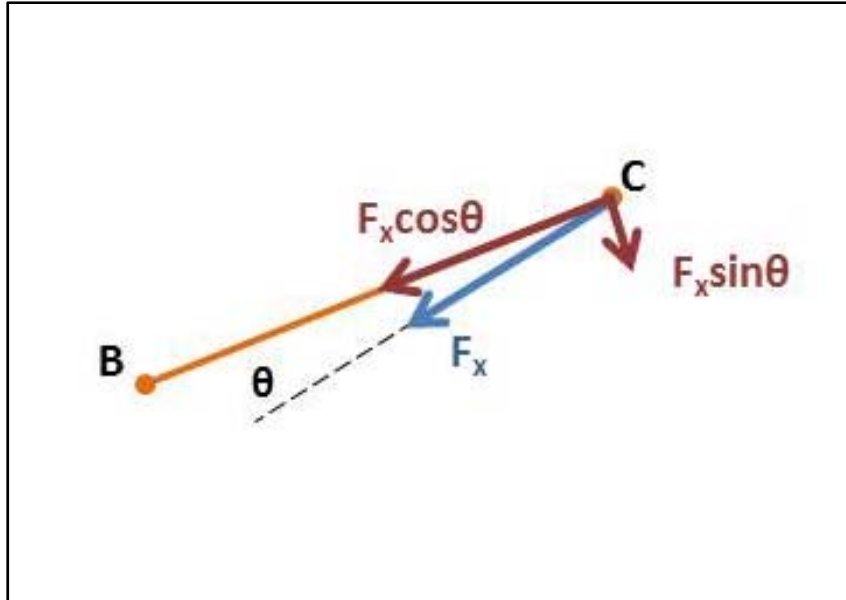


Figure 37: Decomposition of F_x into Parallel and Perpendicular Components

The angle θ is half of the joint angle; for example, if the joint were to be articulated at a 30° angle (in Figure 35 this would be manifested as an angle of 30° between the links AB and CD) then θ would equal 15° .

The same force transformation process can be carried out on this middle link (Figure 38) as well; the difference will be that instead of placing F_x at B, the parallel component $F_x \cos \theta$ will be moved.

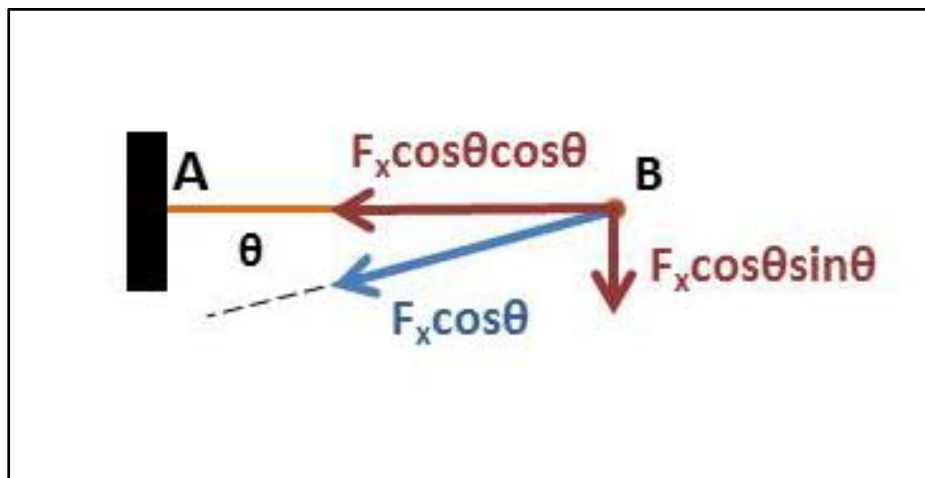


Figure 38: Decomposition of $F_x \cos \theta$ into Parallel and Perpendicular Components

Note that the perpendicular components of the forces were assumed to go entirely to rotating the different links rather than being transmitted to the adjacent one. While these perpendicular forces could be analyzed in the same manner as the parallel components, due

to the fact that the perpendicular components are multiplied by a $\sin\theta$ factor with θ being a small angle, they were deemed to be negligible.

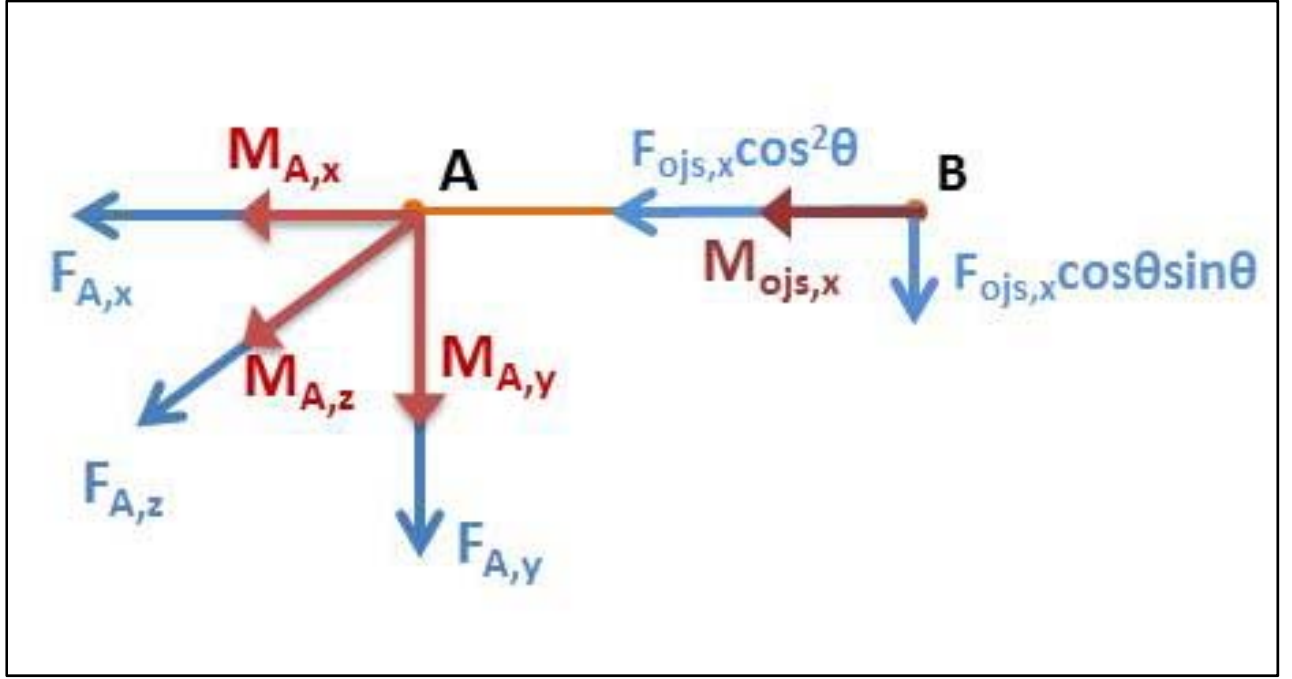


Figure 39: FBD of Link AB

Taking into account this analysis of the axial loading in addition to all of the other considerations noted above, the manner in which loading applied at the shaft side of joint will be transmitted to the flange of the joint can be determined. As discussed before, the only loadings at all transmitted to the flange will be the axial force, $F_{ojs,x}$, and the axial torque, $M_{ojs,x}$. Figure 39 shows the final link AB with the total loading and the corresponding reactions at A.

Summing forces, the relations between reactions and loadings can be written. Due to mechanical constraints, all accelerations were set to zero when applying Newton's Law.

$$F_{A,x} = -F_{ojs,x} \cos^2 \theta \quad (13)$$

$$F_{A,y} = -F_{ojs,x} \cos \theta \sin \theta \quad (14)$$

$$F_{A,z} = 0 \quad (15)$$

Executing a similar procedure for the moments, the reaction \mathbf{M}_A can be computed by summing the moments about point A. Note that the reaction moment's x-component, $\mathbf{M}_{A,x}$, is not computed using Newton's Law; it is written as equal and opposite to the applied torque due to the assumption of perfect torque transmission of the joint. All other components of

the reaction moment are computed using Newton's Law with angular accelerations equal to zero due to mechanical constraints.

$$M_{A,x} = -M_{ojs,x} \quad (15)$$

$$M_{A,y} = 0 \quad (16)$$

$$M_{A,z} = r_{A/B,x} \cdot F_{ojs,x} \cos \theta \sin \theta \quad (17)$$

While the reactions at A have been solved for, in reality, these are distributed among all the bolts on the joint's flange. These forces and moments will now be solved for in terms of \mathbf{F}_A and \mathbf{M}_A . Summing the forces on the flange, the results are as follows.

$$\sum F_X = \sum_{i=1}^4 F_{obj,x_i} + F_{A,x} = m_{oj} a_X = 0 \quad (17)$$

$$\sum F_Y = \sum_{i=1}^4 F_{obj,y_i} + F_{A,y} = m_{oj} a_Y = 0 \quad (18)$$

$$\sum F_Z = \sum_{i=1}^4 F_{obj,z_i} + F_{A,z} = m_{oj} a_Z = 0 \quad (19)$$

Since the flange of the joint is constrained to only rotate in the x-axis, all other angular accelerations were set to zero. The moments about point A can then be summed.

$$\sum M_X = M_{A,x} + \sum_{i=1}^4 r_{b_i/A,y} \cdot F_{obj,z_i} + \sum_{i=1}^4 r_{b_i/A,z} \cdot F_{obj,y_i} + \sum_{i=1}^4 M_{obj,x_i} = J_{XX,A} \alpha_X \quad (20)$$

$$\sum M_Y = M_{A,y} + \sum_{i=1}^4 r_{b_i/A,z} \cdot F_{obj,x_i} + \sum_{i=1}^4 M_{obj,y_i} = J_{YY,A} \alpha_Y = 0 \quad (21)$$

$$\sum M_Z = M_{A,z} + \sum_{i=1}^4 r_{b_i/A,y} \cdot F_{obj,x_i} + \sum_{i=1}^4 M_{obj,z_i} = J_{ZZ,A} \alpha_Z = 0 \quad (22)$$

Applying the assumption about the bolts being unable to sustain any moments and substituting the values of the reactions at A into the above equations, the relation between the shaft loading and the flange bolt loading can finally be obtained.

$$\sum_{i=1}^4 F_{obj,x_i} = -F_{A,x} = -(-F_{ojs,x} \cos^2 \theta) = F_{ojs,x} \cos^2 \theta \quad (23)$$

$$\sum_{i=1}^4 F_{obj,y_i} = -F_{A,y} = -(-F_{ojs,x} \cos \theta \sin \theta) = F_{ojs,x} \cos \theta \sin \theta \quad (24)$$

$$\sum_{i=1}^4 F_{obj,z_i} = -F_{A,z} = 0 \quad (25)$$

$$\sum_{i=1}^4 r_{b_i/A,y} \cdot F_{obj,z_i} + \sum_{i=1}^4 r_{b_i/A,z} \cdot F_{obj,y_i} = J_{XX,A} \alpha_X - M_{A,x} = J_{XX,A} \alpha_X + M_{obj,x} \quad (26)$$

$$\sum_{i=1}^4 r_{b_i/A,z} \cdot F_{obj,x_i} = -M_{A,y} = 0 \quad (27)$$

$$\sum_{i=1}^4 r_{b_i/A,y} \cdot F_{obj,x_i} = -M_{A,z} = -r_{A/B,x} \cdot F_{obj,x} \cos \theta \sin \theta \quad (28)$$

Note that these equations were derived for an instance where the articulation angle, 2θ , of the joint was in the x-y plane of both the shaft and the flange. This is a particular case of joint orientation and is not a general representation.

The next part of the half-shaft to be analyzed is the male spline (Figure 40). Since this analysis is considering the half-shaft to be only rotating with no suspension induced motion, the loadings on the welded side of the spline and the toothed side of the spline will be equal and opposite with the exception of the axial torque which will contain an inertial force term accounting for axial acceleration of the half-shaft.

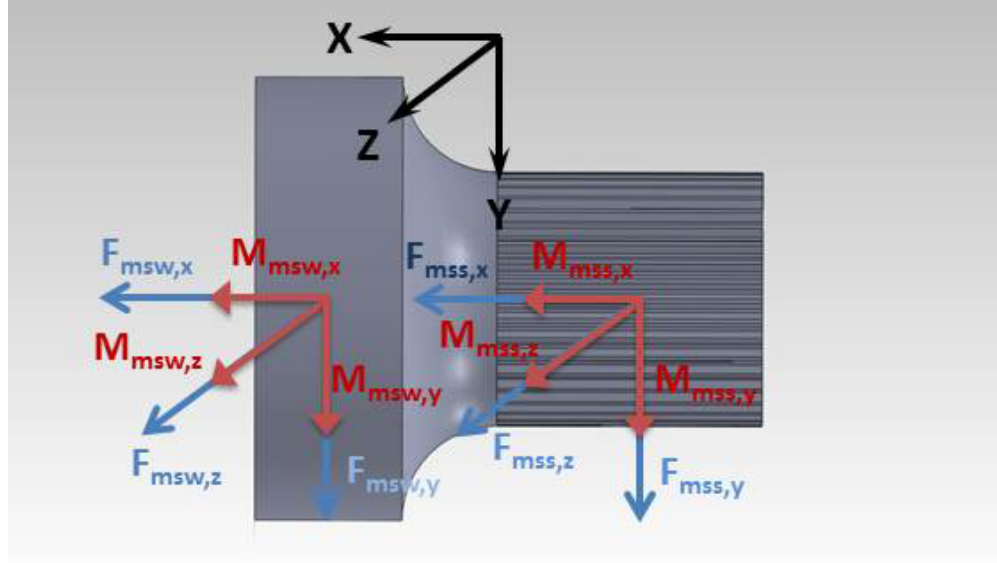


Figure 40: FBD of Male Spline

$$F_{msw,x} = -F_{mss,x} \quad (29)$$

$$F_{msw,y} = -F_{mss,y} \quad (30)$$

$$F_{msw,z} = -F_{mss,z} \quad (31)$$

$$M_{msw,x} = J_{XX}\alpha_X - M_{mss,x} \quad (32)$$

$$M_{msw,y} = -M_{mss,y} \quad (33)$$

$$M_{msw,z} = -M_{mss,z} \quad (34)$$

A similar set of equations can be written for the female spline (Figure 41).

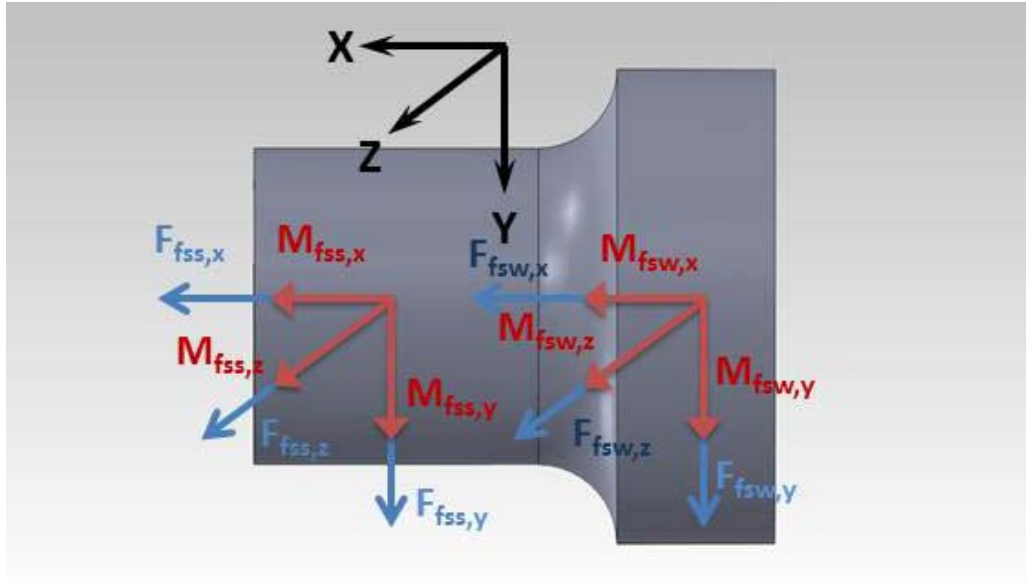


Figure 41: FBD of Female Spline

$$F_{fsw,x} = -F_{fss,x} \quad (35)$$

$$F_{fsw,y} = -F_{fss,y} \quad (36)$$

$$F_{fsw,z} = -F_{fss,z} \quad (37)$$

$$M_{fsw,x} = J_{XX}\alpha_X - M_{fss,x} \quad (38)$$

$$M_{fsw,y} = -M_{fss,y} \quad (39)$$

$$M_{fsw,z} = -M_{fss,z} \quad (40)$$

Finally, the construct developed for the outer Cornay® joint can be applied to the inner joint (Figure 42). For this joint, the output torque, T , from the transfer case is applied.

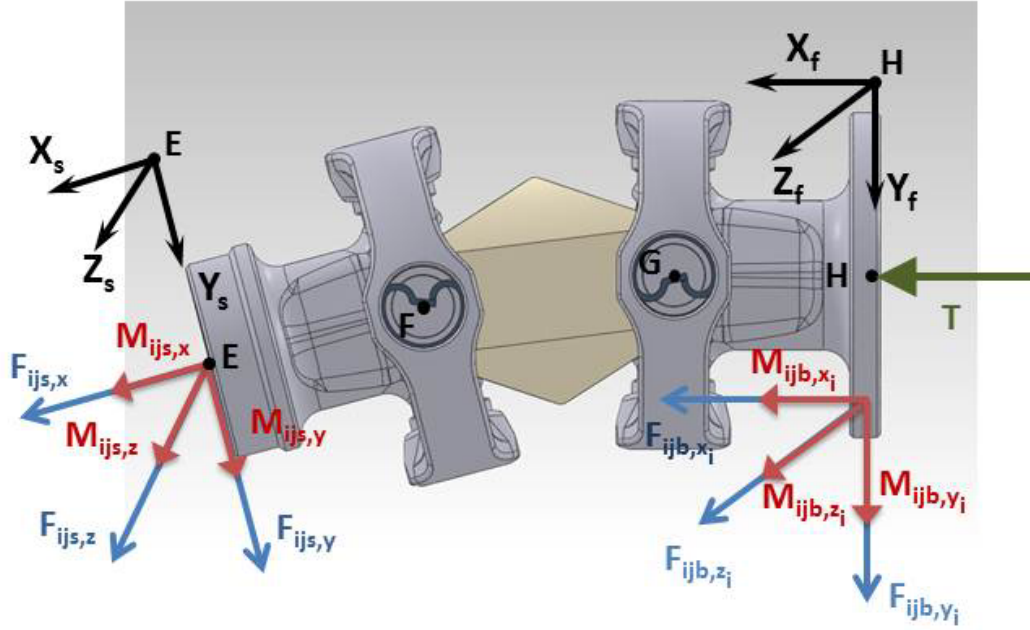


Figure 42: FBD of the Inner Cornay® Joint

$$\sum_{i=1}^6 F_{ijb,x_i} = F_{ijs,x} \cos^2 \theta \quad (41)$$

$$\sum_{i=1}^6 F_{ijb,y_i} = F_{ijs,x} \cos \theta \sin \theta \quad (42)$$

$$\sum_{i=1}^6 F_{ijb,z_i} = 0 \quad (43)$$

$$\sum_{i=1}^6 r_{b_i/H,y} \cdot F_{ijb,z_i} + \sum_{i=1}^6 r_{b_i/H,z} \cdot F_{ijb,y_i} = J_{XX,H} \alpha_X + M_{ijs,x} - T \quad (44)$$

$$\sum_{i=1}^6 r_{b_i/H,z} \cdot F_{ijb,x_i} = 0 \quad (45)$$

$$\sum_{i=1}^6 r_{b_i/H,y} \cdot F_{ijb,x_i} = -r_{H/G,x} \cdot F_{ijs,x} \cos \theta \sin \theta \quad (46)$$

Using the equations (1-46) developed in this section on the full half-shaft analysis, the loads on each component can be computed and then used for stress analysis, part sizing, and material selection.

Male/Female Spline Analysis

The male and female spline are used to account for the 7mm of lateral plunge due to suspension travel as well as make removing the half-shaft, without removing the hub assembly, easier by allowing the shaft to collapse. Shown below in Figure 43 is the torque that is applied to the male spline.

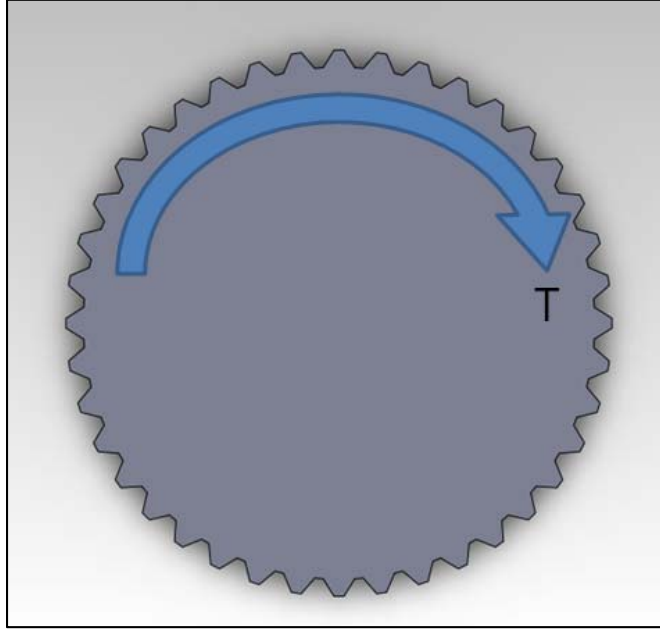


Figure 43: Male Spline Analysis

In order to determine the shear stress seen by the male splined section of the axle due to the torque provided, the following equation is implemented, where T is the torque given in lb·in, K_a is the spline application factor determined by the type of loading placed on the spline D_{re} is the major diameter of the spline and K_f is the fatigue life factor of the spline. The spline factor K_a was determined using a chart from the Machinery's Handbook. Knowing the power source that creates the torque placed on the spline to be an internal combustion engine and assuming a light shock type of load a factor of 2.2 was determined. K_f was determined using a chart out of the same book, assuming 1,000 full torque unidirectional cycles, it was concluded to be 1.8.

$$S_s = \frac{16TK_a}{\pi D_{re}^3 K_f} \quad (47)$$

After utilizing the above equation with a major diameter of 1.61 inches (chosen to be near the current half-shaft diameter), the total shear stress placed on the male spline was ~59 kpsi.

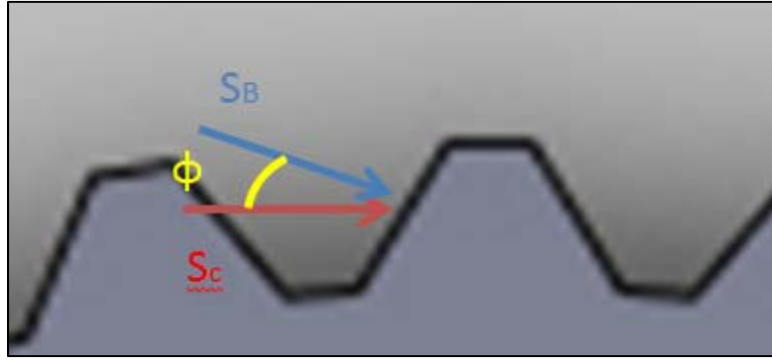


Figure 44: Bursting and Compressive Stress on Spline

In addition to the shear stress due to torque, the compressive stress (S_C) on the teeth as well as the radial bursting stress (S_B), shown above in Figure 44 were calculated using the following equations from [Machinery's], where T is torque, K_a and K_f are the same factors as above, D is the outer diameter, N is the number of teeth, L_e is the effective length or contact length of the spline, h is the depth of teeth engagement and K_m is assumed to be one due to the fact the splines are fixed.

$$S_C = \frac{2TK_mK_a}{9DNL_e h K_f} \quad (48)$$

$$S_B = \frac{T \tan(\phi)}{\pi D t_w L} \quad (49)$$

Φ is used in the calculation above for bursting stress in the radial direction, S_B acts perpendicular to the face of the teeth, ϕ is equal to 30° , t_w is the wall thickness of the internal spline and L is the full length of the spline. After computing these values, the greatest stress seen by the male spline will be the compressive stress which is just over 60 kpsi. On the other hand, the bursting stress is relatively low and is just over 20 kpsi.

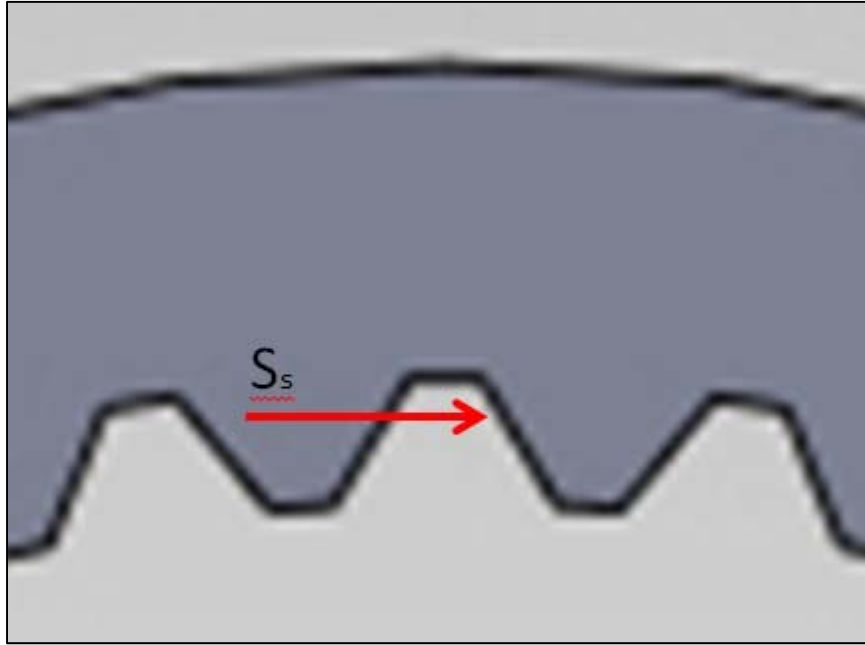


Figure 45: Shear Stress on Female Spline

Shown above in Figure 45 is the direction that the shear stress acts at the pitch diameter of the female spline due to the torque. The following equation is very similar to the shear stress of the male spline due to torque, but the thickness of the female spline must be accounted for by the difference taken between the major diameter (D_{re}) and the minor diameter (D_h) of the female spline.

$$S_s = \frac{16TD_{re}K_a}{\pi(D_{re}^4 - D_h^4)K_f} \quad (50)$$

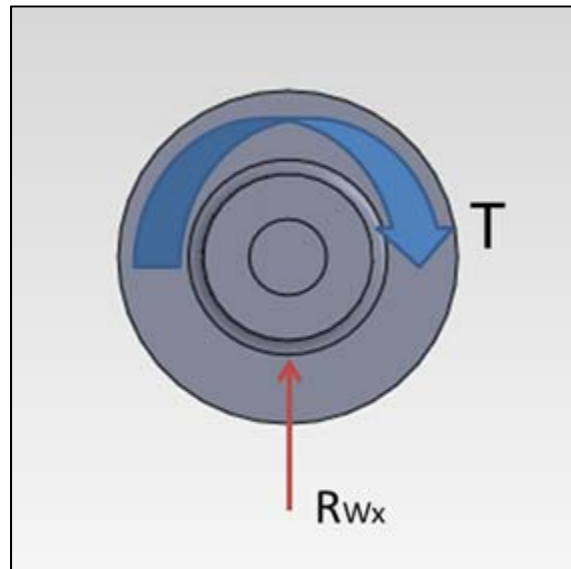
After applying this equation to the torque given as well as the spline parameters the shear stress seen by the female spline is actually less than the male, at a value of 55 kpsi. There are no lateral forces seen within the spline because the lateral motion is taken up by the spline. After reviewing the analysis of the splines, it is clear that the compressive stress on the spline teeth will indeed be the greatest stress and the splines should be designed to accommodate this stress, as well as the material they will be comprised of. Therefore the splines should be made of AISI 8620 steel due to its welding characteristics, machinability and its ability to withstand the stresses created by the torque. The particular characteristics of both the male and female splines are listed in Table 1 below and the material properties of 8620 steel are listed in Section 4.1 later in the report.

Table 1: Male and Female Spline Dimensions

Number of Teeth (N)	40
Female Outer Diameter (D_{oi})	2.00 in.
Major Inner Diameter (D_{re})	1.61 in.
Major Outer Diameter (D_{ri})	1.72 in.
Pitch Diameter (D)	1.67 in.

Spindle Analysis

The shear stress acting on the spindle must also be determined for material selection of the shaft. Shown below in Figure 46 are the force and torque acting on the spindle. The reaction force is placed on the shaft by the bearing in the hub due to the shaft's weight (R_{wx}); this force is very minor in comparison to the torque applied therefore it is negligible for material selection and analysis purposes.

**Figure 46: Shear Stress on Spindle**

To determine the shear stress on a circular, solid shaft the following equation is used:

$$\tau = \frac{rT}{J}, J = \frac{\pi}{2}r^4 \quad (51)$$

Where R is the radius of the shaft, J is the polar moment of inertia and T is the torque given. The shear stress seen by the spindle is calculated to be ~48 kpsi. This is marginally smaller

than the shear stress seen on the splines, therefore the same material can be used, AISI 8620 steel, for the spindle. The parameters of this particular material are listed in Section 4.1 later in the report.

Bolted Connection Analysis

As seen in Figure 19, a bolted connection allows torque transfer from the transfer case to the inner Cornay® joint. An additional bolted connection fixes the outer joint to Flange 1. The following is an analysis of these bolted connections. Note that pictorial representations shown depict Flange 1. The inner bolted connection was analyzed in an identical manner, eliminating the need for detailed analysis images of this connection.

The half-shaft assembly was designed for a maximum torque of “T”. Because torque is conserved across the entire assembly, Flange 1 is subject to torque “T” as seen below.

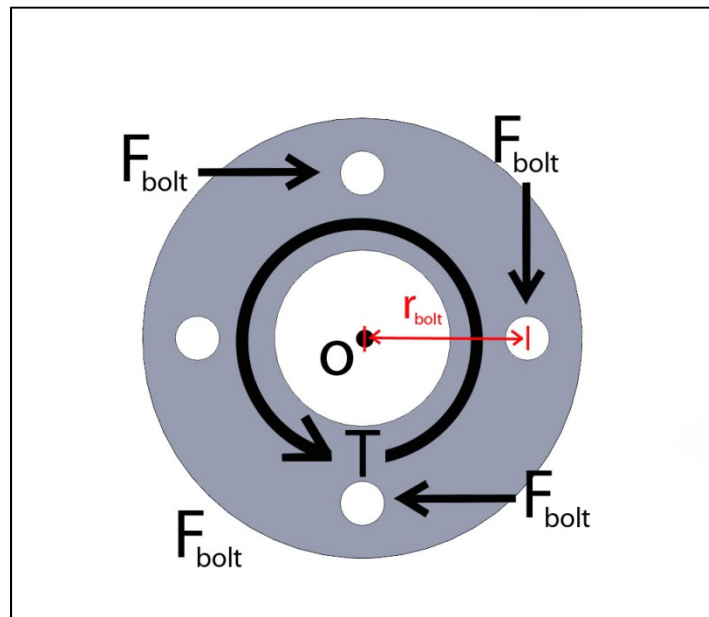


Figure 47: Flange 1 F.B.D.

For the static condition, with the assembly subject to max torque “T”, the sum of the moments about point “o” in Figure 47 is analyzed as follows:

$$\Sigma M_0 = 0 \rightarrow T + (n_{bolts})(F_{bolt}) = 0 \rightarrow |T| = |(n_{bolts})(F_{bolt})| \quad (52)$$

Shear Loading of Bolts:

This applied torque results in forces, denoted “ F_{bolt} ”, across the cross-section of each of the bolts fixing the members, as seen in Figure 47 above.

These forces can be calculated by the following equation:

$$F_{bolt} = \frac{T}{(r_{bolt})(n_{bolts})} \quad (53)$$

Where “ r_{bolt} ” is the distance from flange center to the center of each bolt hole and “ n_{bolts} ” is the number of bolts in the connection. With the bolts in place, each bolt and the flange are loaded as seen below in Figure 48.

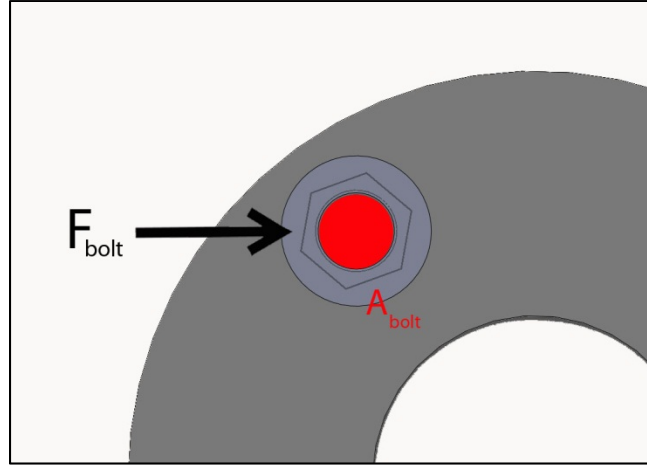


Figure 48: Shear Loading of Bolt

As seen above, “ F_{bolt} ” causes a shear stress, τ , across the cross-sectional area of each bolt, calculated as:

$$\tau = \frac{F_{bolt}}{A_{bolt}} \quad (54)$$

Where “ A_{bolt} ” can take on two different values: if the bolt threads do not extend into the shear plane, “ A_{bolt} ” is the major area of the bolt. If they *do* extend into the shear plane, “ A_{bolt} ” becomes the minor area of the bolt.

For both bolted connections, the values of these parameters are found in the following table. Note that these values reflect the 7/16” [x4] bolts selected for the outer connection and the M8 [x6] bolts of the inner connection.

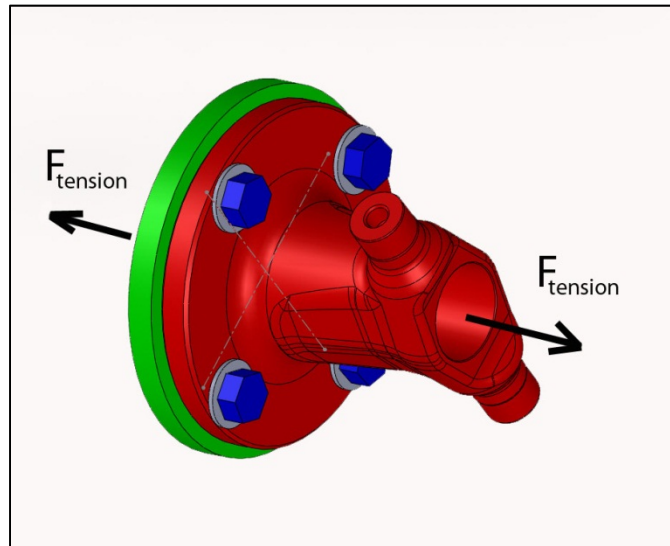
Table 2: Bolts in Shear

Bolted Connection	r _{bolt} [in]	T [in-lbs]	F _{bolt} [lbs]	Portion in shear plane	A _{bolt} [in ²]	τ [ksi]
Inner	1.85	39,838	3,589	Unthreaded:	.0779	46.07
				Threaded:	.0508	70.59
Outer	1.875		5,312	Unthreaded:	.1503	35.33
				Threaded:	.0933	56.93

Based on the above calculations, suitable bolt grades were found. Bolt grades are rated by, among other quantities, minimum yield strength. At the inner connection, Grade 8.8 bolts with a yield strength of 92 ksi were chosen for a safety factor of approximately 1.3. Grade 8 bolts are being used for the outer connection, as they have a shear strength of 130 ksi, giving a safety factor of over 2 for these bolts.

Tensile Loading of Bolts:

These bolts are also subject to tensile loading as seen in Figure 49 below:

**Figure 49: Outer Bolted Connections - Tensile Loading**

In this figure, the outer Cornay® joint has been simplified with only the member to which the bolts are attached visible for ease of illustration. The tensile force, “ F_{tension} ”, is caused by the friction associated with the plunging of the splined shaft when subject to a torque. “ F_{tension} ” is related to the tensile load on each bolt by the following equation, derived from Shigley’s Section 8-7:

$$F_{\text{tension}} = (P)(n_{\text{bolts}}) \quad (55)$$

In this equation, “P” is the maximum tensile load of each of the individual bolts. Due to the repeated plunging nature of the splined shaft, the bolts are subject to fatigue tensile

loading. This loading induces the following alternating stress on each bolt [Shigley's, Eq. 8-39]:

$$\sigma_a = \frac{CP}{2A_t} \quad (56)$$

Where “ A_t ” is the tensile area of the bolt and “ C ”, the fraction of the external load carried by the bolt, is found using the following equations, also found in Shigley's Section 8-7:

$$C = \frac{k_b}{k_b + k_m} \quad (57)$$

In the above equation, “ k_b ” is the stiffness of the bolt, calculated according to Shigley's Eq. 8-17:

$$k_b = \frac{A_d A_t E_{bolt}}{A_d l_t + A_t l_d} \quad (58)$$

In the previous equation, “ A_d ” is the major area of the bolt and l_t and l_d are the threaded and unthreaded lengths of the bolt respectively. Because the washer and joint flange are constructed of similar material, “ k_m ”, the member stiffness is found Shigley's Eq. 8-23 as follows:

$$k_m = AE_{members} d \exp\left(\frac{Bd}{l}\right) \quad (59)$$

“ A ” and “ B ” above are constants found in Table 8-8 of Shigley's. In Equation 59, “ d ” is major bolt diameter, and “ l ” is grip length (in the case of these bolted joints, the combined thicknesses of the washers and Cornay® flanges).

The bolted connection dimensions and parameters pertinent to the above calculations for the outer joint are in the table below:

Table 3: Bolt and Joint Parameters

Bolted Connection	d [in]	A_t [in²]	A_d [in²]	l [in]	l_t [in]	l_d [in]	E_{bolt} [Mpsi]	$E_{members}$ [Mpsi]
Inner:	.3150	.0608	.0779	.529	.984	0	30	30
Outer:	.4375	.1187	.1503	.503	1.000	0	30	30

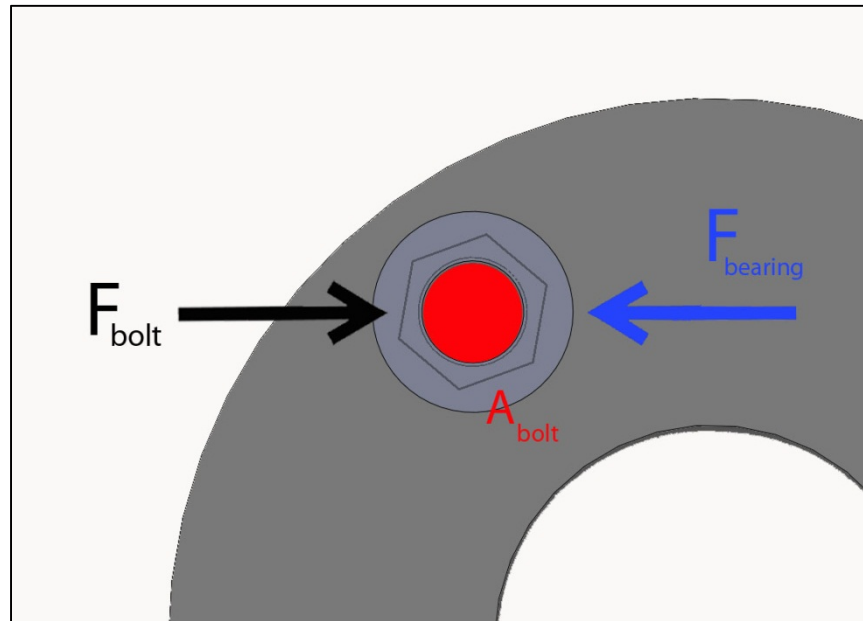
The values in Table 3, the values from Shigley's of $A=.78715$ and $B=.62873$, and the known “ $F_{tension}$ ” (assumed to be 1000 lbs. as a high estimate to ensure robust fastener use) yielded the following:

Table 4: Alternating Stresses on Bolted Connections

Bolted Connection	F_{tension} [lbs]	P [lbs]	k_b [lb/in]	k_m [lb/in]	C	σ_a [psi]
Inner:	1000	166.7	1.854e6	1.103e7	.144	197.3
Outer:		250	3.561e6	1.785e7	.166	175.1

Based on the alternating stresses experienced by the bolts of the inner bolted connection, Grade 8.8 bolt's endurance strength of 18.7 ksi [Shigley's Table 8-17] is beyond adequate in this application. Similarly, at the outer bolted connection, Grade 8 bolts with a maximum endurance strength of 23.2 ksi were deemed suitable for this application.

Bearing Stress on Flange 1:

**Figure 50: Bearing Stress F.B.D.**

As seen in Figure 50, the reaction force of Flange 1 on the bolts inherently induces a bearing stress in the four bolt holes. This reaction force is related to " F_{bolt} " as seen in Equation 60:

$$F_{\text{bolt}} = F_{\text{bearing}} \quad (60)$$

This bearing stress, $\sigma_{bearing}$, becomes:

$$\sigma_{bearing} = \frac{F_{bearing}}{A_{bolt, projected}} = \frac{F_{bearing}}{(d)(h_{flange})} \quad (61)$$

In Equation 61, “ h_{flange} ” is the height of the bolt as seen below in Figure 51:

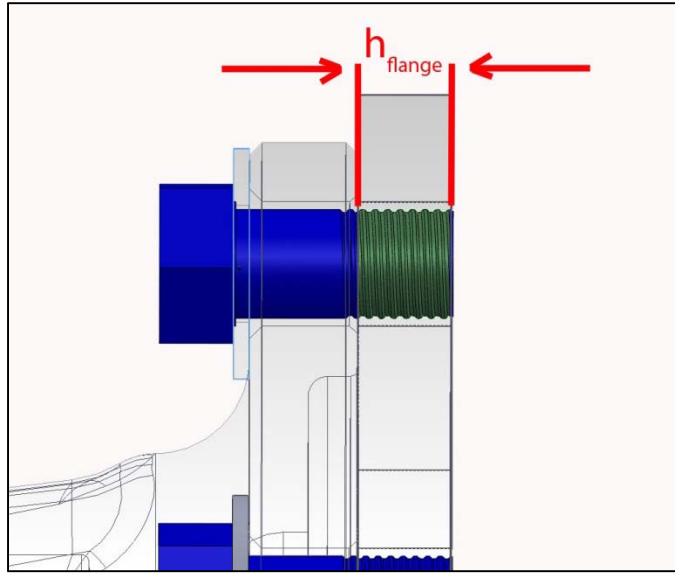


Figure 51: Projected Area of Bearing Stress

In Figure 51 above, the green area is the projected area of the bolt placing a bearing stress on Flange 1.

The resulting bearing stress values, as well as the physical parameters used to derive said stress specific to Flange 1 are tabulated below:

Table 5: Bearing Stress Values

$F_{bearing}$ [lbs]	d [in]	h_{flange} [in]	$\sigma_{bearing}$ [ksi]
5,312	7/16	.372	32.38

The material selected for Flange 1, AISI 8620 steel, is adequately robust for the bearing stress that it is subject to, with a yield strength of approximately 56 ksi. This gives the flange a safety factor of over 1.7 against bearing stress.

Weld Analysis

The proposed design contains a welded joint at the connection of each Cornay® joint and splined shaft. These joints have the same dimensions, and will therefore be fixed by similar welds, analyzed below.

The welds attach the Cornay® joints to the splined shafts as seen in Figure 52:

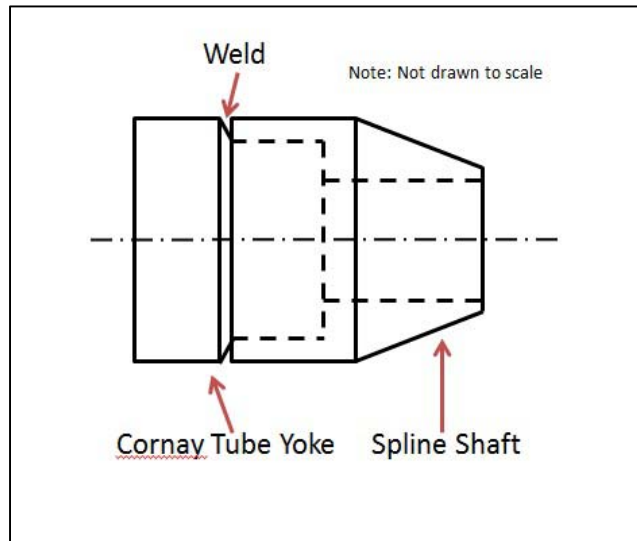


Figure 52: Welded Joint

Generally, welds are subject to primary and secondary shear forces. However, in the case of this welded connection, there is no primary shear. This is the case because the shear force that would be present in the weld is actually taken up by the Cornay® tube yoke as seen below in Figure 53:

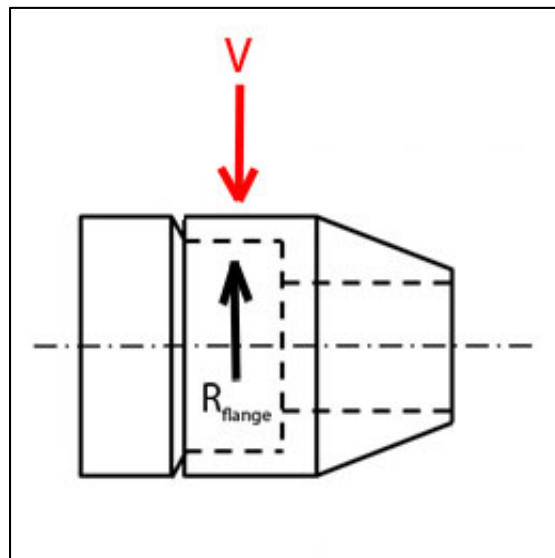


Figure 53: Welded Connection F.B.D.

From the above figure, it is evident that “ R_{flange} ”, the reaction force of the flange on the shear force is equal and opposite, placing no shear force on the weld labeled in Figure 52. Due to

the lack of primary shear, the maximum shear stress in the weld is simplified by the equation below, a variation of Shigley's Eq. 9-5:

$$\tau_{\max} = \tau'' = \frac{Tr}{J} \quad (62)$$

Where “T” is the max torque applied to the weld, “r” is the distance of the point on the weld to the centroid of the weld group, and “J” is the unit second polar moment of area, calculated as follows (for a 45° weld) [Shigley's, Table 9-1]:

$$J = .707hJ_u \quad (63)$$

In the above equation, “h” is the throat size of the weld, which is a design parameter to be determined based on the strength of the weld. For a circular weld group, “J_u”, the unit second polar moment of area is calculated by the equation below.

$$J_u = 2\pi r^3 \quad (64)$$

This assembly is subject to cyclic loading, so weld fatigue must be analyzed. According to Shigley's Table 9-5, a reinforced butt weld like the one being used at this joint has a fatigue stress-concentration factor of 1.2, increasing the effective maximum shear stress in the weld by 20%.

Based on the previous equations, a suitable weld throat and an electrode type were selected. The table below contains the dimensions associated with calculating these parameters. Note that “h”, one of the parameters being solved for, was given a known value. This is because this analysis was iterative, with all iterations performed in Microsoft Office Excel.

Table 6: Weld Dimensions

r [in]	h [in]	J [in³]	J_u [in³]	A [in²]
1.5	.25	3.748	21.205	1.666

Using the above dimensions and equations, the maximum shear stress in the weld was calculated as 15.94 ksi. Introducing a fatigue stress-concentration factor of 1.2, this effectively became 19.13 ksi.

Knowing the maximum stress, the material strength of the weld material was examined. As mentioned, the loading type of this weld is shear. According to Shigley's Table 9-4, the allowable shear stress for a weld in shear is related to the weld's ultimate tensile stress as follows:

$$\tau_{\text{allowable}} = .30S_{ut} \quad (65)$$

Therefore, an E90xx electrode number was chosen, with an ultimate tensile strength of 90 ksi. By the above equation, the allowable shear stress of the weld is 27 ksi. With the allowable and maximum shear stresses known, the safety factor was calculated according to the following equation:

$$n = \frac{\tau_{allowable}}{\tau_{max}} \quad (66)$$

Therefore, this E90xx electrode number weld with a ¼” throat has a fatigue safety factor of 1.41.

2.3. Simulation

Interference Analysis

At this point in the design, the only simulation run on the proposed design has been an interference analysis in SolidWorks. A Cornay® CVX-50 joint model was obtained and then used in a model half-shaft. The model of the Cornay® joint itself is dimensionally identical to the ones found in the prototype design. Also, this joint is rated for a maximum torque of 3700 Nm and for a max articulation angle of 50° which exceed the requirements for the half-shaft design. Once the SolidWorks half-shaft assembly was completed, it was placed in the third axle model provided by the class’s contacts in the USASOC. This whole assembly was then articulated from the bump-stop position (minimum ride height) to the off-road position (maximum ride height). Unfortunately, interference between the half-shaft and the other suspension members was observed. As a result, it was concluded that the Cornay® half-shaft design or HMT 400/600 suspension itself would require modification to fit in the constraining space. The pictures below show the proposed half-shaft design inserted into the suspension model of the Supacat at different ride heights and steering angles.

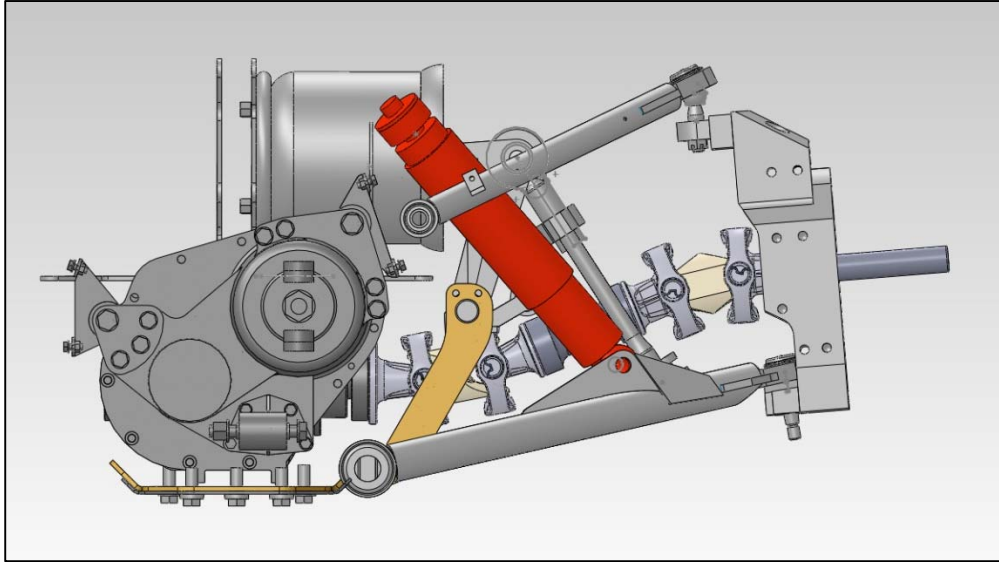


Figure 54: Side View (Bump-Stop Height, 0° Steering Angle)

Above is a side view of the suspension assembly at the vehicles lowest ride height, with steering unarticulated. At this height, there is a clearance issue at the suspension's pushrod, as seen below:

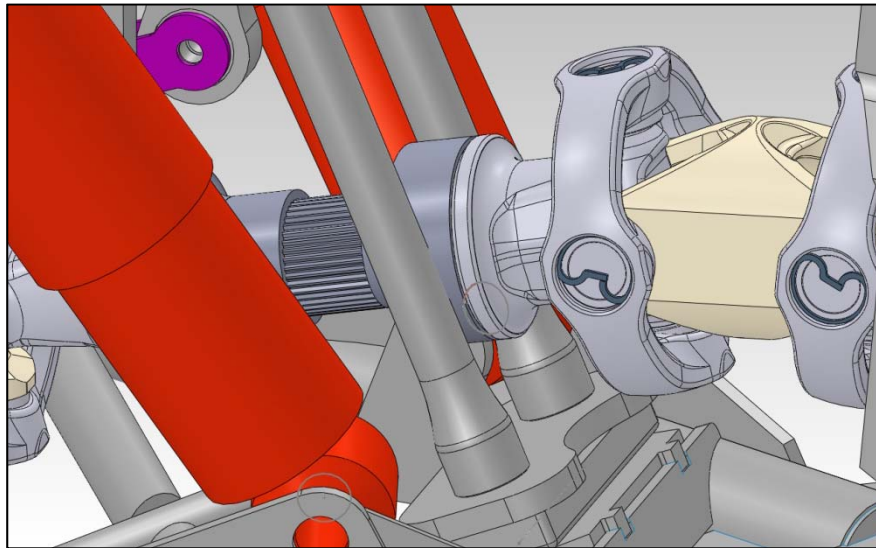


Figure 55: Interference at Pushrod (Bump-Stop Height, 0° Steering Angle)

Another clearance issue is present at this height. The inner Cornay® joint interferes with the suspension assembly as made evident by the figure below.

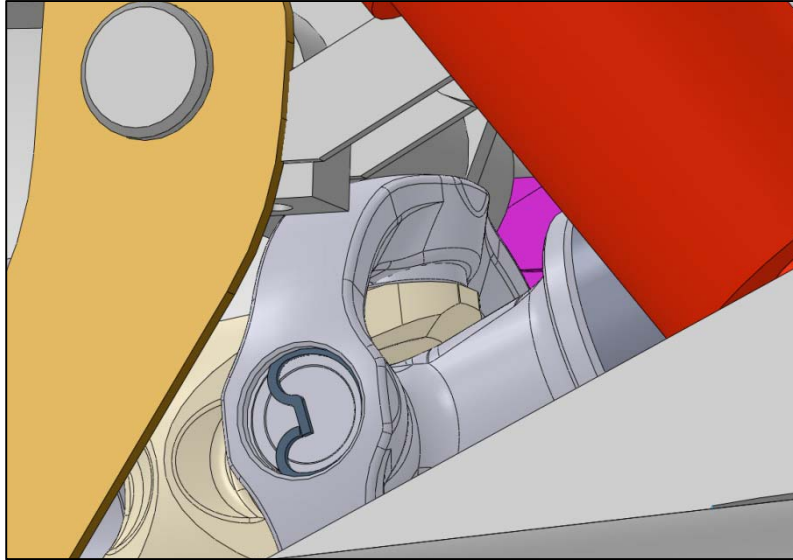


Figure 56: Interference at Inner Joint (Bump-Stop Height, 0° Steering Angle)

Steering articulation was introduced to the simulation and interference was visually analyzed. The assembly at a steering angle of 30° is displayed below.

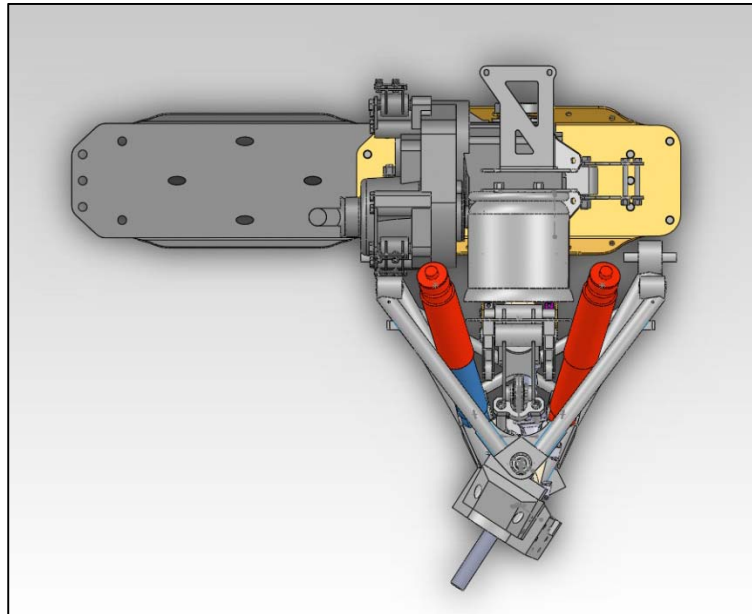


Figure 57: Top View (Suspension Assembly at Full-Lock)

Similar interference issues are present at full-steering lock, with 30° of steering. The interference at the inner joint is similar to the interference with no steering articulation. Interference worsens at the pushrod under full-steering lock as below:

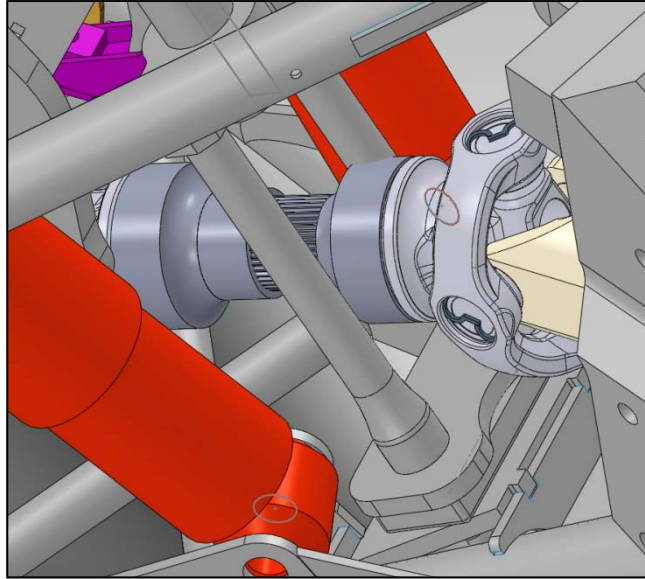


Figure 58: Interference at Pushrod (Bump-Stop Height, Full-Lock)

Altering the ride height the off-road setting has a positive impact on half-shaft clearance in the suspension assembly. An image of this assembly at maximum ride height can be viewed below.

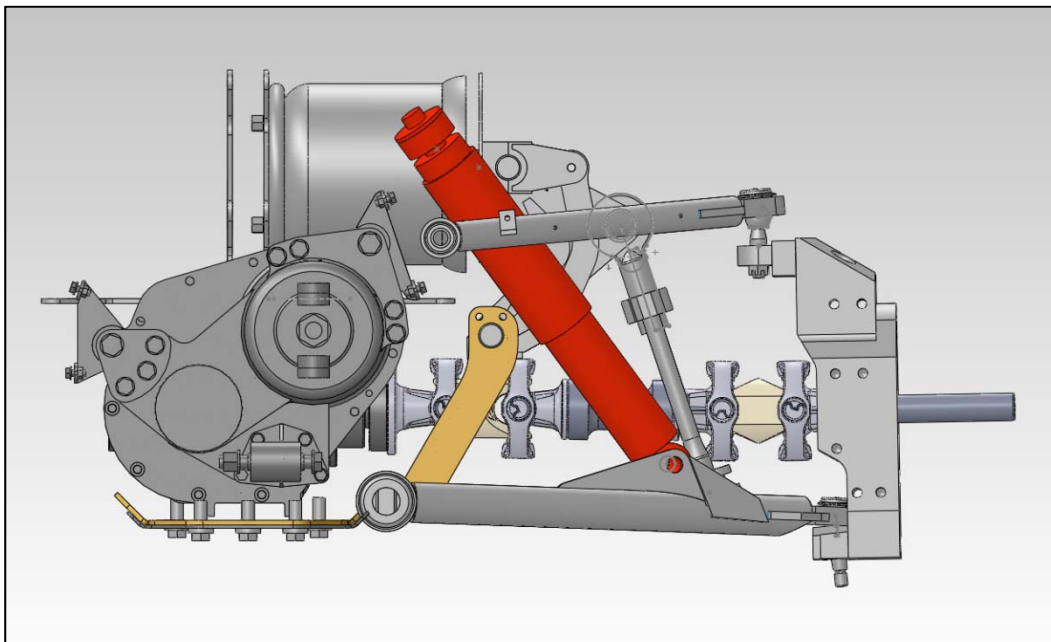


Figure 59: Side View (Off-Road Height, 0° Steering Angle)

At this height, the interference problems previously present at the inner joint are resolved, with no parts in contact as seen in the following figure:

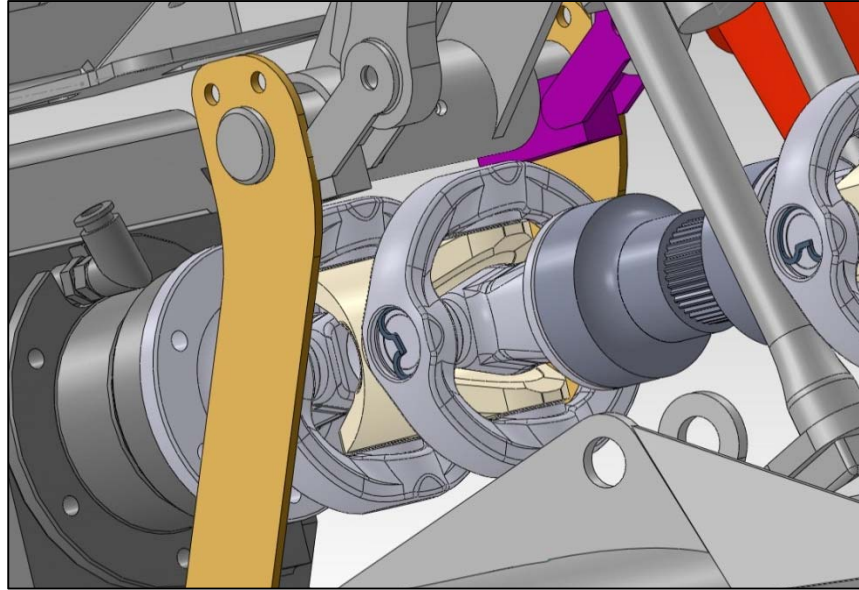


Figure 60: Clearance at Inner Joint (Off-Road Height, 0° Steering Angle)

Note that in the image above, one of the shocks was hidden for ease of viewing the clearance at the inner joint.

The contact of the half-shaft with the pushrod actually worsens at off-road height as evidenced in the following picture:

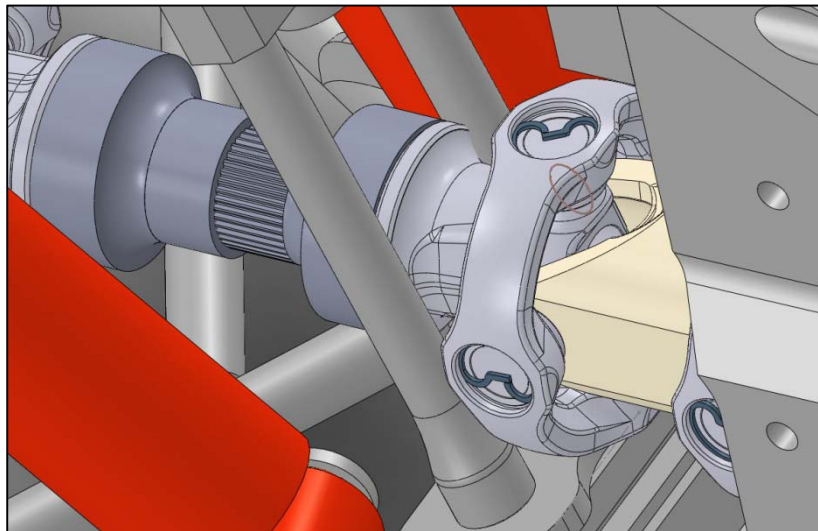


Figure 61: Interference at Pushrod (Off-Road Height, 0° Steering Angle)

Steering articulation has a similar effect on bump stop and off-road heights. No clearance issues are present at the inner joint, but the pushrod interference worsens as seen below:

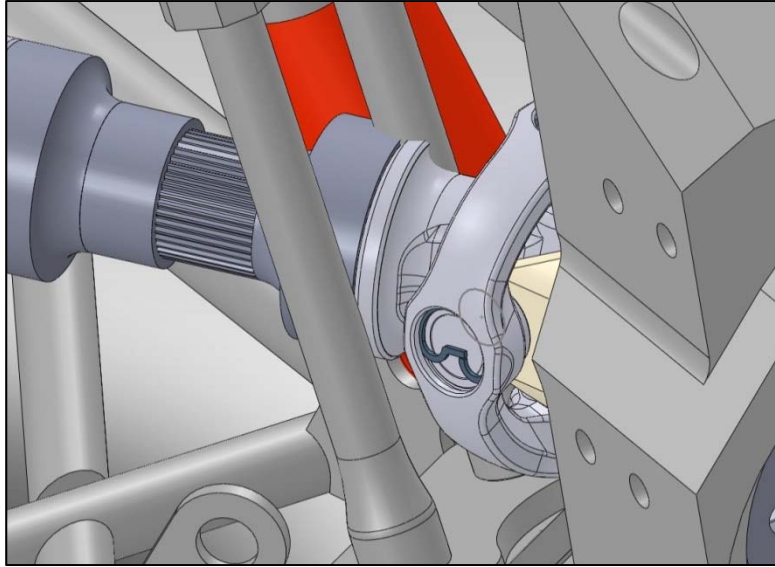


Figure 62: Interference at Pushrod (Off-Road Height, Full-Lock)

The interference simulation made evident quite a few issues with the fit of the half-shaft into the HMT 400/600 suspension assembly. These issues, while present with the prototype, could be eliminated with the production design through methods mentioned in Section 8.

3. Optimization

3.1. Feasibility Study

The following encompasses many of the ideas and inventions researched over the course of this project. The included information was helpful in analyzing and optimizing the possible ideas for utilization in the design of the prototype.

Design I: Split Boot



Figure 63: Split CV Boot

The Split Boot design, shown in Figure 63 above, is one in which the current thermoplastic boot surrounding the outer Rzeppa joint is replaced with an open-type boot. This boot would be constructed of material similar to the current conventional-type boot, with similar internal dimensions. The fundamental characteristic unique to the split boot is its ability to be installed and removed *without* the removal of the half-shaft. Once installed, the split faces would be affixed to one another through the use of both an adhesive along the seam and a bolted connection. The advantage of this design is clear: reduced install time. The removal of the half-shaft assembly requires uninstalling the wheel and hub assemblies, a lengthy process which would be unnecessary with this design. This boot is also very inexpensive to implement and would be highly available relative to other more bespoke solutions. The disadvantages, however, are similar to those of the current conventional boot. The split boot design fails to address the problems imposed by temperature, fatigue, and debris which currently cause boot failures, as well as introducing increased likelihood of lubricant loss. The implementation of the split boot design is recommended more as a temporary fix than a long-term solution.

Design II: Boot Geometry Redesign

This proposed solution for the failure of the current half-shaft addresses the fatigue failure of the grease boot. One of the current design's primary failures is boot cracking due to repeated self-contact and to abrasion from foreign debris. During operation the adjacent corrugations of the boot flex during each rotation of the half-shaft such that the corrugations touch each other. Eventually, this contact, worsened by the presence of grit from the driving surface, wears through the boot causing leakage of the joint lubricant and contamination of the joint itself. This combination results in rapid joint failure. By redesigning the geometry of the boot, it is proposed that the clearance between adjacent corrugations could be widened and the stretch of the boot lessened. This would increase the life of the boot by eliminating the self-contact and reducing the abrasive effect of a small amount of debris between the corrugations. Another advantage to using a boot to correct the half-shaft failure is the relatively small cost. Plastic boots are relatively inexpensive compared to other solutions.

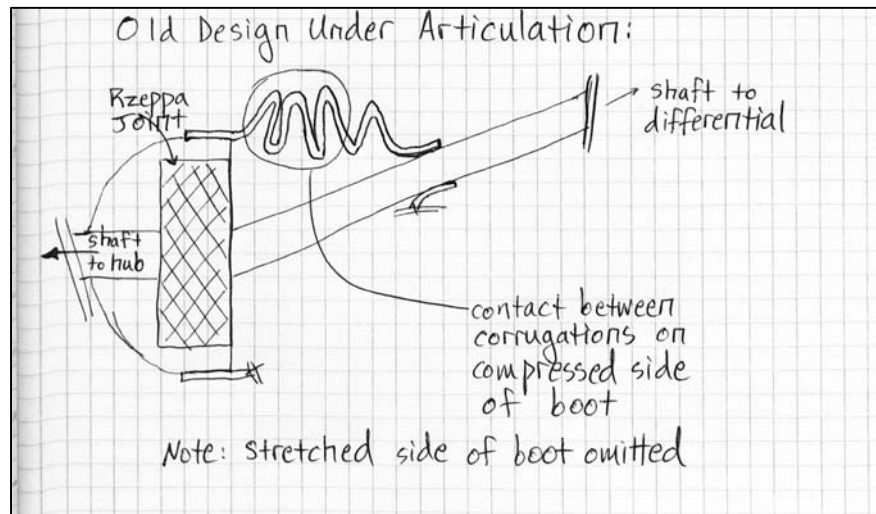


Figure 64: Old Boot Design Compressed

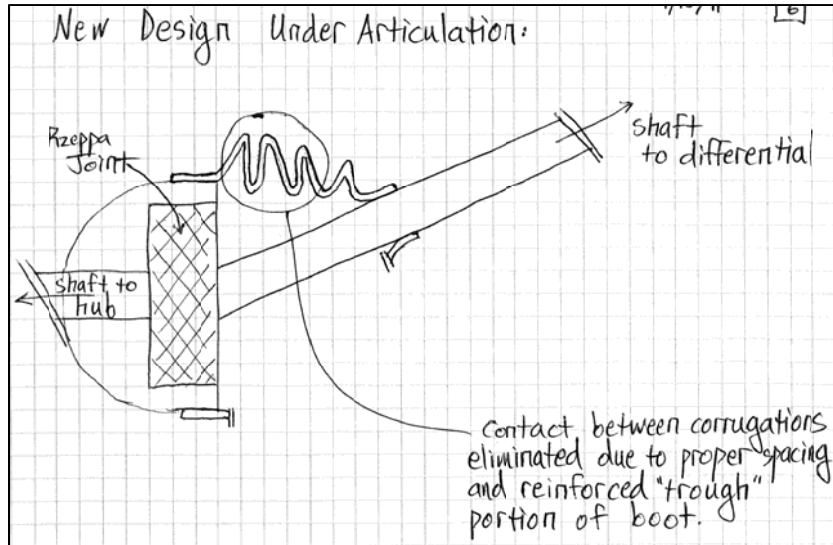


Figure 65: Redesigned Boot Compressed

While this design does address the failure due to self-contact fatigue and due to some abrasion from debris, it does not correct the failure of the boot due to high temperatures or from outright tearing. Furthermore, the manufacturing of such a boot with finely defined geometry would require a precisely constructed mold; whether the facilities available to the senior design class could make such a mold is debatable. As a consequence of these shortcomings, this feasible idea was not chosen as a viable solution.

Design III: Floating Boot

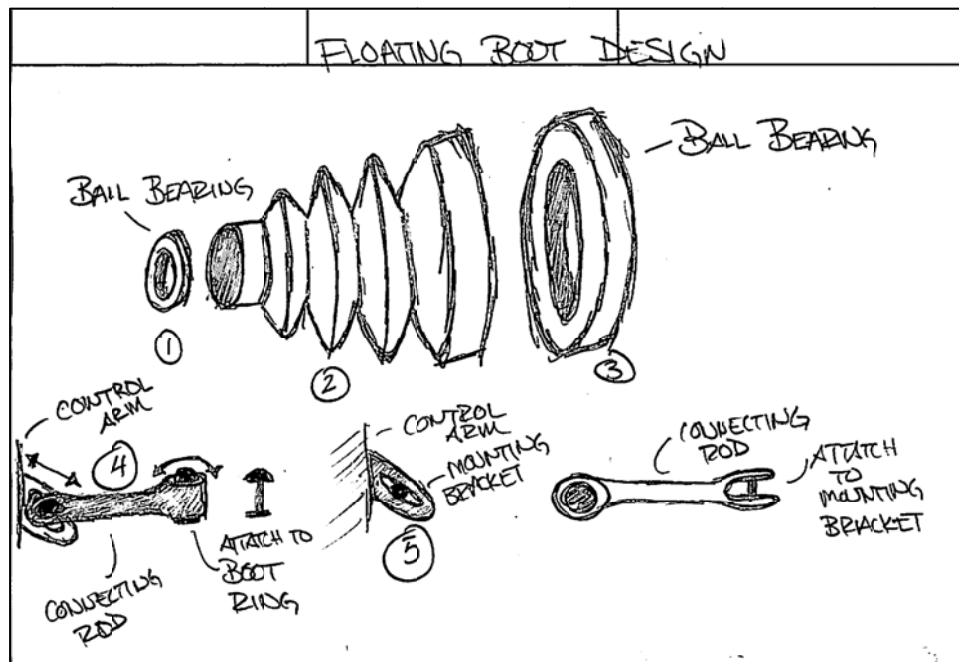


Figure 66: Floating Boot Components

This feasible design implements the idea that the boot will remain stationary as the axle rotates within the boot. If the boot remains stationary as the axle is rotating, less frictional wear will result due to the fact the boot will contact itself less during operation. Also, as debris accumulates on the boot the likelihood that it will wear holes in the boot due to the rubbing of the boot on itself is reduced. If a sharp object with the ability to puncture the boot comes into contact with the boot, only minor punctures will occur rather than a total tear due to the boot rotating itself against the sharp object, thus reducing the amount of grease lost and prevent premature joint failure. A total of two ball bearings are needed on each ends of the joint. A rather large bearing is needed on the output end of the joint. A 45BIH206 Timken ball-bearing with a bore of 4.5 inches would suffice for this design. However, the outer diameter of the bearing is 6.25 inches and would require a larger boot to accommodate for the outer diameter of the bearing. The inside bearing would be a 207W Timken ball-bearing. As with the outer bearing the inner bearing has a larger outer diameter so a larger opening for the boot would also be needed on that end. Each bearing would be pressed onto the shaft at either end of the joint. As shown above in Figure 66 a small bracket would be welded onto the hub to attach the connecting rod that attaches to the clamp which attaches the boot to the larger end of the joint. With this design a more rigid and robust boot could be used do to the less amount of flex or articulation seen by the boot, which greatly elongates the lifespan of the boot. This design still does not reduce the amount of heat generated by the joint, and will still eventually lead to boot failure, which in turn will lead to joint failure. The process of manufacturing, and additional parts of these floating boots actually increases the complexity of replacing the axle. Also, the bearings are intended to be “sealed”, but given the harsh operating environment of the vehicle intrusion is inevitable and foreign particles will find their way into the joint and further deteriorate it. If the bearings fail the joint still has to be removed to replace them, thus creating additional problems with the current design.

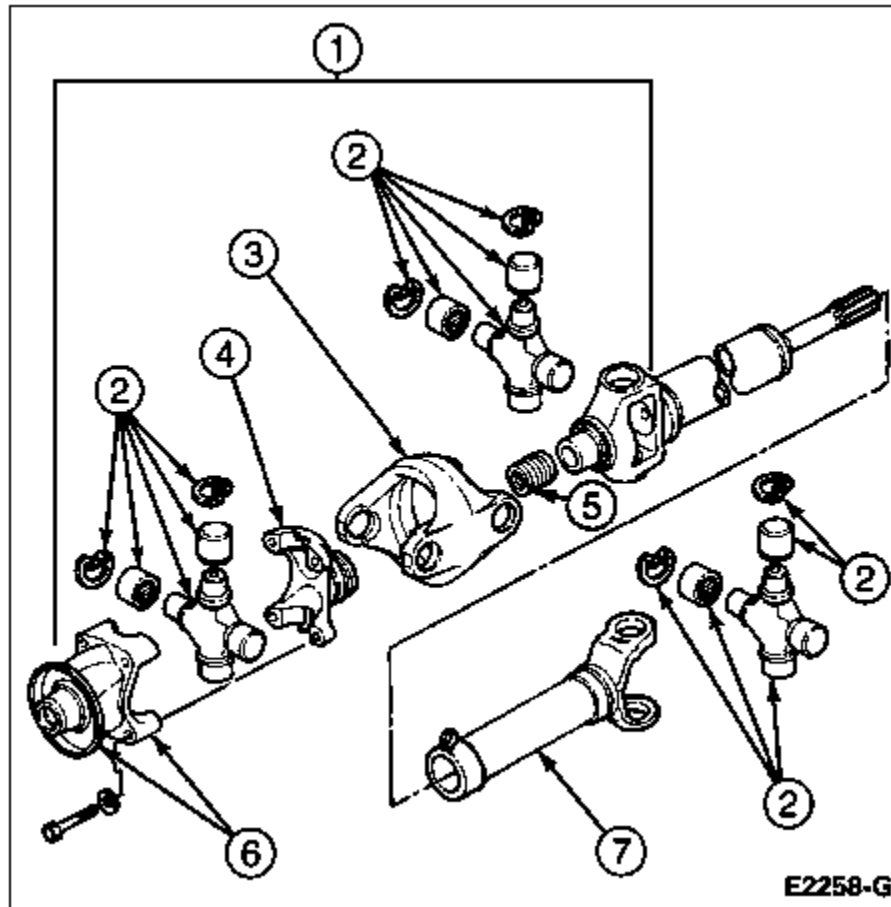
Design IV: Dual Cardan

Figure 67: Dual Cardan CV Joint, Exploded View

This feasible design includes the use of two Dual Cardan constant velocity joints joined together with a splined shaft, replacing the current Rzeppa and Cross Groove joints. The Dual Cardan joint Figure 67 is a near-constant velocity joint designed for transmitting torque. It is often seen in many light-duty applications for transmitting power between transmissions and axles. The joint consists of two universal joints (parts 2) joined together with a coupling yoke (part 3) as well as a centering mechanism (parts 4 and 5), usually of a ball-and-socket design. The ball-and-socket assembly is necessary to maintain equal angles on either side of the coupling yoke. In order to maintain the constant velocity aspect necessary in this type of joint the angle of the input shaft entering the joint and the angle of the output shaft exiting must be equal. A specific advantage to this joint is the fact that it is capable of producing near constant velocity operation without the need for a boot. The main bearing components are housed in sealed “caps” that cannot be damaged easily by any type of debris. The centering ball-and-socket assembly also utilizes a dust cap to prevent particulate intrusion prolonging the life of the joint. Many parts for this style joint are readily available and inexpensive, making it a very cost effective replacement for the current design. It is also possible to eliminate the need to remove the wheel/hub assembly from the vehicle to replace any of the half-shaft components, thus saving time if the joint were to fail. The articulating components of this joint, the two

universal joints, and centering ball-and-socket are also the only components that will experience wear, unless there is total inelastic failure of the metal centering yoke or tube yokes. This is extremely advantageous because the components needed to replace a worn joint are very small and inexpensive.

The downfall to this design is that it is not a true constant-velocity joint. This is due to the fact that throughout its range of articulation, the angle between input and output is not kept perfectly equal as a result of the ball-and-socket style mechanism. The joint is designed such that it maintains as close to constant velocity operation as possible when operating at a specified angle. When this joint is articulated, either under or over its specified angle, the constant velocity property begins to dissipate. When this happens the assembly begins to develop unwanted vibration which can then damage the joint and connected components. For this specific application, it is necessary to articulate, and operate, across a wide array of angles. Furthermore, Dual Cardan constant velocity joints are typically utilized in light-duty applications. This application requires a specific torque rating which is on the upper limits of the readily available Dual Cardan CV components, in fact there is only one such joint that is capable of satisfying the necessary torque rating. In addition to this, the articulation capability of this joint is not quite large enough for the needs of the Supacat. It is feasible that this joint be modified to suit the articulation needs, but at the cost of torque capability.

Design V: Thompson Coupling

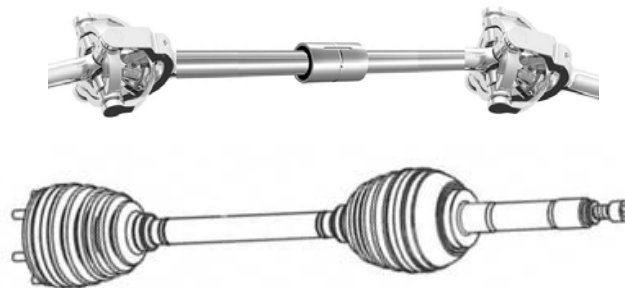


Figure 68: Thompson Design (above) compared to Original Design (below)

This feasible design involves two Thompson Coupling joints replacing the outer Rzeppa joint and inner CV joint. The design would require a splined shaft in between the joints to maintain the specified plunge. According to the specification sheet of the Thompson CV joint 2C-15, this model exceeds our maximum torque by 2000 Nm and the speed by 500 rpm. However the full articulation angle is only 15° and the dimensions are much larger than the current space available.

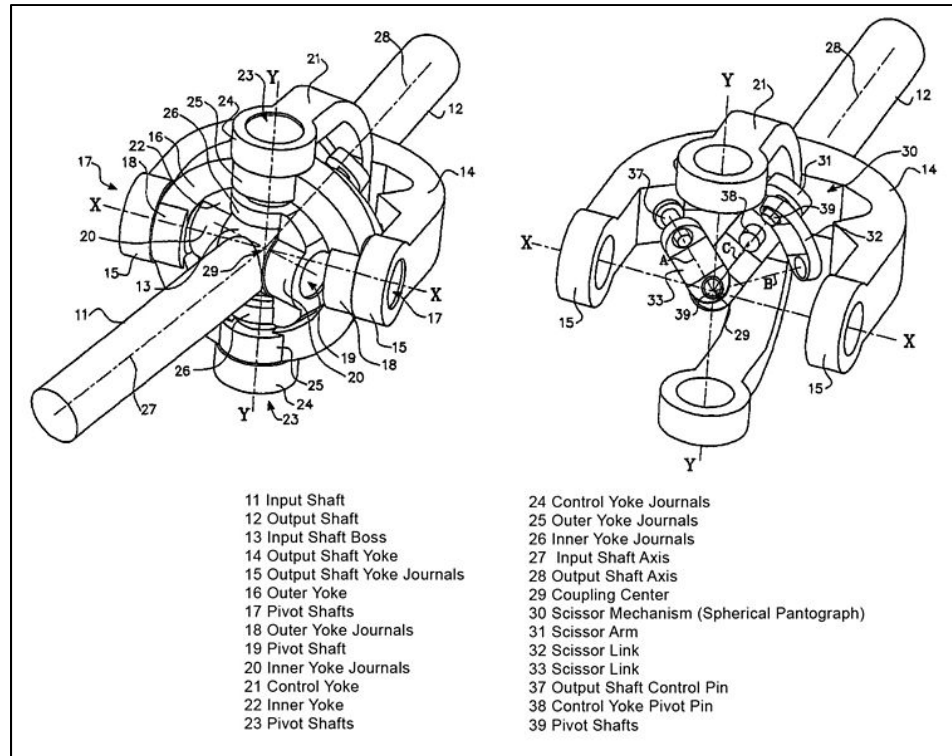


Figure 69: Detailed Drawing of Thompson Coupling

The Thompson Coupling joint, detailed in Figure 69, is a constant velocity joint composed of two Cardan joints assembled within each other with a control yoke. Because of this configuration, this joint eliminates the intermediate shaft present in the typical linear configuration of the double Cardan joint. The Thompson Coupling joint also uses roller bearing running circumferentially instead of ball bearings present in the Rzeppa joints. Finally, the unique spherical four bar scissors linkage constrains the joints in the assembly.

The Thompson Coupling design has significant advantages to the current half-shaft design. The roller bearings result in low friction and vibration, which produces less heat and wear to the joints. Also, there is no lubrication or boot required for the joints, eliminating the main causes of failures to the current design. Overall, this is a more reliable and robust design. However, with this ideal design come obstacles to surmount. The design would require custom or redesigned Thompson joints to achieve the specified articulation angle and clearances. These joint would then be more difficult and expensive to manufacture than the current joints.

3.2. Optimization Methods

The criteria chosen for ranking the feasibility designs described in the previous section are: design for manufacturing, cost, reliability, heat resistance, weight, suitability for the given requirements, ease and frequency of maintenance, and fatigue wear. Each criterion was given a weight factor based on importance for the design. The justification for these weight factors is as follows:

- DFM—5/10: Design for manufacturing was assigned a weight factor of 5 because ease of fabrication is not thought to be of high importance. If extra effort needs to be made to construct the design [i.e. splining], it will be done if it is considered beneficial to the design.
- Cost—4/10: The USASOC stated that the current half-shaft assembly costs approximately \$2300. They also stated that the budget could be raised if a design solved the current boot failure problem, demonstrating flexibility with cost. For this reason, cost only received a weight factor of 4.
- Reliability—9/10: Reliability is of prime importance, as failures are caused by unreliable parts. It was desired that the new design be extremely reliable given the tough conditions to which it will be exposed [road conditions, heat, etc.].
- Heat Resistance—7/10: This relatively high weight factor was assigned considering the high heat that the half-shaft will see, specifically with the large heat generation from the wheel hub at high speeds. The improved design should be impervious to heat-related fatigue issues.
- Weight—2/10: Although a low weight is desired for minimal parasitic loss in this application, it is not necessary. A design's ability to improve reliability and solve the boot-failure problem is paramount to weight loss, thus explaining the low factor assigned to this criterion.
- Suitability—10/10: This factor is most important because the new design should suit the application. This means that it should fit and function properly while addressing the problems of the current design.
- Maintenance—8/10: This weight factor is high due to the importance of simple installation and removal of the improved design. In the event of a failure, repairing the assembly should require minimal labor and time.
- Fatigue—6/10: Fatigue was assigned a 6 because the materials to be used are to be fairly fatigue-proof, exhibiting little wear due to mechanical fatigue. This factor is important in the optimization of the design.

Designs can score 1 (worst) to 5 (best) in each of the criteria. These values were then multiplied by the corresponding weight factor in parenthesis and summed to find a total score for each design. The scores and totals are shown in Table 7.

Table 7: Optimization Table

Feasibility Designs	DFM (5)	Cost (4)	Reliability (9)	Heat Resistance (7)	Weight (2)	Suitability (10)	Maint (8)	Fatigue (6)	Total
Split Boot	5	5	1	2	3	1	5	1	130
Boot Geometry Redesign	1	4	2	2	3	2	2	2	107
Floating Boot	2	4	3	2	3	3	2	3	137
Dual Cardan	3	3	4	5	2	5	4	4	208
Thompson Coupling	3	1	4	5	2	1	3	4	152
Cornay Joint	3	2	5	5	2	5	4	4	213

As shown above, the Cornay® design scored the highest. Because this design scored so well compared to the others, we chose dual Cornay® joints for our improved design.

4. Materials and Design for Manufacturing

Each material for each part that will be used within the prototype must be selected in such a manner that allows for no failure within the specified operating limits of the half-shaft. The selections of these materials must also conform to manufacturing limitations. The following sections explain, in detail, why a certain material was chosen. It will also describe how the individual parts can be made for the prototype as well as the feasibility of manufacturing these parts in production settings.

4.1. Material Selection

Shaft/Spline

The particular material to be used to make the shaft and splines of the prototype must be somewhat easy to machine, weldable, and have good finishing qualities after machining. Also, due to the use of the Cornay® joints, the material must also be compatible for welding to these particular joints. Since the weldable ends of the joints are made out of AISI 4140, it was recommended by Cornay® that either AISI 4140 or 8620 alloy steel was to be used. Below in Table 8 and Table 9 the chemical composition of each steel and their respective physical properties can be seen.

Table 8: AISI 8620 Steel Properties

AISI 8620	
Composition	
Element	Weight %
C	0.18-0.23
Mn	0.70-0.90
P	0.035 (max)
S	0.04 (max)
Si	0.15-0.30
Cr	0.40-0.60
Ni	0.40-0.70
Mo	0.15-0.25
Mechanical Properties	
Density (x1000 kg/m³)	7.7-8.03
Machinability	66%
Poisson's Ratio	0.27-0.30
Elastic Modulus (Gpa)	190-210
Tensile Strength (Mpa)	536.4
Yield Strength (Mpa)	385.4
Elongation (%)	31.3
Reduction in Area (%)	62.1
Hardness (HB)	149
Impact Strength (J)	112.2
T @ 25°C	Annealed at 870°C

Table 9: AISI 4140 Steel Properties

AISI 4140	
Composition	
Element	Weight %
C	0.38-0.43
Mn	0.75-1.00
P	0.035 (max)
S	0.04 (max)
Si	0.15-0.30
Cr	0.80-1.10
Mo	0.15-0.25
Mechanical Properties	
Density (x1000 kg/m³)	7.7-8.03
Thermal Conductivity (W/m-K)	42.7
Poisson's Ratio	0.27-0.30
Elastic Modulus (Gpa)	190-210
Tensile Strength (Mpa)	655
Yield Strength (Mpa)	417.1
Elongation (%)	25.7
Reduction in Area (%)	56.9
Hardness (HB)	197
Impact Strength (J)	54.5
T @ 25°C	Annealed at 815°C

Since neither one of these alloys are difficult to machine, the most important requirement in selecting one of these materials is the ease of welding, which is directly affected by the Carbon content in the steel. The lower the carbon content the easier it is to weld. 4140 is also more expensive per foot of 3 inch round stock. However, 8620 comes in both cold finish and hot-rolled. The hot-rolled is cheaper by a slight margin, but is not as strong and does not finish as well when machining. Therefore in order to produce a sturdy weld to the joints being used as well as machining to a quality finish for the effectiveness of the spline, the shaft and spline will be made of AISI 8620 Cold Finished Alloy Steel for the prototype.

Flange/Spindle

The outer flange and spindle assembly will be mounted into the wheel hub assembly and provide a mounting point for the outer Cornay joint. This part, for prototyping purposes will be made from two separate pieces of material as stated earlier in this report. These two parts will be first machined then welded together. Because they will be attached through welding, it will make the most sense to use the same material. This will provide the strongest and most consistent weld. As the material for the splines will be AISI8620 alloy steel due to it being slightly stronger than AISI4140 (See Table 8 and Table 9), the outer flange and spindle will be made from the same material. The flange will be made from 3/8" thick AISI8620 steel plate (cold rolled), and the spindle will be made from the same 3" outside diameter AISI8620 steel rod (cold finished).

4.2. Mechanisms

Cornay® Joint

The joints used in the prototype will not be fabricated or designed in-house, but rather they will be provided by Cornay®. The Cornay® joint is vastly superior to the dual cardan design for a constant velocity (CV) joint. The main reason is the centering mechanism contained within both the dual cardan and Cornay® joint. While the dual cardan design is only a true CV joint at 0° and some design operating angle, whereas the Cornay® joint will operate at true CV from 0° to the joint's maximum misalignment capability. The reason for this phenomenon is the fact that a dual cardan's centering mechanism moves laterally to divide the articulation angle amongst the input and output shaft. The most popular centering mechanism for the dual cardan is the ball-and-socket. As the joint articulates the socket rotates around the ball and the ball actually moves laterally with respect to the socket. This is clearly shown in Figure 70 below.

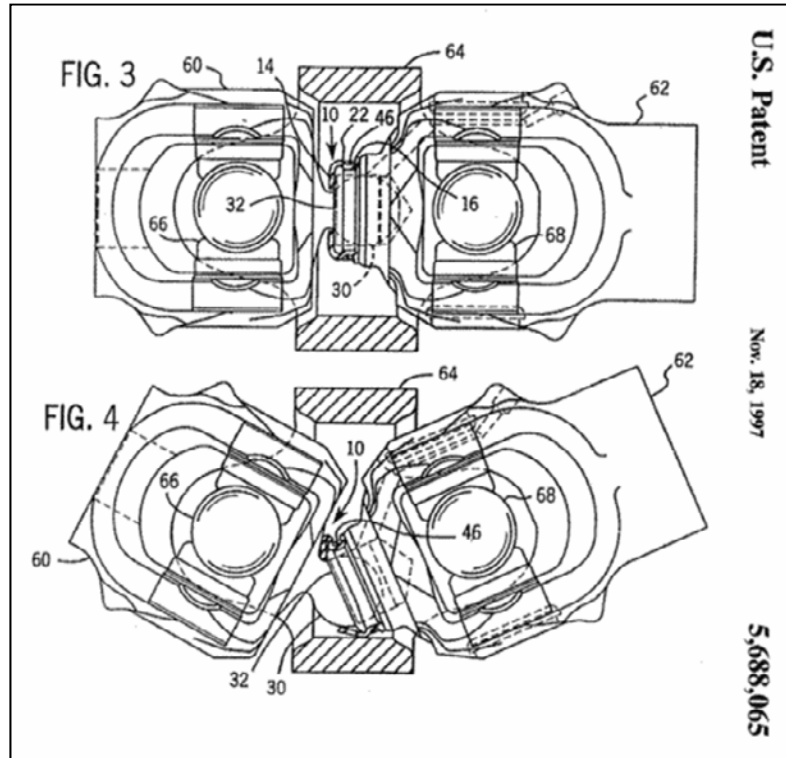


Figure 70: Dual Cardan Centering Mechanism Under Articulation

As the joint articulates it can be seen that the ball actually moves to the left away from the “seat” of the socket. This slight lateral movement causes the centering mechanism to bisect the angular plane of the connecting yoke. This not only causes the joint to move from true CV to relative CV, but this shift causes inertia excitations (vibrations) within the connecting yoke. These vibrations at speeds over 1,000 RPM will eventually deteriorate the connecting yoke and internal bearings within the joint causing premature failure. Another issue with the dual cardan for this application is the inability to source a joint that has both the required articulation and torque capacity. A 1350 capacity dual cardan can withstand the 3,000 Nm of torque, but will not be able to articulate over 30° at relative CV in most cases.

On the other hand, the Cornay® joint’s centering mechanism, which was covered in detail in Section 2.1 does not move laterally under articulation, allowing the centering mechanism to constantly bisect the angular plane between the input and output shafts of the joint. This particular mechanism uses rotation to transfer articulation throughout the joint rather than lateral movement. Below in Figure 71 and Figure 72 it can be clearly seen how the Cornay® joint’s centering mechanism remains in the bisection of the control yoke and angular plane under articulation.

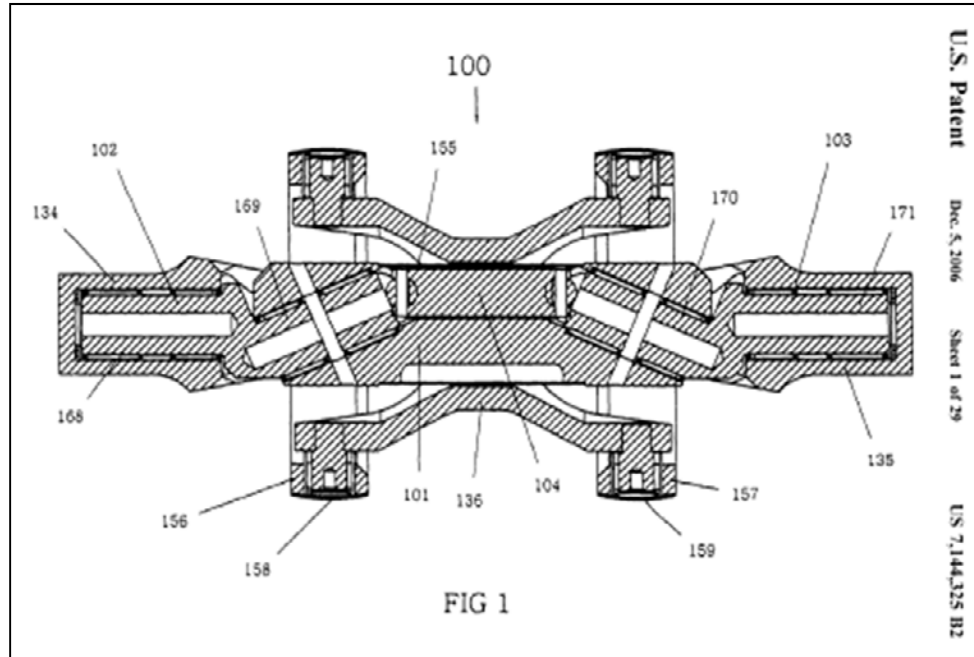


Figure 71: Cornay® Joint - No Articulation

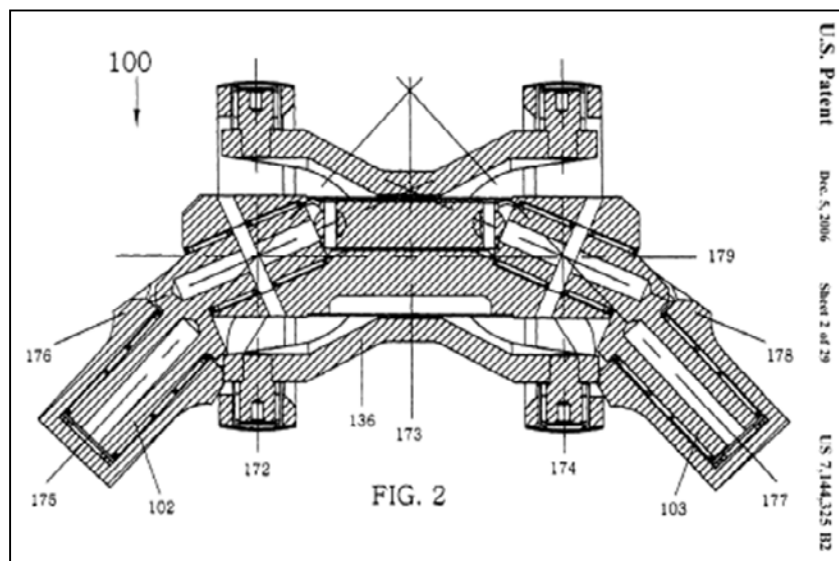


Figure 72: Cornay® Joint – Articulated

Bolts and Washers

The improved half-shaft assembly utilizes two bolted connections: one fixing the transfer case output to the inner joint input flange and one fixing the outer joint output to Flange 1. These connections can be seen in Figure 73 and Figure 74 below:

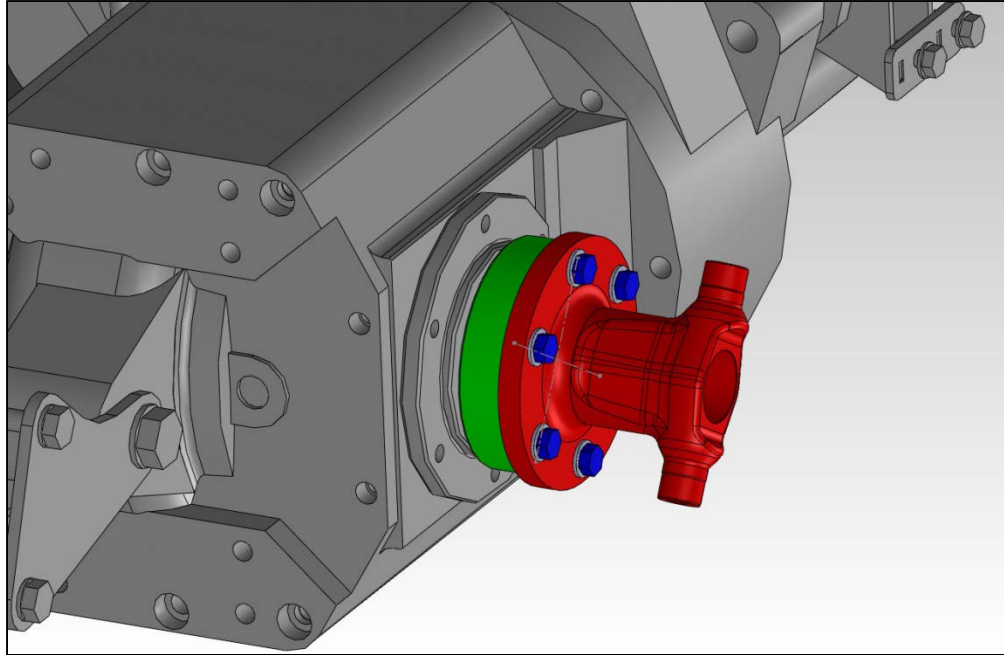


Figure 73: Inner Joint to Transfer Case Bolted Assembly

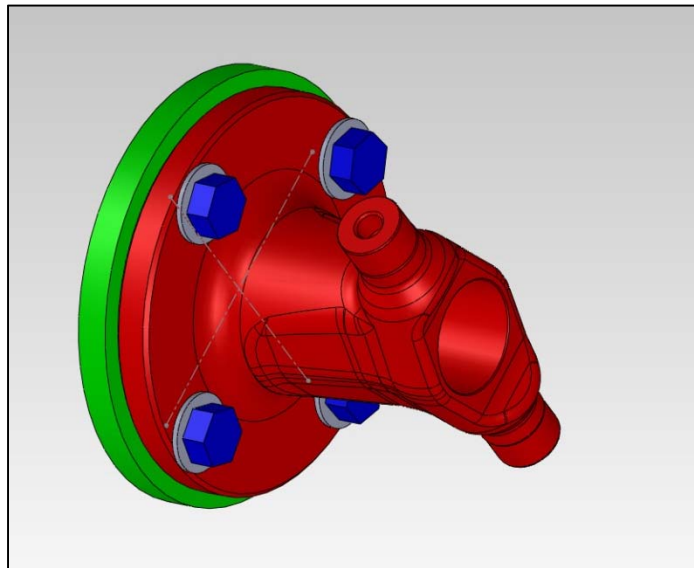


Figure 74: Outer Joint to Flange 1 Bolted Assembly

In each of the above images, the Cornay® joint model was simplified as only the component to which the bolts were fixed. All other components were hidden to better display the bolted connections.

In both bolted connections, lock washers were used to maintain a preload on the bolts, keeping them from loosening under cyclic loading. In the current design, threadlocker is used to perform this function. The use of lock washers instead of threadlocker allows the

simplification of shaft installation and removal, as no curing time is required with lock washers.

Inner Bolted Connection

This connection, seen below in Figure 75, allows the transfer case to be mated with the input flange of the inner Cornay® joint.

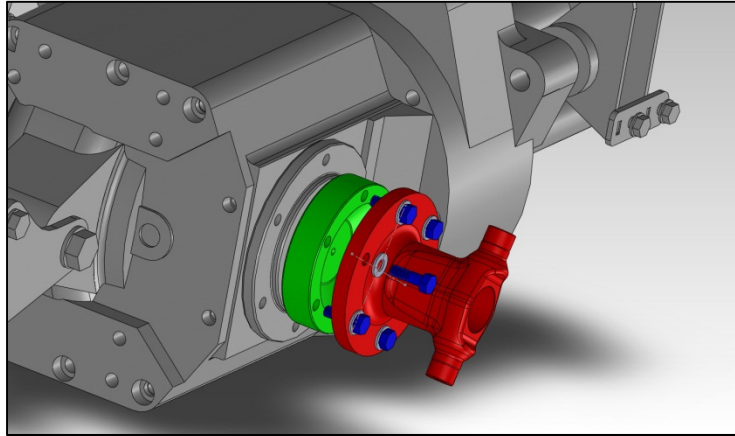


Figure 75: Inner Bolted Connection - Exploded View

List of Hardware:

The bolted assembly in Figure 75 is comprised of the following hardware:

- M8x1.25 bolts, quantity 6
 - Diameter = 8 mm
 - Length = 25 mm
 - Grade 8.8
 - Pitch = 1.25 mm
- 8 mm lock washers, quantity 6

Dimensions:

The use of M8 bolts was chosen based on the thread pattern of the six bolts holes in the vehicle's transfer case, which has 8.5 mm holes tapped for M8 bolts. The 25 mm length was chosen due to the grip length of the connection, found as follows:

$$L_{grip} = t_{cornayflange} + t_{washer} = .438 + .091 = .529 \text{ in.} \quad (67)$$

The threaded bolt portion extending into the transfer case output flange, as seen in Figure 76 was found to sufficiently transmit the torque requirements of the system.

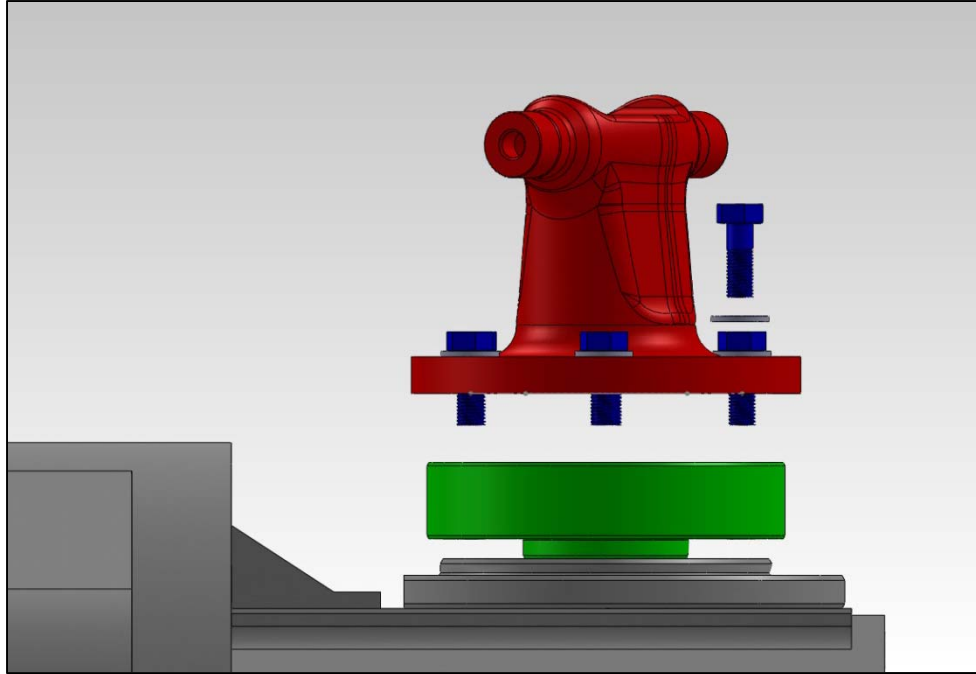


Figure 76: Inner Bolted Connection - Top View, Exploded

Strength:

Grade 8.8 hardware with a yield stress of approximately 92.8 ksi was found to be more than adequate for the torque requirements of the connection. See the analysis section for detailed calculations.

Outer Bolted Connection

The outer bolted connection, which transfers power from the output of the outer Cornay® joint to Flange 1, is seen below in Figure 77 and Figure 78.

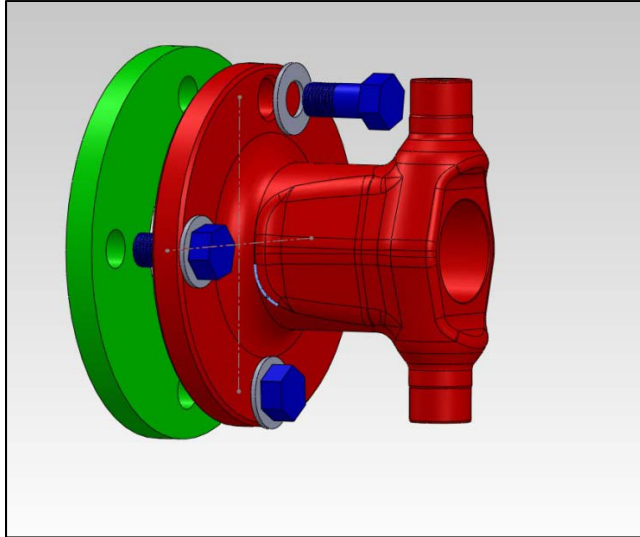


Figure 77: Outer Bolted Connection - Input View

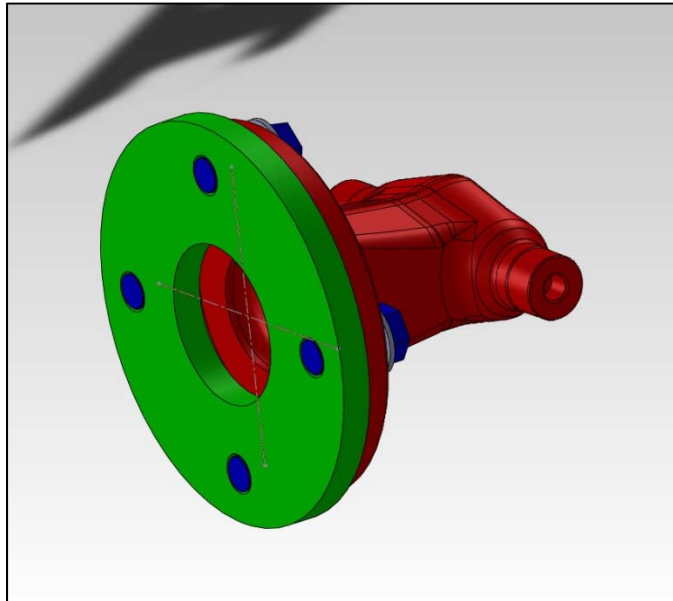


Figure 78: Outer Bolted Connection - Output View

List of Hardware:

This bolted assembly contains the following hardware:

- 7/16"x 1" bolts, quantity 4
 - Diameter = 7/16"
 - Length = 1"
 - Grade 8
 - 20 threads per inch

- 7/16” lock washers, quantity 4

Dimensions:

Four 7/16” bolts are used for this connection because of the bolt pattern used by Cornay® on the output flange of their joint. The length was chosen due to the grip length of the connection as follows:

$$L_{grip} = t_{cornayflange} + t_{washer} = .438 + .065 = .503 \text{ in.} \quad (68)$$

Because these bolts are threaded into Flange 1, which has a 3/8” [.375”] thickness, a length of 1” for the bolts was chosen to ensure that all threads are engaged in the threaded holes of Flange 1, as in Figure 78. The portion of the bolt in contact with Flange 1 sufficiently transmits the required torque without inducing excessive bearing stress on Flange 1. See the analysis section for details.

Strength:

Grade 8 hardware has a yield stress of approximately 130 ksi suitable for the torque requirements of the connection. See the analysis section for detailed calculations.

Cost:

The cost of the hardware used in both inner and outer connections is minimal relative to the entire half-shaft assembly’s cost. A detailed list of individual component costs is available in Section 6.2.

Splined Shaft Boot

In order to keep the lubrication contained within the splined shaft, and to keep dirt and other foreign particles out, a boot is needed. Because this boot is only covering the splined shaft, it does not rotate at an angle. It only experiences the axial plunge of approximately 7 mm, so fatigue failure is not a concern.

Several potential boot options were considered. Dust caps are another option that perform the same role as boots, but cap onto the female spline with a hole the same profile as the male spline to enable the plunge while keeping the grease in. Our design involves a spline with custom dimensions, so it is unlikely there is a dust cap that fits perfectly. A stabilizer boot could also work for the splined shaft; however the material is not as strong as other boots and it is not meant to hold grease in, just keep particles out, so these are not recommended either.

Splined yoke boot kits or universal joint boot kits would work best for our custom application because of their robustness. Several specific boots were found and their specifications are detailed in Table 10 below with the dimensions shown in Figure 79.

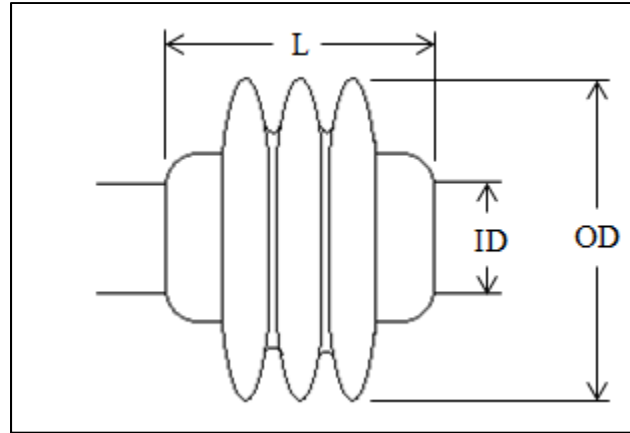


Figure 79: Splined Shaft Boot Dimensions

Table 10: Splined Shaft Boot Options

Manufacturer	Curtis Universal	Spicer	McMaster-Carr
Part No.	CJ654-9K	SPI-212059X	94205K82
ID (in.)	3	3.787	2.23
OD (in.)	6	Not listed	3.25
L (in.)	5.625	7.952	3.52
Material	Polyvinyl Chloride Rubber Blend	Not listed	Neoprene
Attachment	Cable Tie Straps	Metal Clamps	Cable Tie Straps
Temperature Rating	-60° - 220°F	Not listed	-30° - 212°F
Price	\$50.00 (for 1) \$46.57 (for > 1)	\$32.30	\$56.83

For our shaft, the boot would attach best on the large diameter of the female and male splined shaft because there is not enough room on the smaller diameters. Using the large diameter also provides more room to lengthen the boot. The large diameters of the splines are 3 in., which matches the Curtis boot. Using the other two boots would require some minor redesign to be able to attach them. The Curtis boot also has a superior temperature rating and does not require grooves in the shaft to retain it. The Spicer boot does use metal clamps, which would provide a tighter seal than the cable tie straps. A pair of 3 in. metal clamps that would be needed for the Curtis boot can be bought separately for a minimal cost.

4.3. Assembly Details

The assembly will be constructed from several components. The components consist of the following:

- 2 Cornay Joints, received fully assembled from Cornay

- 1 Female Spline
- 1 Male Spline
- 1 Spindle
- 1 Flange

The female spline, male spline, spindle and flange will all need to be machined with the exception of a few components that make up the spline sections. Details are included below regarding the machining and assembly of each individual component as well as the overall half-shaft.

There exist three different responsibilities of team members which include Shop Fabricator, Weldor and Machinist. Each of these responsibilities are assigned to specific areas of the available MAE416 laboratory: the Assembly area, Machine area, and Welding booth. Within each of these areas exists a variety of machines and tools. The available tools with respect to each area are as follows but are not limited to:

Welding Booth:

- MIG Welder
- TIG Welder
- Stick Welder
- Plasma Cutter

Machine Area:

- Lathe
- Drill Press
- Mechanical Press
- Mill
- Belt Sander
- Bench Grinder

Assembly Area:

- Socket Set
- Ratcheting Wrenches
- Screwdrivers

All individuals have been trained, as required, on how to operate the supplied tools and machinery in their respective areas. This along with knowledge learned elsewhere will enable the students within the group to construct the components of the prototype as the following describes.

Flanges

The flange that will connect the outer joint to the spindle will be made out of AISI8620 cold rolled steel sheet of 3/8" thickness. First, using the SolidWorks drawing as a template to draw a circle on the metal sheet, a rough outline cut will be made with a plasma cutter in order to obtain an approximate disk prepared for machining. Next a piece of 1 inch OD, 4 inch length

round stock will be machined so that it has a $\frac{1}{2}$ " tip of $\frac{1}{2}$ " diameter. At the center of the disc a $\frac{1}{2}$ " hole will be drilled using the drill press (See

Figure 80 below). The machined piece of round stock will then be inserted into the approximate disc and welded in place. Care must be taken to ensure that the rod protrudes at exactly 90° from the surface of the disc (See Figure 81 below).

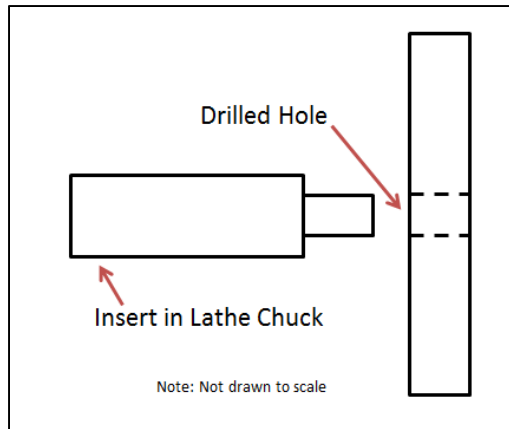


Figure 80: Flange Machining Step 1

This can be done through magnetic holders, tack welded, then turning the assembly on the lathe and checking for any visible wobble.

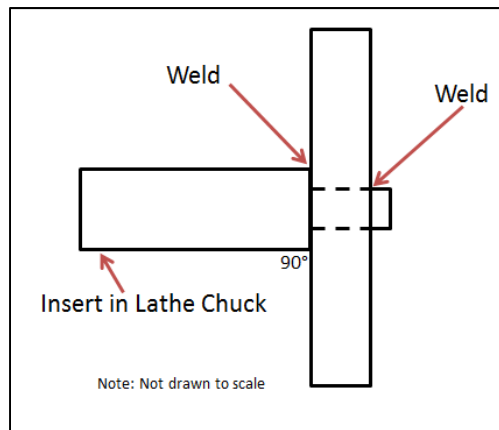


Figure 81: Flange Machining Step 2

The round stock end will then be placed in a lathe and the disc will be lathed down in increments of 0.05 inches until 0.02 inches remain for a final pass of 0.02 inches. Then a file will be used to remove burrs on the edges of the disc. The round stock will then be cut off, and a mill will be used in 0.05 inch increments to mill down each face of the disc to its final thickness. A hole will then be drilled in the center for the spindle using the mill. Using the SolidWorks drawing as a template the centers of each bolt hole will be marked on the disc and the holes drilled out again using the mill, then tapped with the drill press. A file will again be used to remove any burrs from the edges of the holes and the center hole. Scotch Brite will then be used to remove any marker remaining on the disc and clean up the surfaces of the disc.

Spindle

The spindle will be made from AISI8620 cold finished steel round stock of 3" outside diameter. The rough round stock will then be placed in the lathe. Two quick passes at a depth of 0.05 inches will be made to ensure the surface is round. Following the previous step, the output end of the spindle (to be located in the hub) will be lathed to near desired specifications. A hole will then be made in the end of the shaft and then later tapped using a drill press for the specified bolt to secure the spindle into the test rig (See Figure 82 below).

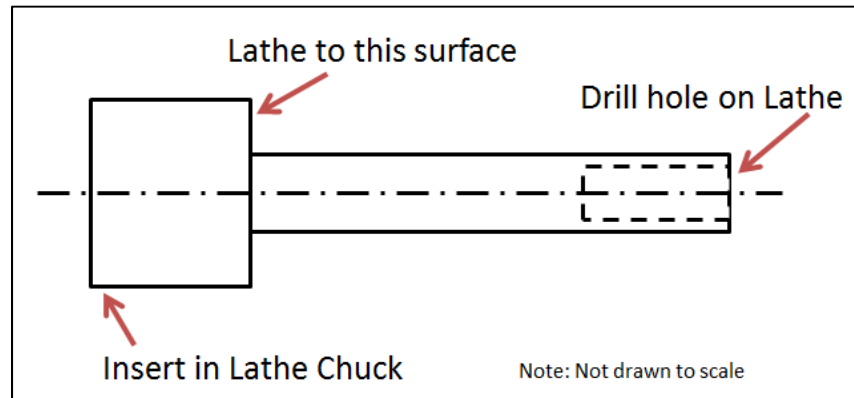


Figure 82: Spindle Machining Step 1

The round stock will then be flipped around, and the input end of the spindle (to be mated to the flange) will be machined to near desired specifications (See Figure 83 below).

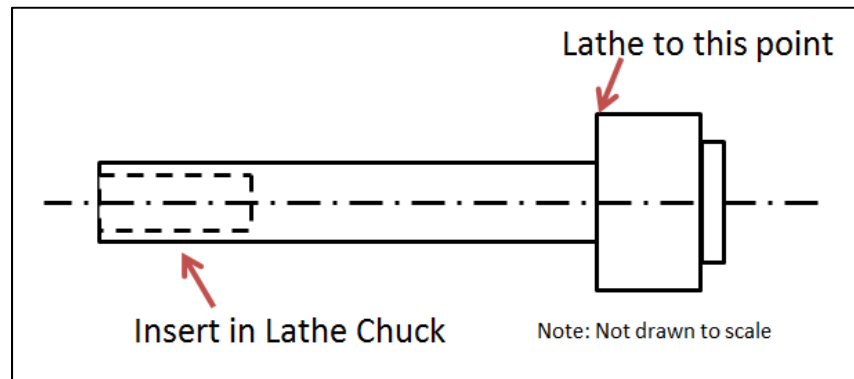


Figure 83: Spindle Machining Step 2

Next, the remaining round stock will be lathed down to near the desired diameter, and a finishing pass removing 0.02 inches will be made to achieve the required diameter of the spindle. Measurements will be taken to ensure all dimensions are exact and, if needed, additional passes of the lathe will be done to ensure exact specifications. A file will then be used to remove any burrs on the edges of the spindle.

Female Spline

The female spline section will consist of two parts, a female spline section to be purchased, as well as an adapter to attach to the tube yoke end of the Cornay® joint to which the female spline section will be attached. The adapter will be made from AISI8620 cold finished steel round stock of 3” outside diameter. The rough round stock will be placed in the lathe and the end which will house the tube yoke of the Cornay® joint will be machined first. This will require taking material only from the inside of the round stock (See Figure 84 below).

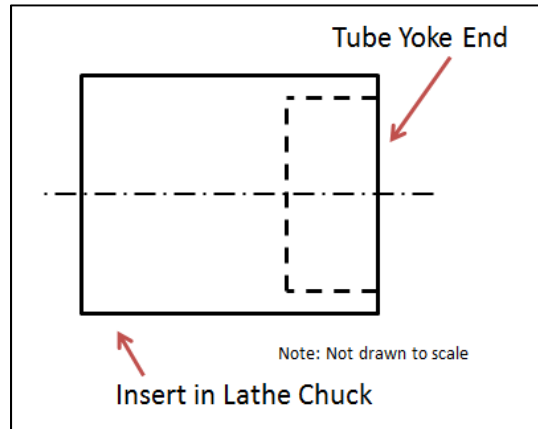


Figure 84: Female Spline Adapter Step 1

The round stock will then be flipped and the end to house the female spline will be machined next to specification. A hole will be machined through the entirety of this adapter at a dimension that matches the outside diameter of the female spline sleeve (See Figure 85 below).

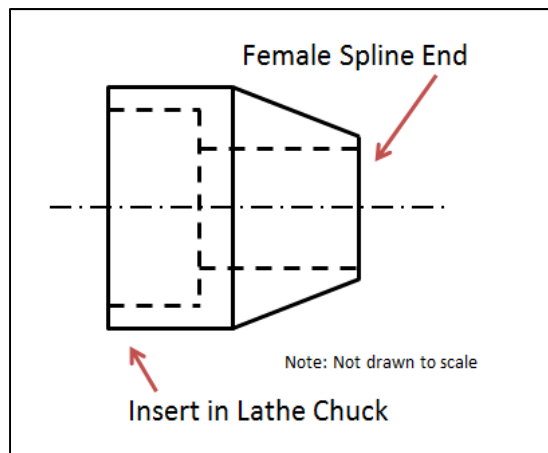


Figure 85: Female Spline Adapter Step 2

To mate these two parts, the female spline section will be inserted so that the back side lays flush with the end of the through hole that lies within the end of the adapter to be mated to the tube yoke of the Cornay® joint. This female spline will then be welded to the adapter inside

the opening for the tube yoke as well as around the exposed opposite end (See Figure 86 below).

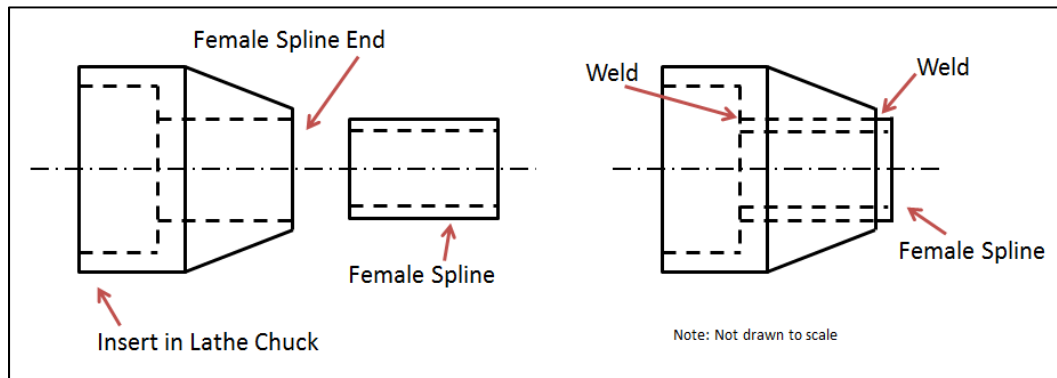


Figure 86: Female Spline Adapter Step 3

Male Spline

The male spline section will consist of three parts, both a male and female spline section to be purchased, as well as an adapter to attach to the tube yoke end of the Cornay® joint to which the splined parts will be attached. The adapter will be made from AISI8620 cold finished steel round stock of 3" outside diameter. The rough round stock will be placed in the lathe and the end which will house the tube yoke of the Cornay® joint will be machined first (See Figure 84 above). This will require taking material only from the inside of the round stock. The same steps taken to machine the female spline adapter above will be taken (See Figure 85, and Figure 86 above). This will allow for the male splined section to simply be inserted into the female section and welded from within the tube yoke end of the adapter (See Figure 87 below).

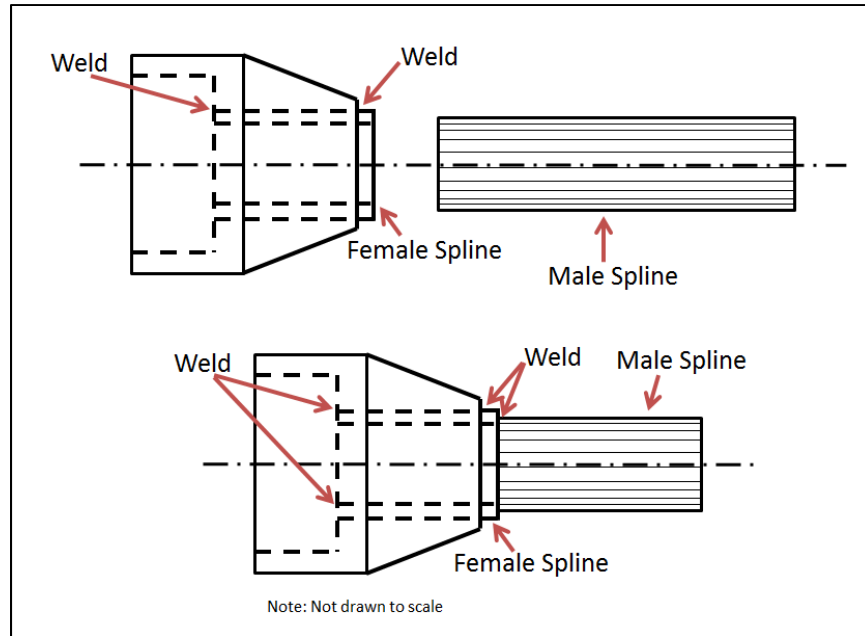


Figure 87: Male Spline Adapter

This process of assembly will eliminate the need to weld the male spline on the slip-section (facing the female spline adapter) thus preventing any lock-up as a result of the male spline over-inserting into the female adapter and jamming against the weld.

Cornay® Joints

The Cornay® joints will be received from Cornay® fully assembled. With the joints being pre-assembled from the manufacturer will leave two simple processes for assembly: welding of each spline adapter to their respective joints. As a result of the machining process of the spline adapters, they will simply slide onto the tube yoke ends of the Cornay® joint and be ready to weld (See Figure 88 below).

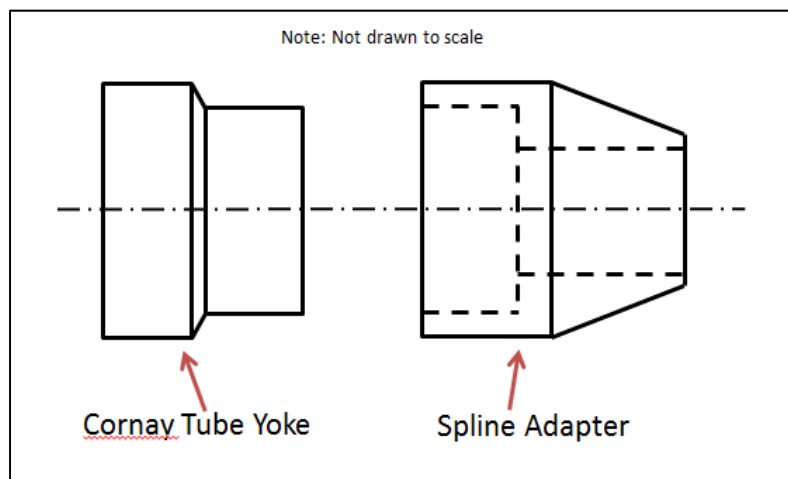


Figure 88: Tube Yoke to Spline Adapter

One weld bead will be run around the full circumference of the tube yoke at the location of the shoulder which will be butted against the end of the adapters (See Figure 89 below).

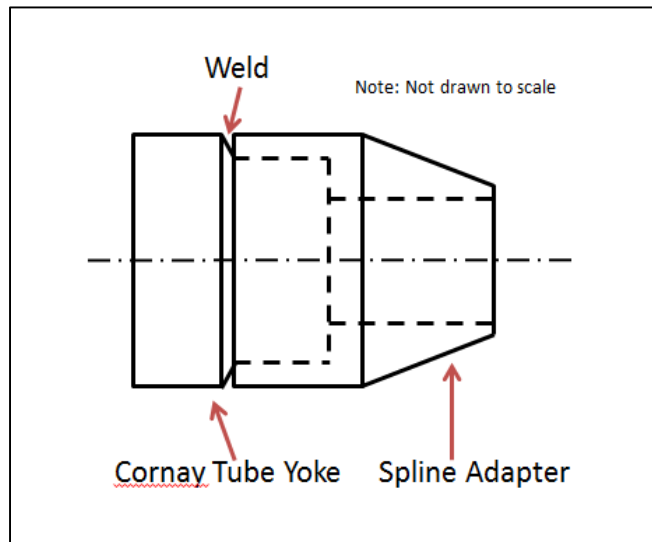


Figure 89: Tube Yoke to Spline Adapter Weld

Complete Assembly

From here, the only assembly remaining will be that of insertion and fastening. The male spline which is welded to the outer Cornay® joint will be inserted into the female spline which is welded to the inner Cornay® joint. Next the 4-bolt flange of the outer Cornay® joint will be bolted to the flange/spindle assembly using 7/16"-20 x 1.00" Grade 8 bolts. This will complete the full assembly of the prototype, which will render it complete for testing. To see a full assembly, please reference Figure 19 in Section 2.1.

4.4. Design for Manufacturing

The improved half-shaft assembly was designed with ease of manufacturing in mind. This is evident both in the implementation of purchased components and the design of the fabricated components.

Purchased Components

The purchased components of this assembly are the two Cornay® joints. These joints are identical except for the bolt patterns at their flanges. Although this difference means introducing an extra feature into the joints, it also ensures that there are no errors present in reinstallation of the joint after maintenance procedures. Once the splines are welded on the joints, the locations of the splined shafts are ensured according to the assembly detailed in Section 4.3, with the male spline at the outer joint and the female and the inner. If a technician were to remove and reinstall joints with a common bolt flange pattern, he may mistakenly assemble with the male spline at the inner joint, altering the geometry of the assembly. With different bolt pattern on each joint flange, this mistake is impossible to make.

Fabricated Components

All fabricated components of the prototype were designed such that they could be created using only the available tooling listed in Section 4.3. The fabricated components of the assembly are Flange 1, the spindle, and the splined shafts.

Flange 1

As stated above, Flange 1 was designed with a four-bolt pattern to ensure no confusion in assembly. This design eliminates the error of bolting the spindle to the inner Cornay® joint.

Spindle

The spindle was designed to simply mirror the current design and allow proper compatibility of the improved assembly with the vehicle. Note that for the production design, Flange 1 and the spindle are to be machined from one piece of stock, eliminating the need for the weld between the components necessary only for prototype fabrication. Reducing these parts to a common one eliminates overall design complexity and simplifies the fabrication of the part.

Splined Shafts

The final fabricated components, the splined shafts, exploited the design of the Cornay® tube yoke. By fabricating these components with a recessed section and allowing them to fit over the Cornay® tube yoke, the need to manually center these shafts before welding them to the Cornay® joints was eliminated. Eliminating the manual centering process greatly reduces the total assembly time of the improved half-shaft.

5. Prototype Testing

The prototype's suitability was tested in a fabricated test rig. This suitability was comprised of two criteria: fit into the vehicle and torque lost to rotating the shaft. The rig was created to recreate the geometry of the HMT 400/600 at various ride heights and steering angles. Installation of the prototype into the test rig therefore ensured a suitable fit into the actual vehicle. The second criteria, torque loss, conveys the prototype's efficiency by quantifying lost torque in rotating the half-shaft assembly. This criteria was tested at varying ride heights and steering angles. A description of the test rig and testing procedure is found below.

5.1. Test Design

The half shaft-assembly will be tested in the test rig shown in Figure 90 and Figure 91. This rig will mimic the Supacat HMT's half-shaft geometry at varying ride heights, testing both the assembly's vertical articulation and its steering angle.

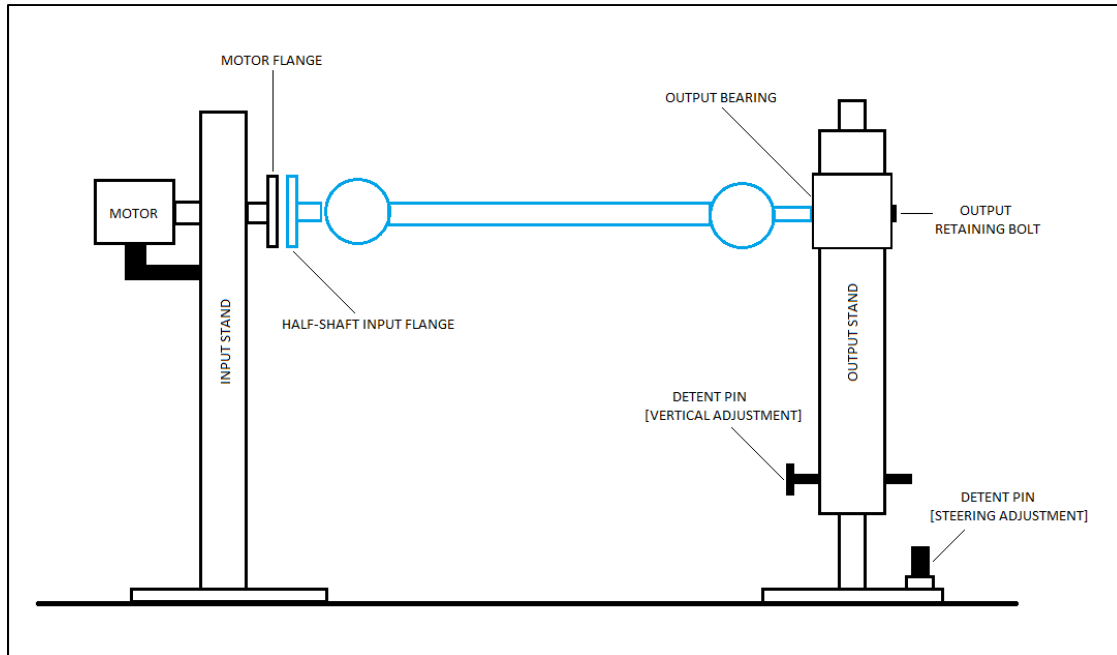


Figure 90: Side View of Test Rig

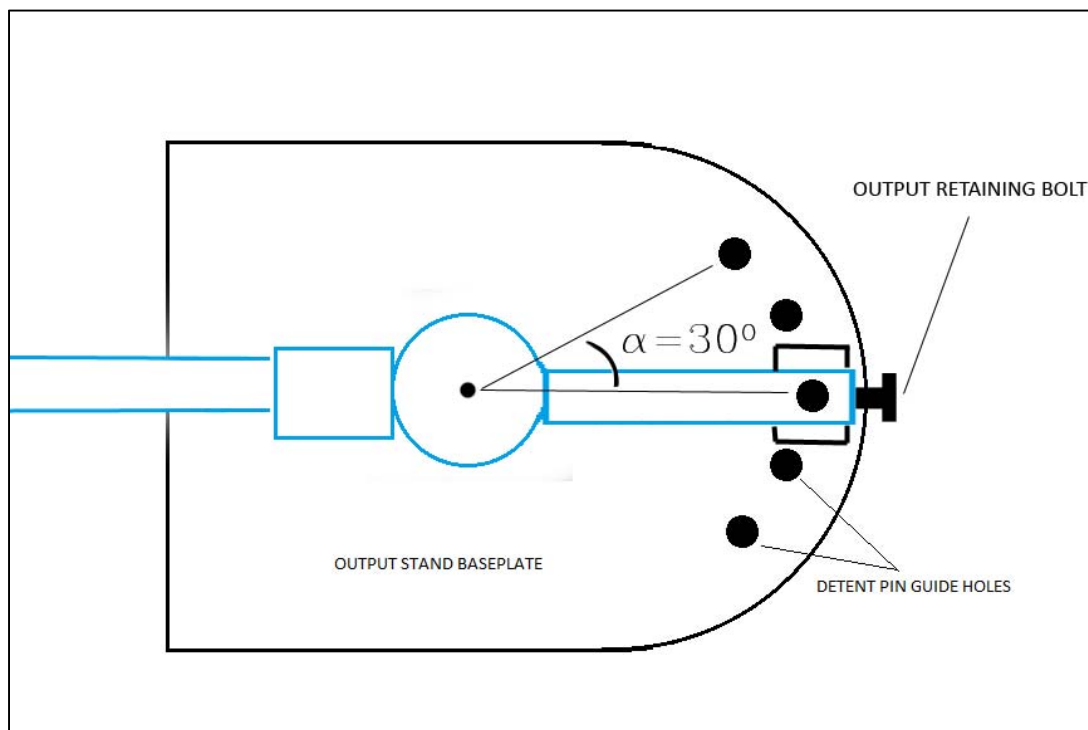


Figure 91: Top View of Test Rig

Test Rig Description

Once installed into the rig, the prototype will be driven by a motor attached to the input stand and connected to the prototype at its input flange. The output of the half-shaft will be bolted into the output bearing seen in Figure 90 on the output stand. This bolted connection is

identical to the one seen at the hub of the HMT. As seen in Figure 90, a sleeve on the output stand is allowed to move vertically to mirror the bump-stop, on-road, and off-road positions of the HMT. Figure 92 shows this vertical articulation. This sleeve is fixed in various vertical positions by the insertion of the detent pin for vertical adjustment into one of three guide holes, as seen in Figure 90 and Figure 92.

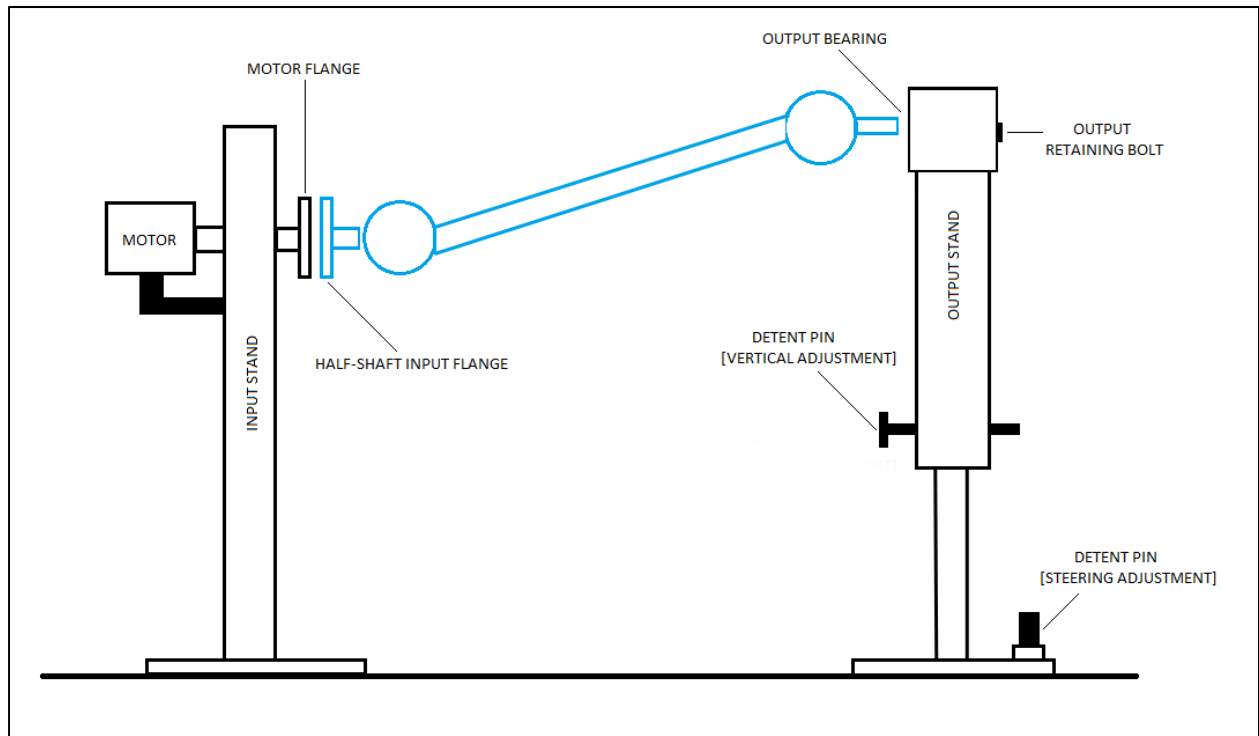


Figure 92: Side View of Test Rig - Vertically Articulated

The steering capability of the half-shaft is recreated by the design through the rotation of the output stand. Figure 91 and Figure 93 clearly show this function. The output stand, which is fixed to a steering alignment arm, is allowed to rotate about the center of the outer joint. The alignment arm, like the vertical adjustment sleeve, is locked into place by a detent pin inserted into one of five guide holes as seen in Figure 91 (zero steering angle) and Figure 93 (30° steering angle).

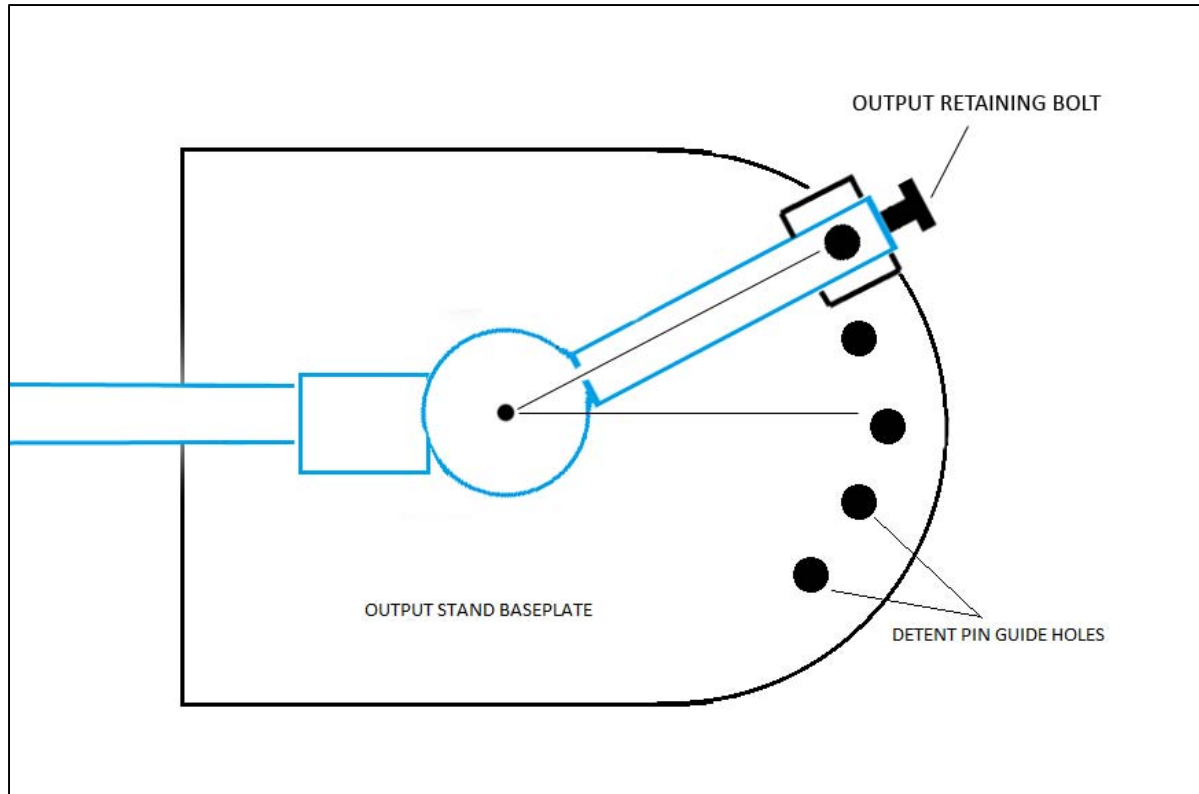


Figure 93: Top View of Test Rig - 30° Steering Angle

Testing Procedure

The testing procedure for the prototype will test the articulation ability of the half-shaft as well as give some idea of the required torque to drive the entire assembly at different suspension heights and steering angles. After installing the prototype into the test rig, the motor was driven with a constant voltage DC power supply. A timing-light was used to measure the half-shaft speed while the current provided to the motor was measured with a multi-meter. Below is the detailed test procedure followed:

1. Install the prototype into test rig by inserting the prototype output shaft into the output bearing and affixing it to the retaining bolt. Next, bolt the test rig input flange to prototype input flange.
2. At zero speed, test both vertical and steering articulation by inserting the two detent pins into the varying guide holes. Ensure proper motion and absence of binding.
3. At zero speed move the half-shaft to the bump-stop position and zero steering angle.
4. Start motor; use timing light to measure speed and use multi-meter to measure motor current.
5. Stop motor and increment the steering angle by 10° and repeat step 4.
6. Repeat steps 4 and 5 for the on-road position and the off-road position.

5.2. Statistical Analysis of Data

Below is the class data for the bump stop position.

Table 11: Shaft Speed and Current at Bump Stop

Team	Steering Angle	Speed (RPM)	Motor Current (A)
Ramrod	0°	608	3.5
	10°	608	3.5
	20°	608	3.5
	30°	606	3.5
Thundacats	0°	587	4.1
	10°	592	4.0
	20°	N/A	N/A
	30°	N/A	N/A
Gravity	0°	102	5.1
	10°	N/A	N/A
	20°	N/A	N/A
	30°	N/A	N/A

Chauvenet's Criterion was applied once to the shaft speed data above in order to eliminate outliers. This process involves calculating the initial mean value and standard deviation of the data set with N values:

$$x_m = \frac{1}{N} \sum_{i=1}^N x_i = 530.1429 \text{ rpm}$$

$$\sigma_{N-1} = \left\{ \frac{1}{N-1} \sum_{i=1}^N (x_i - x_m)^2 \right\}^{1/2} = 188.9907 \text{ rpm}, N < 20$$

Then d_i/σ for each data point was calculated, where $d_i = x_i - x_m$. These results are in Table 12. The error function is then calculated using the formula below:

$$P(z) = 1 - \frac{1}{2N} = 0.9286, \quad \frac{1}{2}P(z) = 0.4643$$

The $1/2P(z)$ value is used to look up a z value:

$$z \equiv \frac{d_{max}}{\sigma} = 1.81$$

Any data points with a d_i/σ value greater than the above z value is eliminated. The resulting data set is then used to find the class average.

Below is a table summarizing Chauvenet's Criterion for the shaft speed at the bump stop position:

Table 12: Chauvenet's Criterion for Shaft Speed at Bump Stop

Team	Steering Angle	Shaft Speed (RPM)	d/σ	Eliminate?	New Set
Ramrod	0°	608	0.411962875	no	608
	10°	608	0.411962875	no	608
	20°	608	0.411962875	no	608
	30°	606	0.401380342	no	606
Thundacats	0°	587	0.300846283	no	587
	10°	592	0.327302614	no	592
Gravity	0°	102	-2.265417865	yes	-
				Average:	601.5

The same procedure is applied to the current values at the bump stop position with the following results:

Table 13: Chauvenet's Criterion for Current at Bump Stop

Group	Steering Angle	Input Current (A)	d/σ	Eliminate?	New Set
Ramrod	0°	3.5	-0.647585678	no	3.5
	10°	3.5	-0.647585678	no	3.5
	20°	3.5	-0.647585678	no	3.5
	30°	3.5	-0.647585678	no	3.5
Thundacats	0°	4.1	0.359769821	no	4.1
	10°	4	0.191877238	no	4
Gravity	0°	5.1	2.038695652	yes	-
				Average:	3.6833

Below are the class results for the on-road articulation position:

Table 14: Shaft Speed and Current at On-Road

Team	Steering Angle	Speed (RPM)	Motor Current (A)
Ramrod	0°	628	3.0
	10°	621	3.1
	20°	621	3.1
	30°	619	3.2
Thundacats	0°	658	2.4
	10°	626	3.1
	20°	604	3.6
	30°	N/A	N/A
Gravity	0°	660	2.25

Design and Delivery of HMT Half-Shaft Prototype

	10°	642	2.6
	20°	624	2.7
	30°	N/A	N/A

Tables 15 and 16 below summarize the resulting data sets for the shaft speed and current data at the on-road position after applying Chauvenet's Criterion.

Table 15: Chauvenet's Criterion for Shaft Speed at On-Road

Team	Steering Angle	Shaft Speed (RPM)	d_i/σ	Eliminate?	New Set
Ramrod	0°	628	-0.12942835	no	628
	10°	621	-0.523340718	no	621
	20°	621	-0.523340718	no	621
	30°	619	-0.635887109	no	619
Thundacats	0°	658	1.558767515	no	658
	10°	626	-0.241974741	no	626
	20°	604	-1.479985041	no	604
Gravity	0°	660	1.671313906	no	660
	10°	642	0.658396387	no	642
	20°	624	-0.354521132	no	624
				Average:	630.3

Table 16: Chauvenet's Criterion for Current at On-Road

Team	Steering Angle	Input Current (A)	d_i/σ	Eliminate?	New Set
Ramrod	0°	3.0	0.231757108	no	3.0
	10°	3.1	0.475711959	no	3.1
	20°	3.1	0.475711959	no	3.1
	30°	3.2	0.71966681	no	3.2
Thundacats	0°	2.4	-1.231971997	no	2.4
	10°	3.1	0.475711959	no	3.1
	20°	3.6	1.695486213	no	3.6
Gravity	0°	2.25	-1.597904273	no	2.25
	10°	2.6	-0.744062295	no	2.6
	20°	2.7	-0.500107444	no	2.7
				Average:	2.905

Finally, the off-road position class data is shown below.

Table 17: Shaft Speed and Current at Off-Road

Team	Steering Angle	Speed (RPM)	Motor Current (A)
Ramrod	0°	621	3.1
	10°	620	3.2
	20°	620	3.1
	30°	615	3.1
Thundacats	0°	666	2.3
	10°	650	2.6
	20°	614	3.2
	30°	N/A	N/A
Gravity	0°	522	2.95
	10°	462	2.89
	20°	420	3.67
	30°	N/A	N/A

Below are also the resulting shaft speed and current data sets after Chauvenet's Criterion is applied.

Table 18: Chauvenet's Criterion for Shaft Speed at Off-Road

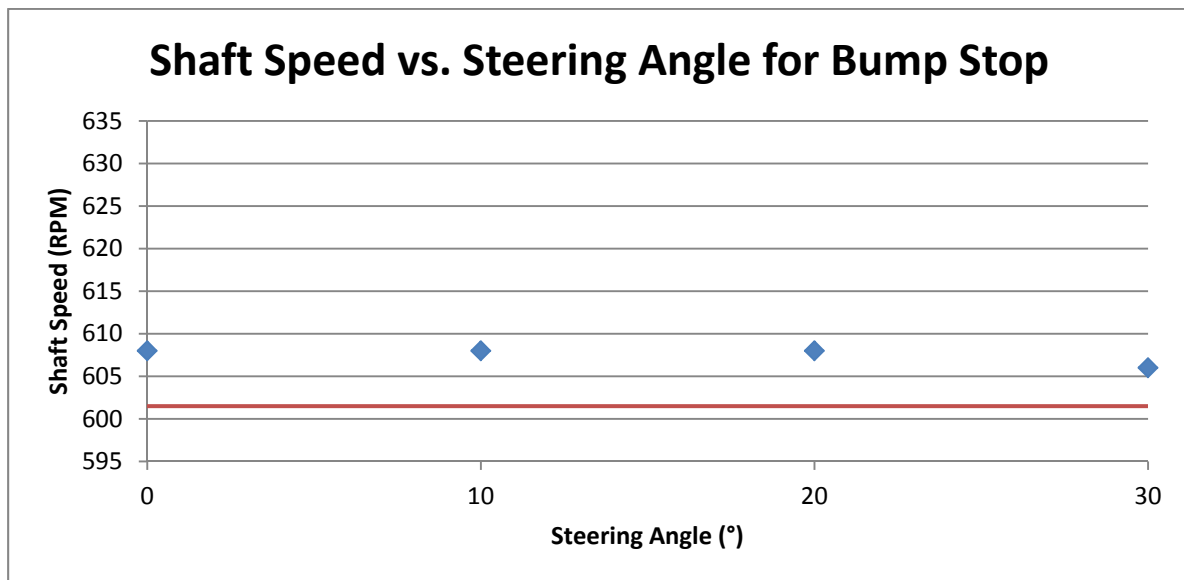
Team	Steering Angle	Shaft Speed (RPM)	d/σ	Eliminate?	New Set
Ramrod	0°	621	0.480245949	no	621
	10°	620	0.4682398	no	620
	20°	620	0.4682398	no	620
	30°	615	0.408209057	no	615
Thundacats	0°	666	1.020522641	no	666
	10°	650	0.828424262	no	650
	20°	614	0.396202908	no	614
Gravity	0°	522	-0.708362775	no	522
	10°	462	-1.428731698	no	462
	20°	420	-1.932989944	yes	-
				Average:	598.8889

Table 19: Chauvenet's Criterion for Current at Off-Road

Team	Steering Angle	Input Current (A)	d_i/σ	Eliminate?	New Set
Ramrod	0°	3.1	0.241503891	no	3.1
	10°	3.2	0.512856577	no	3.2
	20°	3.1	0.241503891	no	3.1
	30°	3.1	0.241503891	no	3.1
Thundacats	0°	2.3	-1.9293176	yes	-
	10°	2.6	-1.115259541	no	2.6
	20°	3.2	0.512856577	no	3.2
Gravity	0°	2.95	-0.165525139	no	2.95
	10°	2.89	-0.32833675	no	2.89
	20°	3.67	1.788214203	no	3.67
				Average:	3.09

Our data points are graphed below versus the steering angle with the class average shown as a horizontal line.

The three graphs below show our half-shaft's speed versus steering angle for the bump stop, on-road, and off-road positions. Because the voltage of the motor is a constant 24V, the speed of the shaft varies inversely with resistance. So when the speed of the shaft is higher, there is less resistance, heat, and friction present, which is favorable.

**Figure 94: Shaft Speed at Bump Stop Compared to Class Average**

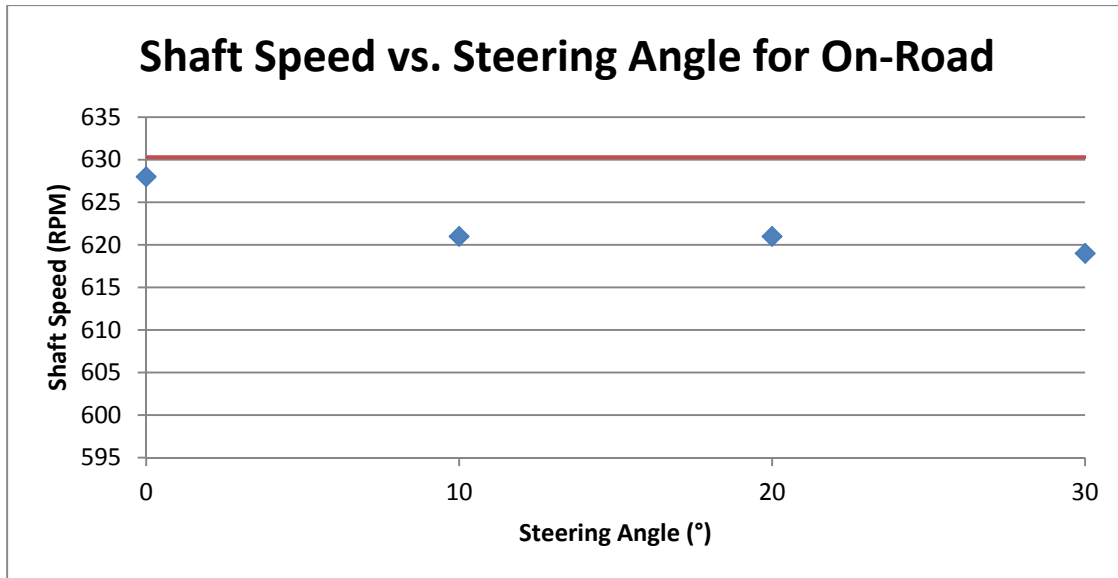


Figure 95: Shaft Speed at On-Road Compared to Class Average

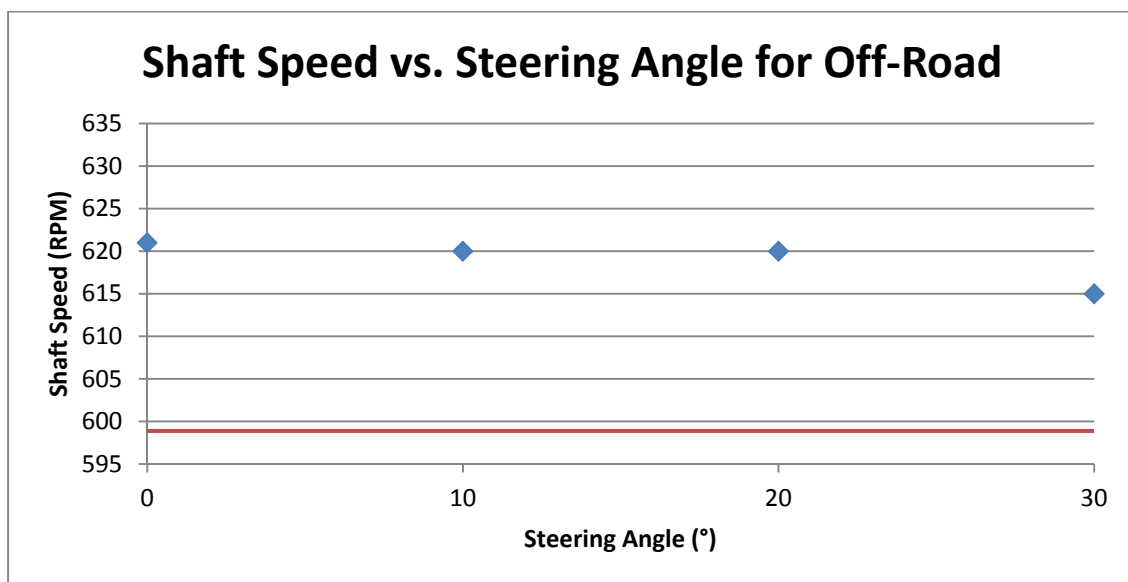


Figure 96: Shaft Speed at Off-Road Compared to Class Average

All three articulation angles have shaft speeds ranging from 606 rpm to 628 rpm. The on-road position has the highest speeds (619-628 rpm), then the off-road position (615-621 rpm), and followed by the bump stop position (606-608 rpm). The bump stop and off-road positions produced shaft speeds that were above the class averages at those articulation angles. At the on-road position, our shaft speeds were not far below the class average. It should also be noted that our shaft speeds did not vary much as the articulation angle changed, and varied even less as the steering angle changed. This shows that the Cornay® joints performed equally well at low angles, high angles, and angles in between.

The graphs below show our input current versus the steering angle for the same three articulation angles. The current going through the motor of the test rig is directly related to the torque required. Therefore, a lower current is desirable because it is more efficient.

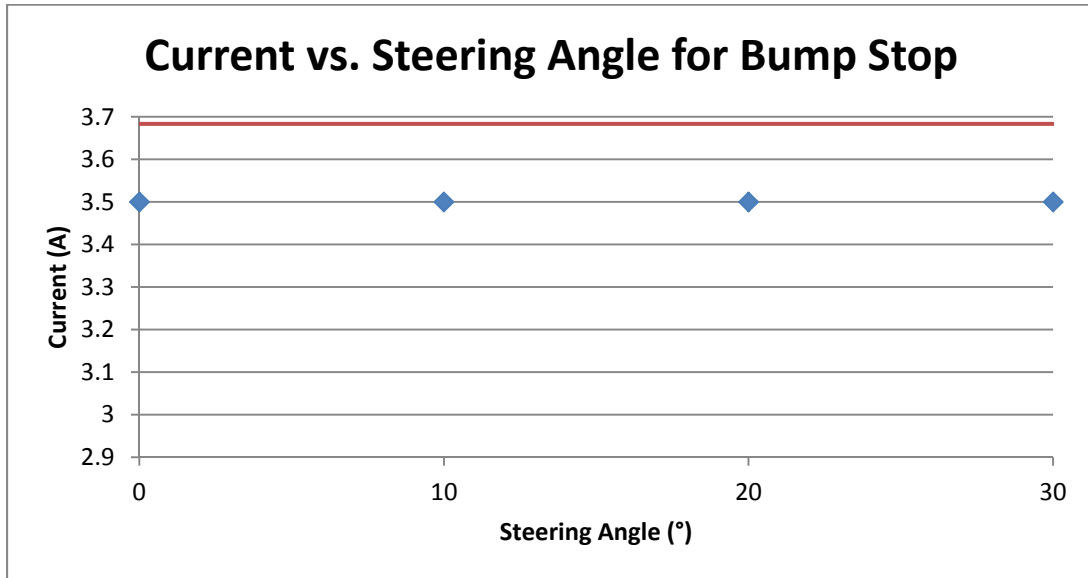


Figure 97: Current at Bump Stop Compared to Class Average

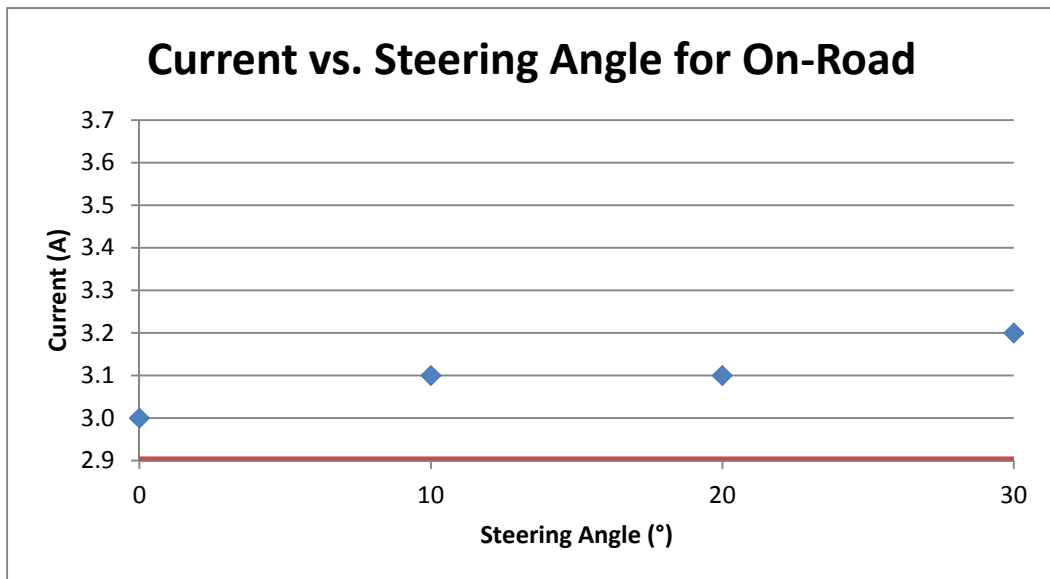


Figure 98: Current at On-Road Compared to Class Average

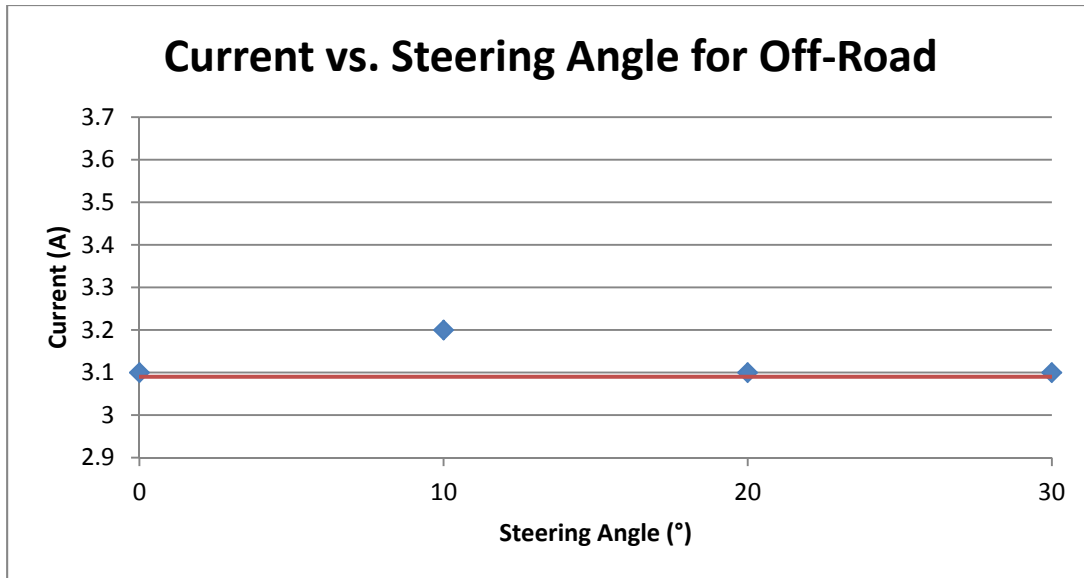


Figure 99: Current at Off-Road Compared to Class Average

The input current for the various articulation angles ranged from 3.0A to 3.5A. The current for the on-road and off-road positions were roughly equal (3.0-3.2A vs. 3.1-3.2A) and for the bump stop position, the current was at a constant 3.5A. The current is lower than the class average at the bump stop position, about equal at off-road, and slightly higher at on-road. Because these values were averaged from a fluctuating voltmeter by hand, the currents are not exact readings. If this test were performed again, software should be used to cancel out the noise we were seeing and capture more accurate data. However, these results agreed with the shaft speed data in that there was small to no variation in current as the shaft was articulated to different angles.

Overall, our half-shaft prototype tested well at all the required angles, resulting in consistently high speeds and low currents. These results indicate an efficient half-shaft design with low friction, resistance, and heat.

6. Economics/Cost

6.1. General Economics

Current Rzeppa Design Cost

The current cost of the half-shaft assembly is tabulated below.

Table 20: Current Design Cost

Mechanism	Cost per Unit	Quantity	Total Cost
Driveshaft Assembly	\$2115.00	1	\$2115.00
		Total Cost:	\$2115.00

There is also a maintenance kit that contains a replacement outboard sleeved boot. The total cost of this kit is \$317.00 and will be used in the cost analysis section. Note that all prices for the current design include labor costs.

Recommended Design Cost

The cost of the improved half-shaft assembly is made up of mechanism costs and raw material costs. The cost for the mechanisms comprising the design and the materials for all of the components manufactured in house can be seen below in the “Recommended Design Cost” Table 21. Note that although this does not include the labor and assembly costs, the cost for the joints is high due to it being in pre-production phase. This price will decrease significantly if the part reaches the production phase and, therefore, the current cost of the joint absorbs the labor costs.

Table 21: Recommended Design Cost

		Description	Cost per Unit	Quantity	Total Cost
Mechanism	CV Joint	Cornay® CVX-50	\$2,500.00	2	\$5,000.00
	Male Spline	1.128” OD (1062-20-2-117) 12” L	\$18.00	1	\$18.00
	Female Spline	2” OD (BS-1062-20-2-1215) 2” L	\$17.42	2	\$34.84
	Inner Bolts	M8x1.25x25 mm, Grade 8.8	\$0.1731	6	\$1.04
	Inner Lock Washers	8 mm	\$0.0357	6	\$0.21
	Outer Bolts	7/16”-20x1”, Grade 8	\$0.2650	4	\$1.06
	Outer Lock Washers	7/16”	\$0.0579	4	\$0.23
	Splined Shaft Boot	3” ID	\$46.57	1	\$46.57
	Metal Clamps	3” D	\$0.51	2	\$1.02
Material	AISI 8620 Hot Rolled 1/2” Plate	12” x 12”	\$80.32	1	\$80.32
	AISI 8620 Cold Finished 3” Rod	12” L	\$41.44	1	\$41.44
				Total Cost:	\$5224.73

Each Cornay® CVX-50 joint has an approximate cost of \$2,500. These joints are in a pre-production stage and machined from solid stock making the cost at this time rather expensive. The price per unit would decrease significantly if the part were to reach the production phase.

All material price projections were taken from the vendors we purchased the material from.

Cost Analysis

A total cost equation for one half-shaft was found for each of the half-shaft designs using the total cost of each as the fixed costs. The maintenance costs were used as the variable costs.

For the current design, the maintenance cost was found using a life of 1600 miles, a boot replacement rate of 50% and a complete shaft failure rate of 50%. So the average of the boot repair kit cost (\$317.00) and the half-shaft assembly cost (\$2115.00) is the variable cost per 1600 miles. This results in the following equation for the total cost of the current design:

$$y[\text{cost}] = \$2115.00 + \left(\frac{\$1216.00}{1600 \text{ miles}} \right) x[\text{miles}] \quad (69)$$

For the recommended design, the maintenance cost was found using an estimated life of 10,000 miles. The half-shaft assembly cost (\$5224.73) is the variable cost per 10,000 miles. This results in the following equation for the total cost of the recommended design:

$$y[\text{cost}] = \$5224.73 + \left(\frac{\$5224.73}{10,000 \text{ miles}} \right) x[\text{miles}] \quad (70)$$

Graphing these equations below in Figure 100 shows the intersection of the two lines, which is the break-even point (at 13,092 miles). After this point, using our recommended design saves the sponsor money compared to the current design.

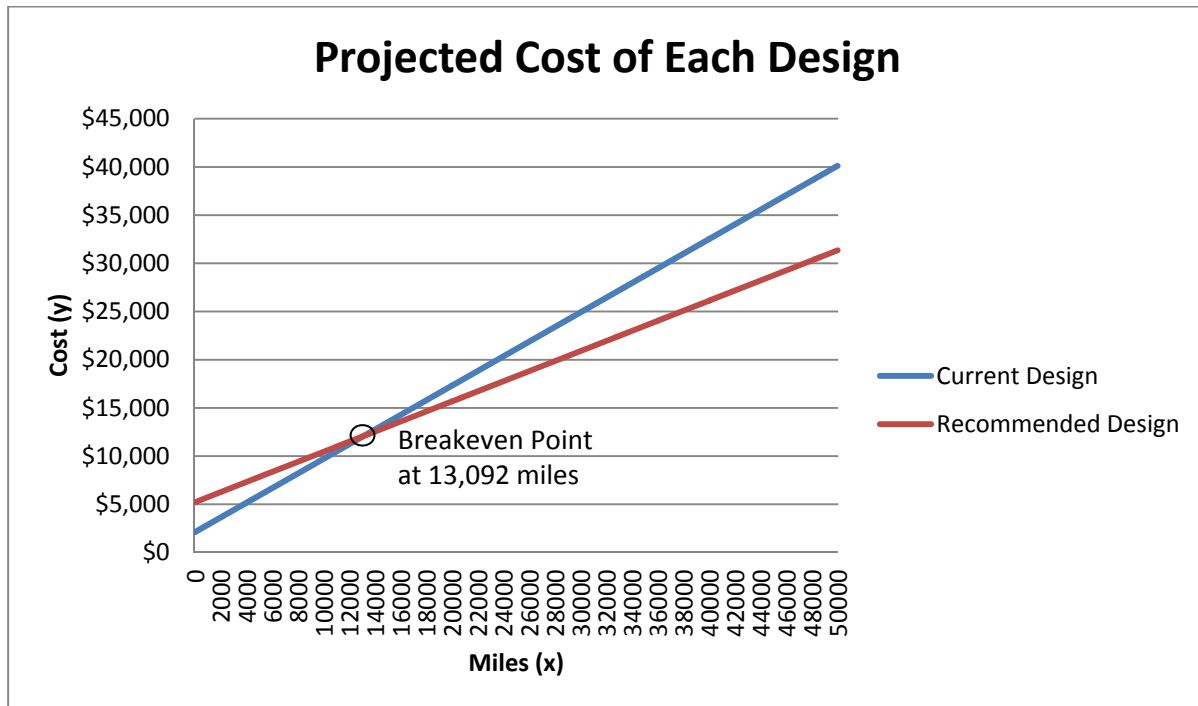


Figure 100: Break-even Chart

The increased life-span of the recommended design over the current design would result in a savings of \$8766.62 for each half-shaft over a period of 50,000 miles.

6.2. Cost

The total cost of the prototype is detailed below in Table 13. All the receipts of the materials purchased were turned in as the components were purchased.

Table 22: Prototype Cost

		Description	Cost per Unit	Quantity	Line Total
Mechanism	CV Joint	Cornay® CVX-50	\$0.00	2	\$0.00
	Male Spline	1.128" OD (1062-20-2-117) 12" L	\$9.00	1	\$9.00
	Female Spline	2" OD (BS-1062-20-2-1215) 2" L	\$8.71	2	\$17.42
	Inner Bolts	M8x1.25x25 mm, Grade 8.8	\$0.1731	9	\$1.56
	Inner Lock Washers	8 mm	\$0.0357	96	\$3.43
	Outer Bolts	7/16"-20x1", Grade 8	\$0.2650	25	\$6.63
	Outer Lock Washers	7/16"	\$0.0579	25	\$1.45
Material	AISI 8620 Hot Rolled 1/2" Plate	12" x 12"	\$80.32	1	\$80.32
	AISI 8620 Cold Finished 3" Rod	12" L	\$41.44	3	\$124.32
Tools	Tap	8 mm-1.25	\$7.98	1	\$7.98
				Sub-Total	\$252.11
				Tax	\$1.42
				Shipping and Handling	\$84.52
				Total	\$338.05

7. Quality Engineering

7.1. Deliverables

- (4) – Group Presentations
 - Feasibility Study
 - Preliminary/Critical Design
 - Detailed Design
 - Final Design
- (5) – Feasible Design Solutions
- (5) – Engineering Notebooks
- (3) – Reports

- Preliminary/Critical Design
- Detailed Design
- Final Design
- (1) – Prototype
- Detailed Shop Drawings

7.2. Safety

Safety is a vital part of any engineering project because if the design, assembly or manufacturing process is remotely unsafe than the costs are dramatically increased as well as liability. Each member of the design team at N.C. State has been certified in a respective field, whether welding, machining or fabrication. The weldors have completed a training course involving the use of machine operation and the practice of MIG, TIG and Stick welding as well as the use of a plasma cutter. The machinist was certified on both the lathe and mill. The shop fabricators were trained a variety of tools including a band saw, drill press and various grinders to accomplish sanding, tapping, drilling, cutting and grinding. If at any point anyone is using equipment they are not certified on or not following the safety guidelines listed below their badge will be punched. After three punches they are banned from the shop.

Required Attire:

- Safety glasses or face shield if necessary
- Long pants
- Close-toed, non-canvas shoes (safety-toed shoes preferable)
- No long sleeves
- No loose or baggy clothing
- No dangling jewelry
- Pull back long hair in a band and tuck into collar or hat
- No gloves while machining
- Do not wear highly flammable clothing
- Welding gloves, jacket and mask (FOR WELDING ONLY)

Required Procedures:

- Never look away from your work while tool or machine is on
- Turn off machinery anytime you are not at the machine
- Do not operate machinery or tools while ill, taking strong medication or under the influence of other drugs or alcohol
- Keep workspace clean and neat
- Do not use a tool in any manner it was not intended
- Make sure work is secured before attempting to work on it, especially metal and while lathing
- No food or drink
- No smoking

The manufacturer should also follow these standard guidelines as well as OSHA regulations while making these individual parts.

During assembly and installation of the half-shaft gloves and eye protection should be worn at all times. Goggles are needed to prevent debris from entering the eyes during the removal of the previously installed half-shaft and the installation of the new half-shaft. Gloves are required to prevent cuts and contusions due to sharp metal objects and tight clearances during removal and installation. Also long sleeves are recommended to prevent cuts to the wrist and arms during the removal and installation process.

7.3. Impact on Society

This Senior Engineering Design Project, like many others, has a profound effect on several fronts. Primarily, as this project is an educational venture, the student and engineering group gain an invaluable amount of knowledge regarding mechanical engineering, design, and manufacturing. Upon the completion of the project the student learns how to take the bulk of their engineering education and apply it to real world scenarios. The student learns how to take an engineering problem and find a solution through methods of teamwork, brainstorming, feasibility studies, mechanical design, prototyping, assembly, testing and debugging. This is made possible through the College of Engineering at NC State University, and its vast resources.

The second beneficiary to this project is the University itself. Through partnerships, such as this one with the USASOC, the University is able to further its reputation in the engineering community. This would not be possible without the already incredible reputation of the University, but this works as a perpetual machine towards improving relationships with outside companies and contractors while also benefitting the students. The education that NC State provides, along with the mechanical resources such as the MAE416 laboratory where the prototyping for this course was realized, the students gain the skills to better prepare them for futures in Mechanical Engineering and Management fields. The success that the students will encounter in their professional fields will ultimately come back to the University, solidifying its reputation and future partnerships in the Engineering community.

Lastly the partnered company, in this instance the USASOC, gains valuable engineering work and problem solutions that are eligible for implementation in real world applications. Specific to this project, the USASOC plays a vital role in National Security as well as the protection of our troops overseas. This partnership is different from other Engineering Design projects in that the partnered company does not gain specific profits as a result, but that the outcome is one that helps to protect the sole reason why we are able to have this educational opportunity in the first place. It also benefits the entire public as well by allowing anyone else to have the same opportunity to learn, gain valuable experience and ultimately allow them to provide for themselves as well as their respective universities and companies.

In summary, this project is beneficial to the students, the University, the USASOC and our military, as well as helps to solidify the reason we, as students, are able to have this opportunity. Going forward this wheel of education, partnership and experience, will continue to revolve providing invaluable opportunities for students, companies, and the University alike.

7.4. Ethics

Throughout the engineering education at NC State University, students learn the vital role that ethics plays in education as well as everyday life and the professional society. It was absolutely necessary for the group to maintain an ethical approach throughout all stages of this project. The following is a brief overview of the aspects of the project and the ethical requirements that were met:

- Provide a viable solution to the problem presented by the USASOC that will be feasible for implementation and fall within the specification requirements
- All incorporated designs that were not realized by the team were given credit to their respective owners
- The design of the half-shaft itself was scrutinized to maintain full functionality of the proposed design
- All sources of outside information were cited appropriately and credit given to their respective authors

Throughout the project, the main guideline for ethical practices was taken from the National Society of Professional Engineers Code of Ethics. The Fundamental Canons, which follow, give a brief outline:

“Engineers, in the fulfillment of their professional duties, shall:

1. Hold paramount the safety, health, and welfare of the public.
2. Perform services only in areas of their competence.
3. Issue public statements only in an objective and truthful manner.
4. Act for each employer or client as faithful agents or trustees.
5. Avoid deceptive acts.
6. Conduct themselves honorably, responsibly, ethically, and lawfully so as to enhance the honor, reputation, and usefulness of the profession.”⁸

It was paramount that Team Ramrod follow these guidelines to ensure all aspects of this project resulted in the most appropriate outcome, as well as all team members gain the most from this project without taking anything away from the functionality of the design, the University, other team members, other groups or students, or the USASOC.

8. Concluding Remarks

The shortcomings of the Supacat HMT 400/600’s current half-shaft assembly have made themselves evident through the high failure rate of CV boots. These failures prompted the development of an improved, bootless design intended to increase product life and robustness.

The decision to pursue the design outlined above did not come about without the investigation of alternative solutions. These included dual cardan joints, Thompson couplings, and alternative boot designs. Ultimately, the dual Cornay® joints were deemed superior for the application, with their high range of articulation and torque capacity.

The dual Cornay® joint configuration detailed in this report has many advantages over the current design. Most importantly, the catastrophic boot failure problem has been solved. With the implementation of twin bootless joints, there is no potential for lubricant loss due to extreme

thermal conditions or abrupt impact caused by debris. The increase in reliability, in combination with the advantage of the design's relative ease of installation and removal, means less vehicle down time and higher confidence in performance over questionable terrain. Equally important are the financial savings associated with this design. Savings projections of \$8766.62 over 50,000 miles for each half-shaft were found, along with a break-even point of only 13,092 miles.

The proposed design, combined with a joint geometry redesign or variations in vehicle suspension components, provide an excellent solution to the Supacat HMT 400/600's boot joint failure problem.

Despite its advantages, the proposed design does have its drawbacks, particularly in fitment. The joint model used for the prototype fails to fit into the HMT's suspension assembly without considerable modification. The Cornay® joints being used are off-the-shelf models, Cornay® would be able to manufacture and design a proprietary joint for the use particularly for the HMT 400 to fix the clearance issues without modifying the suspension. Combined with stronger components, a smaller design with similar torque capacity is feasible. Another means of addressing the fitment problem is through a redesign of a few suspension components of the vehicle, particularly the pushrod assembly, which limits available assembly space currently. This redesign could allow the prototype to be installed into the HMT 400/600 without interference to suspension components.

References

1. "Cornay CVX-50 Fact Sheet." *Cornay*. Cornay Company, n.d. Web. 13 Oct 2011. <http://www.cornay.com/pdfs/Cornay_CVX-50_fact_sheet.pdf>.
2. "Constant Velocity Joint." *Wikipedia*. Wikimedia, 12 Oct 2011. Web. Sept 2011. <http://en.wikipedia.org/wiki/Constant-velocity_joint>.
3. Oberg, Erik, Franklin D. Jones, Holbrook L. Horton, and Henry H. Ryffel. *Machinery's Handbook*. 27th ed. New York: Industrial Press Inc., 2004.
4. *Universal Joint and Driveshaft Design Manual: Advances in Engineering Series*. No. 7. Warrendale, PA: Society of Automotive Engineers, Inc. 1979.
5. Thompson, Glenn Alexander. "Constant velocity coupling and control system therefor." US Patent 7144326. 5 Dec. 2011
6. "Thompson Constant Velocity Joint (TCVJ) 2C - 15 Specification." *Thompson Couplings Limited*. 2009. Thompson Couplings Limited. 8 Sept. 2011. <<http://www.thompsoncouplings.com/documents/pdf/Product%20Drawings/2C-15%20Drawing.pdf>>.
7. "Universal Joint Couplings for Joint Applications: Parts and Assemblies." *Spicer Parts*. Aug. 1981. Dana Holding Corp. 8 Sept. 2011. <<http://www2.dana.com/pdf/IJ900.pdf>>.
8. "Universal Joint Kits and Center Bearings for Passenger Cars and Trucks." *Spicer Parts*. May 2008. Dana Holding Corp. 15 Sept. 2011. <<http://www2.dana.com/pdf/K350-1-DSSP.pdf>>.
9. "Rzeppa joint." The Free Dictionary. 14 Oct. 2011. Farlex. <<http://encyclopedia2.thefreedictionary.com/Rzeppa+joint>>.
10. Cason, Rick. Telephone Interview by Brandon Novak. October 2011.
11. Jaynes, Jesse. High Angle Driveline. Phone Interview. 19 Sept. 2011.
12. Matt and David Craddock. Brakes, Inc. Personal Interview. 27 Sept. 2011.
13. ZAGG | *InvisibleSHIELD* | *IPhone, iPod Cases, Screen Protectors, Covers, Shields, Skins*. Web. 21 Oct. 2011. <<http://www.zagg.com/>>.
14. "File:UJoint1.png." *Wikipedia, the Free Encyclopedia*. Web. 21 Oct. 2011. <<http://en.wikipedia.org/wiki/File:UJoint1.png>>.
15. "Figure 28-7. Tracta Constant Velocity Joint." *Repair and Maintenance Manuals - Integrated Publishing*. Web. 21 Oct. 2011. <<http://www.tpub.com/content/automotiveenginemechanics/TM-9-8000/TM-9-80000560.htm>>.
16. Budynas, Richard G. and Keith Nisbett. *Shigley's Mechanical Engineering Design*. 9th ed. New York: McGraw-Hill. 2010.
17. "Boot Kits & Lubrication." *Curtis Universal*. Curtis Universal Joint Company, n.d. Web. 19 Oct 2011. <<http://www.curtisuniversal.com/boot-kits-and-lubrication.html>>.
18. "Spicer 212059X." *Northern Drivetrain*. Northern Drivetrain, LLC, n.d. Web. 19 Oct 2011. <<http://www.northerndrivetrain.com/product/SPI-212059X.html>>.
19. "Bellows for Universal Joints." *McMaster-Carr*. McMaster-Carr, n.d. Web. 17 Oct 2011. <<http://www.mcmaster.com/#universal-joint-boots/=ekufqf>>.
20. "Metal Clamp, 3 inch." *Hardware World*. Hardware World, n.d. Web. 19 Oct 2011. <<http://www.hardwareworld.com/Metal-Clamp-3-inch-p38H28M.aspx>>.
21. Cantrell, Sean. "RE: NCSU MAE 416: Cost of Current Half-Shaft." Email to Eric Boros. 17 Oct 2011.

22. Newnan, Donald G., Ted G. Eschenbach, and Jerome P. Lavelle. *Engineering Economic Analysis*. 11th ed. New York: Oxford University Press, Inc. 2011.

Appendices

A1: Bolt Grade Markings and Strength Chart from K-T Bolt Manufacturing Inc.

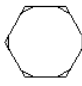

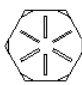


Head Markings	Grade or Class	Material	Nominal Size Range (Inches)	Mechanical Properties		
				Proof Load (psi)	Minimum Yield Strength (psi)	Minimum Tensile Strength (psi)
American Bolts						
 No Markings	Grade 2	Low or Medium Carbon Steel	1/4 thru 3/4	55,000	57,000	74,000
			Over 3/4 thru 1-1/2	33,000	36,000	60,000
 3 Radial Lines	Grade 5	Medium Carbon Steel, Quenched and Tempered	1/4 thru 1	85,000	92,000	120,000
			Over 1 thru 1-1/2	74,000	81,000	105,000
 6 Radial Lines	Grade 8	Medium Carbon Alloy Steel, Quenched and Tempered	1/4 thru 1-1/2	120,000	130,000	150,000
Stainless markings vary. Most stainless is non-magnetic	18-8 Stainless	Steel alloy with 17-19% Chromium and 8-13% Nickel	1/4 thru 5/8		40,000 Min. 80,000 – 90,000 Typical	100,000 – 125,000 Typical
			3/4 thru 1		40,000 Min. 45,000 – 70,000 Typical	100,000 Typical
			Above 1			80,000 – 90,000 Typical
Metric Bolts						
 8.8	Class 8.8	Medium Carbon Steel, Quenched and Tempered	All Sizes thru 1-1/2	85,000	92,000	120,000
 10.9	Class 10.9	Alloy Steel, Quenched and Tempered	All Sizes thru 1-1/2	120,000	130,000	150,000
Stainless markings vary. Most stainless is non-magnetic	A-2 Stainless	Steel alloy with 17-19% Chromium and 8-13% Nickel	1/4 thru 5/8		40,000 Min. 80,000 – 90,000 Typical	100,000 – 125,000 Typical
			3/4 thru 1		40,000 Min. 45,000 – 70,000 Typical	100,000 Typical
			Above 1			80,000 – 90,000 Typical
Tensile Strength: The maximum load in tension (pulling apart) which a material can withstand before breaking or fracturing. Yield Strength: The maximum load at which a material exhibits a specific permanent deformation Proof Load: An axial tensile load which the product must withstand without evidence of any permanent set.						

Figure 101: Bolt Grade Markings and Strength Chart

A2: Cornay Drawing

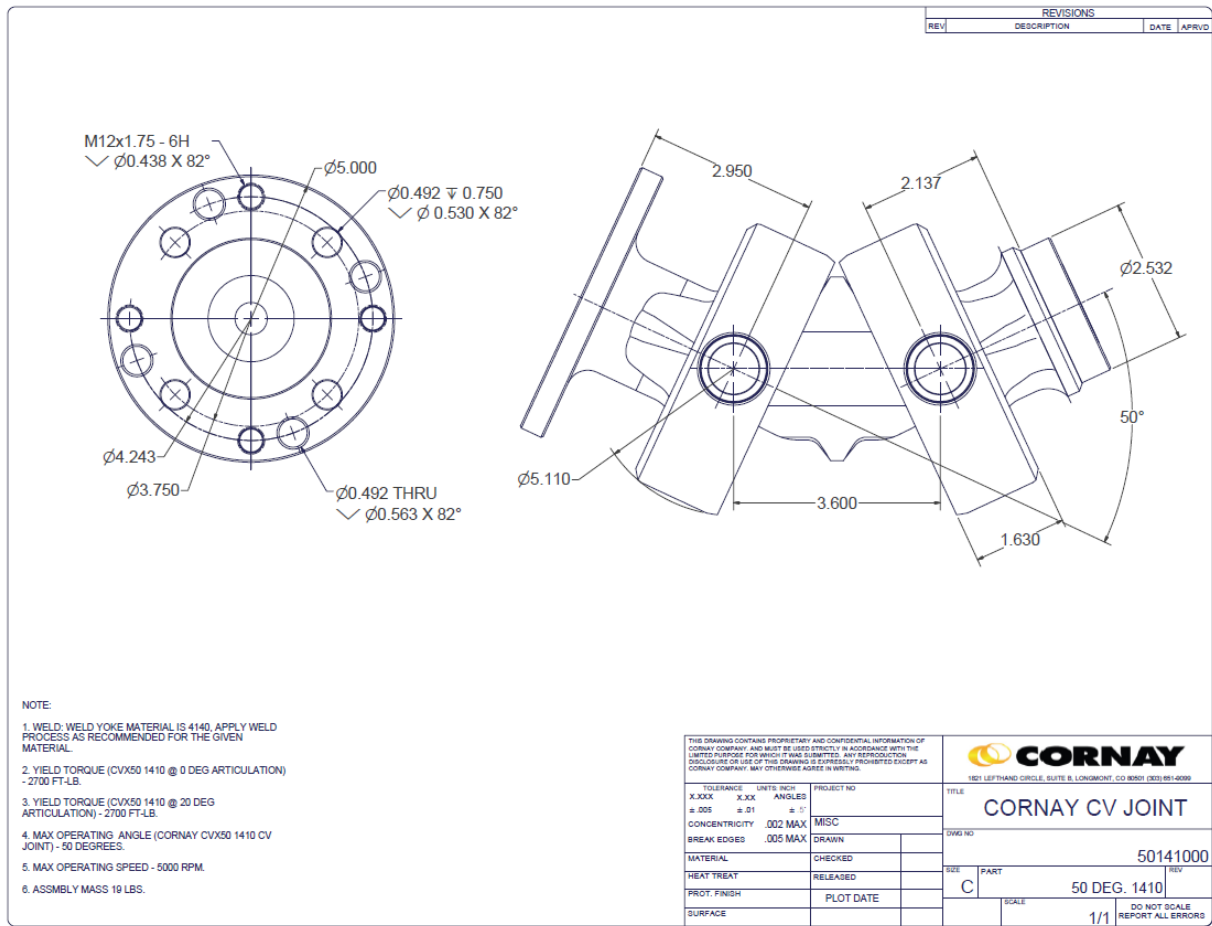


Figure 102: Cornay Joint Drawing

A3: Shop Drawings

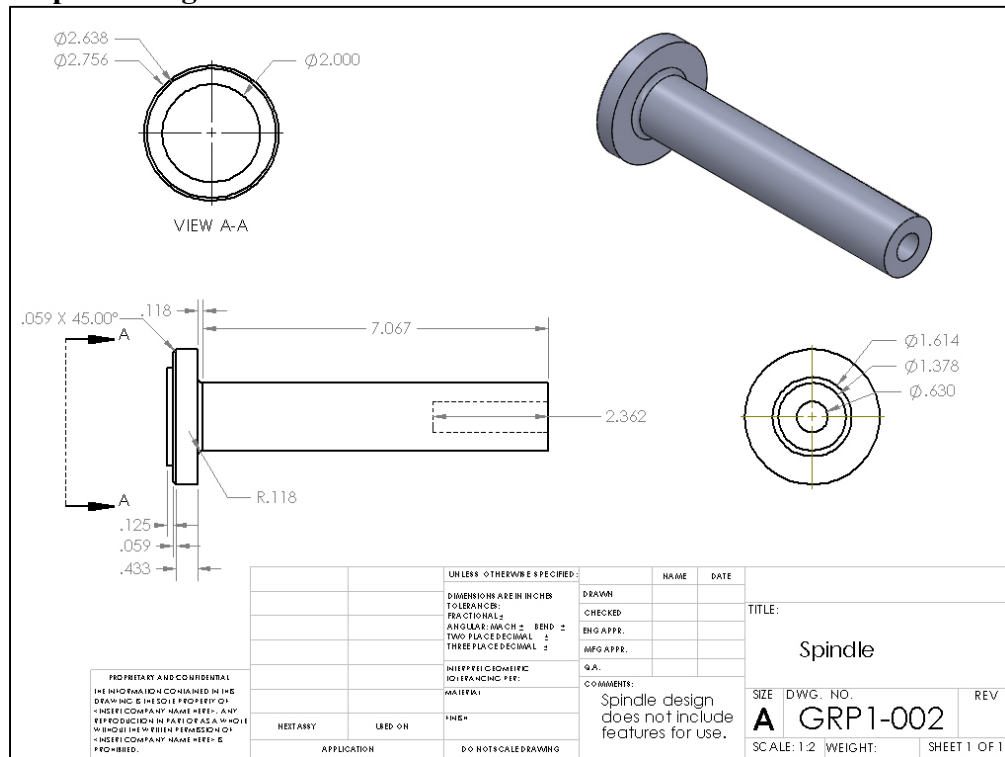


Figure 103: Spindle Drawing

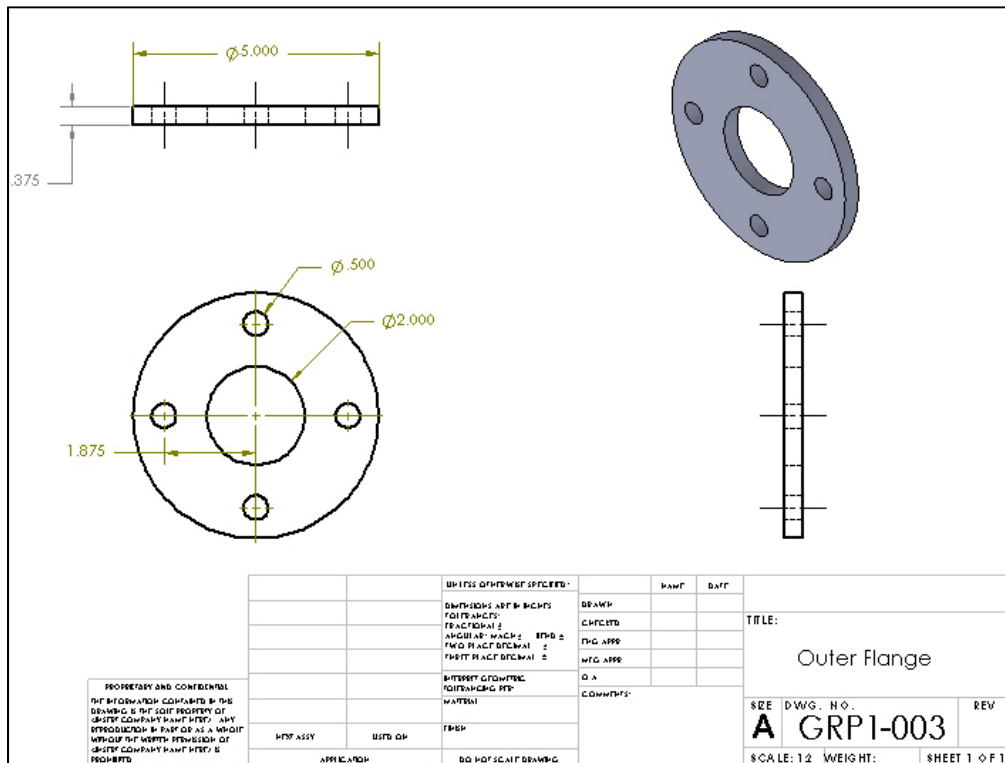


Figure 104: Outer Flange Drawing

Design and Delivery of HMT Half-Shaft Prototype

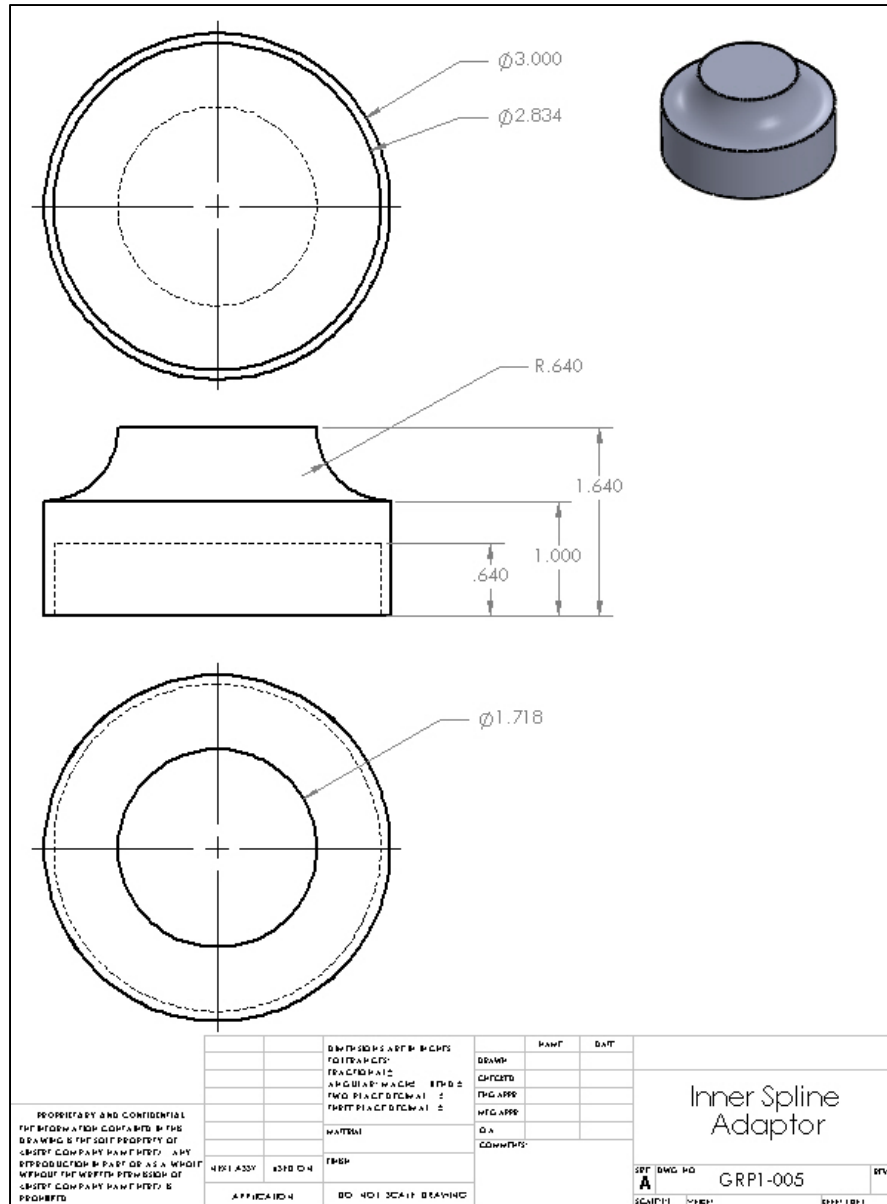


Figure 105: Inner Spline Adaptor Drawing

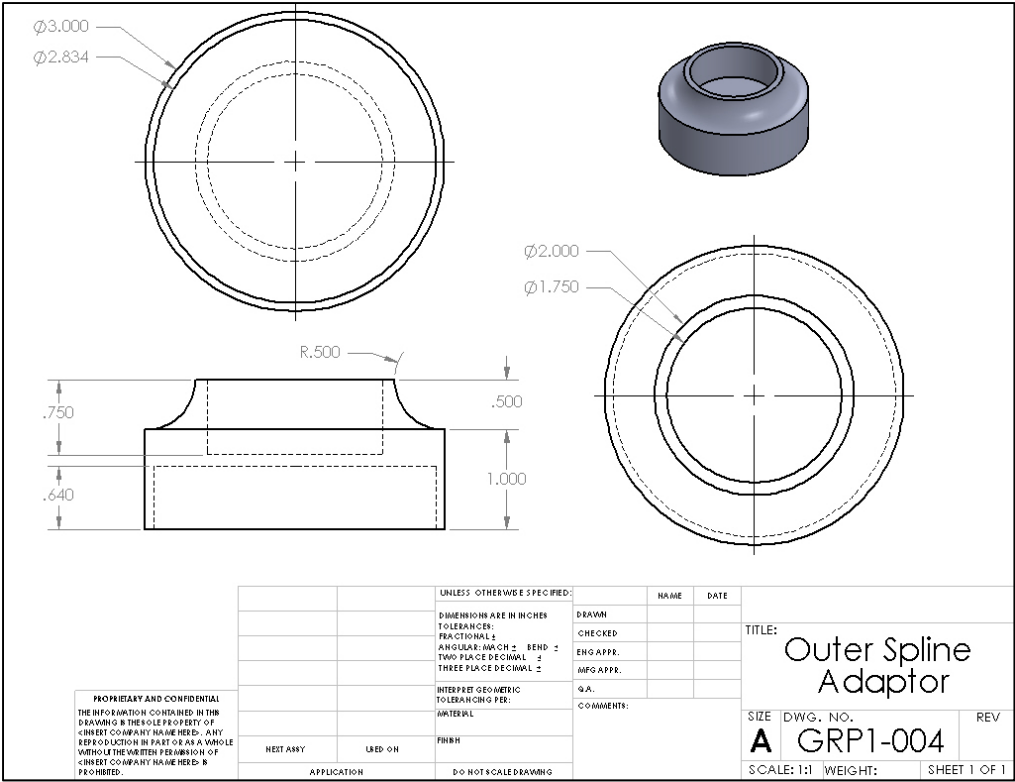


Figure 106: Outer Spline Adaptor Drawing

- ¹ Rzeppa
- ² Rzeppa Def
- ³ Cornay Fact Sheet
- ⁴ InvisibleSHIELD
- ⁵ Thompson Coupling
- ⁶ Ujoint Wikipedia
- ⁷ WIKIPEDIA SPLINE
- ⁸ NSPE